Development of Transparent and Flexible Field Emission Displays Using ZnO Films

by

ZURITA BINTI ZULKIFLI

A thesis submitted in partial fulfillment of the requirements for the degree of

DOCTOR OF ENGINEERING

Field of Environmental Ceramic Materials
Department of Frontier Materials
Graduate School of Engineering
Nagoya Institute of Technology

Supervised by:

Prof. Dr. Masaki Tanemura

Table of Contents

List of figures i
List of tables v
Abstract vi
Acknowledgment vii
CHAPTER 1 **1**
Introduction 1
1.0 Advancement in Transparent and Flexible Devices Technology 1
1.1 Research motivation and objectives 2
1.2 Thesis outline 4
1.3 References 6
CHAPTER 2 **8**
Background of Display Technology 8
2.0 Introduction 8
2.1 Working mechanism of display technology 9
2.1.1 Cathode ray tube 9
2.1.2 Liquid Crystal Display 9
2.1.3 Plasma display Panel 10
2.1.4 Field Emission Display 10
2.2 Cathode and Phosphor materials of FED 12
2.3 Zinc oxide (ZnO) and related doping materials 13
2.3.1 General Properties of ZnO 13
2.3.2 Doping materials 15
2.4 Growth Methods of ZnO Thin film 15
2.5 ZnO nanostructures and growth mechanism 16
2.6 References 17
CHAPTER 3 **23**
Methodology and Characterizations 23
3.1 Introduction 23
3.2 Preparation for ZnO thin film 23
3.3 Co-sputtering technique 25
3.4 Preparation of nanostructured ZnO film 26
3.5 Field Emission measurement 28
3.6 Electron emitters' efficiency 28
3.7 Sample characterizations and instrumentations 30
3.7.1 Sheet resistance 30
3.7.2 Surface profiler 31
3.7.3 Scanning Electron Microscopy (SEM) 31
3.7.4 UV-Vis Spectrometer 32
3.7.5 Atomic Force Microscopy (AFM) 32
3.7.6 X-Ray Diffraction (XRD) 33
3.7.7 X-ray Photoelectron Spectroscopy (XPS) 33
3.7.8 Raman Spectroscopy 34
3.8 References 35

CHAPTER 4 **36**
Fabrication of Nanostructured ZnO Films for Transparent Field Emission Displays **36**
4.0 Introduction 36
4.1 Experimental Procedure 37
4.2 Results and Discussion 38
4.3 Conclusions 46
4.4 References 47
CHAPTER 5 **50**
Effect of surface morphology on the field emission property for ZnO films **50**
5.0 Introduction 50
5.1 Experimental Details 51
5.1.1 Sample preparations 51
5.1.2 Sample Characterizations 51
5.2 Result and Discussion 52
5.3 Conclusion 57
5.4 References 58
CHAPTER 6 **61**
Highly transparent and conducting C:ZnO thin film for field emission display **61**
6.0 Introduction 61
6.1 Experimental details 62
6.1.1 Thin film preparation 62
6.1.2 Characterization 65
6.2 Results and Discussion 66
6.2.1 Morphology, electrical and optical properties 66
6.2.2 X-ray Photoelectron spectrometer (XPS) 70
6.2.3 Luminescence emission properties 72
6.2.4 Field emission application 73
6.3 Conclusion 74
6.4 References 76
CHAPTER 7 **79**
Fabrication of transparent graphene-ZnO nanocone based field emission display **79**
7.0 Introduction 79
7.1 Experimental details 80
7.1.1 Thin film preparation 80
7.1.2 C:ZnO nanocones film preparation 81
7.1.3 Synthesis of graphene and transfer process 81
7.1.4 Sample characterizations 82
7.2 Results and Discussion 82
7.3 Conclusion 87
7.4 References 88

CHAPTER 8 **91**
Fabrication of transparent and flexible carbon doped ZnO field emission display on plastic substrate **91**
8.0 Introduction 91
8.1 Experimental details 93
8.1.1 C:ZnO thin and nanostructured film preparations 93
8.1.2 C:ZnO films characterizations 94
8.2 Results and Discussion 94
8.3 Conclusion 100
8.4 References 102
CHAPTER 9 **106**
Conclusion and Future Development **106**
9.0 Conclusions 106
9.1 Future development 107
List of Publications **108**
List of Conferences **109**

List of figures

Figure 1-1: Schematic diagram of current approach of FED structure....3

Figure 1-2: The proposed FED structure 4

Figure 2-1: Development of display technology 8

Figure 2-2: Comparison between CRT and FED....11

Figure 2-3: Surface barrier in field emission 12

Figure 2-4: The crystal structure of ZnO [23] 14

Figure 2-5: Schematic diagram of direct band gap ZnO material 15

Figure 3-1: Schematic diagram of RF sputtering system....24

Figure 3-2: Schematic diagram of RF sputtering chamber....24

Figure 3-3: (a) Top and (b) side view of ZnO target 26

Figure 3-4: Schematic diagram of incident angle normal to the substrate 27

Figure 3-5: Sputtering yield curve....27

Figure 3-6: Schematic diagram of FED prototype....28

Figure 3-7: Sheet resistance measurement....30

Figure 3-8: Resistance measurement 31

Figure 3-9: Definition of arithmetic, root mean square and peak to valley roughness in AFM measurement 32

Figure 4-1: SEM image of as-deposited ZnO on glass substrate.....38

Figure 4-2: SEM images of ZnO nanocones fabricated by Ar^+ ion irradiation at ion-incidence angle of 30˚. (a) Low- and (b) high-magnification SEM images. 39

Figure 4-3: TEM image of ZnO thin film....40

Figure 4-4: XRD patterns of (a) as-deposited ZnO film, and nanostructured ZnO film ion-irradiated at ion-incidence angles of (b) 30˚and (c) 45˚. 41

Figure 4-5: Field emission property of ZnO nanocones irradiated at ion-incidence angle of 30˚. 42
Figure 4-6: SEM images of ZnO nanocones fabricated by Ar+ ion irradiation at ion-incidence angle of 45˚. (a) Low- and (b) high-magnification SEM images. 43
Figure 4-7: Field emission property of ZnO nanocones irradiated at ion-incidence angle of 45˚. The inset figure is the corresponding FN plot. 44
Figure 4-8: SEM image of ZnO nanocones fabricated by Ar^+ ion irradiation at ion-incidence angle of 60˚ 44
Figure 4-9: Field emission property of ZnO nanocones irradiated at ion-incidence angle of 60˚. The inset figure is the corresponding FN plot. 45
Figure 5-1: SEM images of (a) as-deposited ZnO thin film and (b) ZnO nanocones induced on the film surface by ion irradiation after 3 min. 52
Figure 5-2: Initial FE property of ZnO nanocones before the stability test. 53
Figure 5-3: Stability test at electric field of 12 V/μm for 60 minutes in a vacuum condition. 54
Figure 5-4: Field emission properties of ZnO nanocones after the stability test. 55
Figure 5-5: Surface morphology of ZnO nanocones at the emission area 56
Figure 5-6: Surface morphology of ZnO nanocones at out of the emission area 56
Figure 6-1: RF Sputtering schematic diagram 63
Figure 6-2: Top view of graphite plate position on the ZnO target 64
Figure 6-3: AFM images of undoped and carbon doped ZnO thin film 66
Figure 6-4: Raman spectra of undoped and C doped ZnO thin film 68
Figure 6-5: Transmittance spectra of undoped and carbon doped ZnO thin films 70
Figure 6-6: XPS spectrum of C doped ZnO 71
Figure 6-7: CL spectra of undoped and carbon doped ZnO thin film 73

Figure 6-8: FE property of C doped ZnO film as the phosphor layer and SWCNT as the field emitter. Inset figures are (a) the FN plot and (b) light emission from C doped ZnO film.....74

Figure 7-1: (a) Highly transparent pristine C:ZnO nanocone film and (b) SEM image of C:ZnO nanocones on the glass substrate after 10 min ion beam irradiation at RT. 83

Figure 7-2: (a) A low magnification and (b) high magnification of SEM images of hybrid graphene-C:ZnO nanocones film (red arrows shows the fold of graphene).....84

Figure 7-3: Transmittance spectra of pristine C:ZnO nanocones and graphene-C:ZnO nanocones film.....84

Figure 7-4: (a) Raman spectra of pristine C:ZnO nanocones and (b) hybrid graphene-C:ZnO nanonocones film.....85

Figure 7-5: FE properties of pristine C:ZnO and hybrid graphene-C:ZnO nanocones film. Inset indicates the F-N plot for field enhancement factor of the emitters. 86

Figure 7-6: Stability test for graphene-C:ZnO nanocones film in 50 min at 1200V 87

Figure 8-1: C:ZnO thin film deposited at high RF power 94

Figure 8-2: SEM image of C:ZnO on arylite substrate deposited at high RF power.....95

Figure 8-3: C:ZnO thin film on arylite substrate deposited at low RF power 95

Figure 8-4: Typical SEM images of C:ZnO nanocone emitters on an arylite substrate at (a) low magnification and (b) high magnification.....96

Figure 8-5: (a) The transmittance spectra of C:ZnO thin and nanoconces film. Transparent and flexible C:ZnO (b) anode film and (c) nanocone emitters. 97

Figure 8-6: (a) FE properties of transparent and flexible C:ZnO FED and the inset figure is the corresponding FN plot. (b) Stability test of transparent and flexible C:ZnO nanocones emitters for 1 hr.....98

Figure 8-7: (a) FE property of transparent and flexible C:ZnO anode film with CNT as the cathode material. (b) Red light emission observed from FE measurement and (c) CL spectra shows the dominant peak at 646 nm at the visible wavelength which is corresponding to the red colour wavelength. 100

List of tables

Table 6-1: Sputtering condition of C:ZnO thin film.....63

Table 6-2: Electrical and transmittance property of undoped and C:ZnO thin films 67

Table 7-1: Sputtering condition of C:ZnO thin film.....80

Abstract

Electronic displays have been renaissance in today's technology with the demand of transparent and flexible features. Transparent and flexible display may offers a low cost electronic devices, lightweight, foldable, convenient and also become environmental friendly devices. In this thesis, Field Emission Display (FED) concept was applied to study the potential materials and nanostructure features in order to achieve for the goals. ZnO material was chosen because it has wide energy band gap which is a significant property for a transparent device applications. The ability to emit light from ZnO-based material was also the reason why ZnO is the best candidate to be selected in this research work. To achieve the flexible FED, arylite was attempted for both substrates, the anode (screen) and the cathode (emitters), respectively. Transparent ZnO nanocones film for the electron emitters of FED had successfully fabricated at room temperature by Ar^+ ion irradiation technique. To improve the conductivity of ZnO, carbon source from graphite plate and sheet of graphene were employed as the dopant material and coating layer, respectively. Both materials showed excellent performance in electrical and optical properties with ZnO. The details of the challenges and achievements upon the fabrication of transparent and flexible FEDs using ZnO films were revealed in this thesis.

Acknowledgment

In the name of Allah, the Most Gracious and the Most Merciful. Alhamdulillah with His blessed, in any circumstance, I managed to complete my thesis without any obstacles.

I dedicate special appreciation to my honorable supervisor, Prof. Dr. Masaki Tanemura for his invaluable advices, suggestions, comments and courage towards my three years struggling on the research works. He generously and continuously offered his time and effort to make sure I grabbed all the chances to gain knowledge and experiences as much as I can under his supervision. The opportunities given had boost up my confidence level in writing skill and paper presentation in the international conferences.

I also would like to express my gratitude to my thesis reviewers, Prof. Dr. Tetsuo Soga and Prof. Dr. Ichikawa Yo towards their comments and suggestions on improving the thesis contents.

I am grateful and thankful to work with Assistant Prof. Dr. Golap Kalita for his guidance in completing my research and publication work. I thank Dr. Subramanian for his efforts to teach me in using many equipment in which I have no experienced in handling it before. I am greatly appreciate Dr. Mohd Zamri Mohd Yusop for his kindness in helping me in research as well as in all necessaries arrangement since my first day living in Nagoya.

Sincere thanks to all my colleagues, lab mates, my senior Dr. Sukreen Hana, Prof. Dr. Mohamad Rusop, Malaysian students in Nagoya especially Saufi Rosmi, Yazid Yaakob, Norhana Abdul Rashid and Nazri Sokri for their moral supports and continuously cheerful spirit towards completion this journey. I am thankful to those who involved indirectly in this research. Your contribution and kindness are means a lot to me.

A special thanks also goes to Universiti Teknologi Mara, Shah Alam and Ministry of Education Malaysia for their financial support. Without their offer, I would not be able to study abroad and survive living in Japan.

Last but not least, I gladly acknowledge my debt and deepest gratitude to my beloved parents Mr. Zulkifli Abdullah and Mrs. Joriah Kasmuni, also to all my family members for their valuable advice and courage even though we are far from each other. Thanks to the technology that makes me feel we are always close with each other. Thank you very much for your endless love and prayers.

CHAPTER 1

Introduction

1.0 Advancement in Transparent and Flexible Devices Technology

Transparent electronics is an emerging technology that involves wide band-gap semiconductor (> 3 eV). To achieve for a transparent electronics devices, electronic circuitry and all components must be transparent in visible too. Until today, transparent conductive oxide (TCO) materials especially indium tin oxide (ITO) were widely being applied in the fabrication of transparent electronic component and electrodes [1-3]. However, the development of transparent and conductive film is still looking for the best material to challenge ITO [4,5]. Recent needs in device applications to have lightweight, transparent and conductive, foldable and cheap devices, have limit the ITO material to be used due to the failure of ITO film under bending condition, limited indium source and costly material. Thus, the future needs have stimulated researchers to find for the suitable materials that comply with transparent, conductive and fit to be fabricated on flexible substrate.

The interesting of having transparent devices is because it can be applied in a very wide area of applications. Fabrication of transparent paper can be applied for electronics devices such as thin films transistors (TFTs), organic light emitting diode (OLED), solar cell and others [6]. A transparent camera could possibly improve the security system. In military system and for a common use such as in extreme sport, a real time wearable display could be useful for the head up display (HUD) [7,8]. Another interesting application in display technology is where a window can be engineered to become a smart window [9]. The purpose is such to double function the window glass by transform it to be as a display. For example,

an automobile windscreen and aircraft cockpit window can visualize information to the driver or pilot in which it is identical with a global positioning system (GPS) and radar system. Transparent display also could be fascinating for a computer and smart phone screen [10,11].

1.1 Research motivation and objectives

Transparent electronics applications can only be implemented if the base materials comply with higher transmittance property in the visible wavelength. The main objectives of this work were to employ ZnO film as the phosphor screen and emitters of transparent and flexible display. For a flat transparent display, there are several technologies have been applied such as transparent OLED, liquid crystal display (LCD) and field emission display (FED). FED development offers a thinner panel display than LCD, wide view angle, high image quality than cathode ray tube (CRT) and consume less power. The advantages of FED will makes the future dreams comes true. Many literatures could be found in developing FED with various techniques and materials. However, only several reports of transparent FED could be found and the stability of emission is still questionable [12]. Thus, the efforts in undertaking these issues were reported in this thesis.

In general, field emission is a process of exciting electrons from solid-state materials into a vacuum by the electric field. FED structure consists of emitters as the cathode materials, and phosphor layer coated on ITO as the anode material. Several types of substrate were used to fabricate the emitters such as glass, silicon and sapphire [13-15].

The surface roughness of nanostructure films has to take into consideration when fabricating transparent FED. High aspect ratio of electron emitters would be a merit to enhance high current density; however, it also may increase the roughness of film surface morphology. The higher surface roughness could reflect more light due to light scattering on

the surface compare to transmit the light thru the nanostructure film. Thus, it can reduce the transmittance property of nanostructured film. It is quite challenging to attain for both criteria. For the anode materials, a phosphor layer coated on the conductive materials also may affect the transmittance property. Fig. 1-1 shows the existing type of FED structures while in Fig. 1-2 shows the potential fabrication of ZnO film to achieve a fully transparent and flexible ZnO-based FED. The potential shortage of indium could stimulate the exploring of ZnO to be as the based material of transparent FED. CNTs are well-known material that could exhibit high current density at a low electric field [16]. However, the preparation of CNTs emitters is expensive due to the higher cost of single wall or multiwall CNTs.

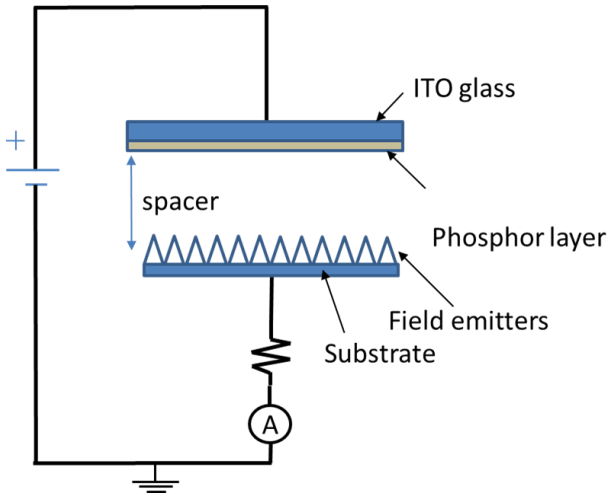

Figure 1-1: Schematic diagram of current approach of FED structure

Therefore, transparent and flexible FED was fabricated using ZnO material owing to the advantages of highly transmittance material, low cost material and it is a direct band gap semiconductor. A big contribution of ZnO in display technology is a potential material to replace the conventional powder phosphor. Defect formation in ZnO-based material creates trap states in the forbidden energy band which are responsible for any light emission in the visible wavelength. The new FED structure employed ZnO-based material as the phosphor layer as well as the material for electron emitters. Taking for granted of the phosphor

property from ZnO film, thus, there is no need to deposit a layer of phosphor material which was done in the conventional fabrication of FED. This technique can reduce the fabrication cost and improve the transmittance property of anode layer. The fabrication of ZnO nanocones emitters was done at room temperature which is suitable for any substrate that has a limitation with heat. Hence, fabrication of ZnO nanostructured film on flexible substrate that offers a light weight, foldable and durability FED can be realized in future. For that reasons, the new structure shown in Fig. 1-2 could be a promising transparent and flexible ZnO-based field emission display.

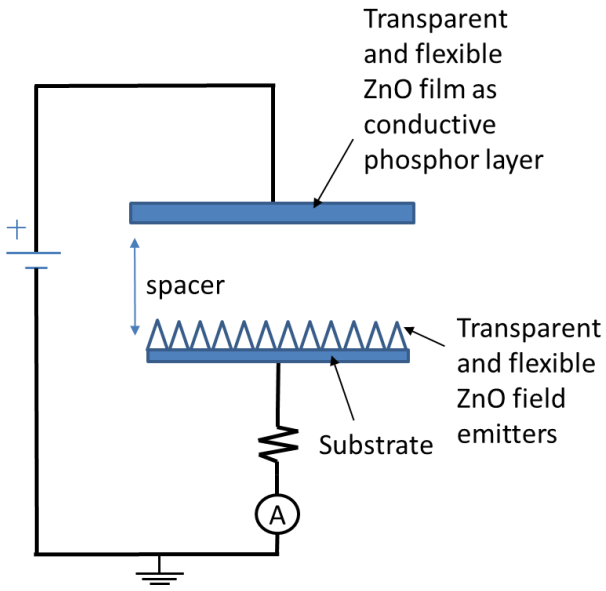

Figure 1-2: The proposed FED structure

1.2 Thesis outline

The thesis comprises nine chapters which are arranged as follows. Chapter 2 describes in details the background and history of vacuum devices especially FED, emitters materials, techniques to fabricate the emitters and preparation method to fabricate the phosphor layer.

Chapter 3 explained the flow of ZnO thin film and nanostructured film fabrication, characterization methods and equipment related with the characterization. Field emission

measurement conducted in this experiment was explained with an aid of schematic diagram of the FED prototype.

Chapter 4 deals with the fabrication of nanostructured ZnO films for transparent field emission displays. A highly transparent field emitter was achieved by Ar^+ ion irradiation onto highly transparent and conducting ZnO films deposited on glass substrates at 60˚ ion incident angle

Chapter 5 describes on the stability of ZnO nanocones. An emission test was conducted for 1 hr and the emission property before and after the test was reported. SEM images were taken to study the surface morphology.

Chapter 6 represents the highly conductive and transparent C:ZnO thin film. The conductivity of ZnO thin film was improved by doping process. Carbon from graphite plates was used as the dopant material and co-sputtered with ZnO target by Argon in a small chamber. The result showed changes in sheet resistance but not so much affected the transmittance property.

Chapter 7 presented a highly transparent hybrid graphene-C:ZnO nanocones film. The hybrid film was employed as the field emitters (FE) which showed an improvement in the emission property compared to the pristine C:ZnO nanocones film.

Chapter 8 explained the challenges of fabricating ZnO-based thin film on flexible substrate. The deposition thin film was done at a low temperature and low RF sputtering to avoid damage on the substrate. Arylite was used as the flexible substrate. High transparent anode and cathode ZnO-based film was achieved for the transparent and flexible field emission display.

Finally, the conclusions for this thesis are drawn in Chapter 9.

1.3 References

[1] H. Liu, V. Avrutin, N. Izyumskaya, Ü. Özgür, and H. Morkoç, "Transparent conducting oxides for electrode applications in light emitting and absorbing devices," *Superlattices Microstruct.*, vol. **48**, no. 5, pp. 458–484, 2010.

[2] J. B. Franklin, J. B. Gilchrist, J. M. Downing, K. a. Roy, and M. a. McLachlan, "Transparent conducting oxide top contacts for organic electronics," *J. Mater. Chem. C*, vol. **2**, no. 1, pp. 84, 2014.

[3] T. Minami, "Substitution of transparent conducting oxide thin films for indium tin oxide transparent electrode applications," *Thin Solid Films*, vol. **516**, no. 7, pp. 1314–1321, 2008.

[4] K. Ellmer, "Past achievements and future challenges in the development of optically transparent electrodes," *Nat. Photonics*, vol. **6**, no. 12, pp. 809–817, 2012.

[5] H. Wu, D. Kong, Z. Ruan, P.-C. Hsu, S. Wang, Z. Yu, T. J. Carney, L. Hu, S. Fan, and Y. Cui, "A transparent electrode based on a metal nanotrough network," *Nat. Nanotechnol.*, vol. **8**, no. 6, pp. 421–5, 2013.

[6] H. Zhu, Z. Fang, C. Preston, Y. Li, and L. Hu, "Transparent paper: fabrications, properties, and device applications," *Energy Environ. Sci.*, vol. **7**, no. 1, p. 269, 2014.

[7] C. W. Hsu, B. Zhen, W. Qiu, O. Shapira, B. G. DeLacy, J. D. Joannopoulos, and M. Soljačić, "Transparent displays enabled by resonant nanoparticle scattering," *Nat. Commun.*, vol. **5**, pp. 3152, 2014.

[8] R. S. Laramee and C. Ware, "Rivalry and interference with a head-mounted display," *ACM Trans. Comput. Interact.*, vol. **9**, no. 3, pp. 238–251, 2002.

[9] J. Zhou, Y. Gao, Z. Zhang, H. Luo, C. Cao, Z. Chen, L. Dai, and X. Liu, "VO_2 thermochromic smart window for energy savings and generation," *Sci. Rep.*, vol. **3**, pp. 3029, 2013.

[10] K. Hong, J. Yeom, C. Jang, G. Li, J. Hong, and B. Lee, "Two-dimensional and three-dimensional transparent screens based on lens-array holographic optical elements," *Opt. Express*, vol. **22**, no. 12, pp. 14363–74, 2014.

[11] T. He, A. Xie, D. H. Reneker, and Y. Zhu, "ARTICLE A Tough and High-Performance Transparent Electrode from a Scalable and Transfer-Free Method," *ACS Nano*, vol. **8**, no. 5, pp. 4782–4789, 2014.

[12] P. Ghosh, M. Z. Yusop, S. Satoh, M. Subramanian, A. Hayashi, Y. Hayashi, and M. Tanemura, "Transparent and flexible field electron emitters based on the conical nanocarbon structures," *J. Am. Chem. Soc.*, vol. **132**, no. 12, pp. 4034–5, 2010.

[13] H.-M. Kim, T. W. Kang, K. S. Chung, J. P. Hong, and W. B. Choi, "Field emission displays of wide-bandgap gallium nitride nanorod arrays grown by hydride vapor phase epitaxy," *Chem. Phys. Lett.*, vol. **377**, no. 5–6, pp. 491–494, 2003.

[14] S. P. Lau, H. Y. Yang, S. F. Yu, H. D. Li, M. Tanemura, T. Okita, H. Hatano, and H. H. Hng, "Laser action in ZnO nanoneedles selectively grown on silicon and plastic substrates," *Appl. Phys. Lett.*, vol. **87**, no. 1, pp. 013104, 2005.

[15] Z. Wang, X. Qian, J. Yin, and Z. Zhu, "Tube-like ZnO Arrays by a Simple Chemical Solution Route," *Langmuir*, vol. **20**, no. 24, pp. 3441–3448, 2004.

[16] D. Ghosh, P. Ghosh, M. Z. Yusop, M. Tanemura, Y. Hayashi, T. Tsuchiya, and T. Nakajima, "Transparent and flexible field emission display device based on single-walled carbon nanotubes," *Phys. status solidi - Rapid Res. Lett.*, vol. **6**, no. 7, pp. 303–305, 2012.

CHAPTER 2

Background of Display Technology

2.0 Introduction

A huge and heavy screen could be seen in those days on the office table or at the corner of living hall. The bulk display screen is called cathode ray tube (CRT) which requires vacuum to operate. Sir William Crooke was a pioneered of vacuum tube in 1878 [1]. His innovation was followed by developing a modern day x-ray machine. In 1897, Sir Karl F. Braun applied the vacuum tube concept to invent in developing of oscilloscope. The technology of cathode ray tube was further used by researcher to develop television. In 1926, Kenjiro Takayanagi, one of the founders of JVC of Japan succeeded to come with the first world black and white (B&W) television. The next few years later, DuMont and Zenith produced the first commercial electronic B&W television. Figure 2-1 shows the development in display technology. The display technology is moving towards lightweight, cheap and bright display from CRT to FED.

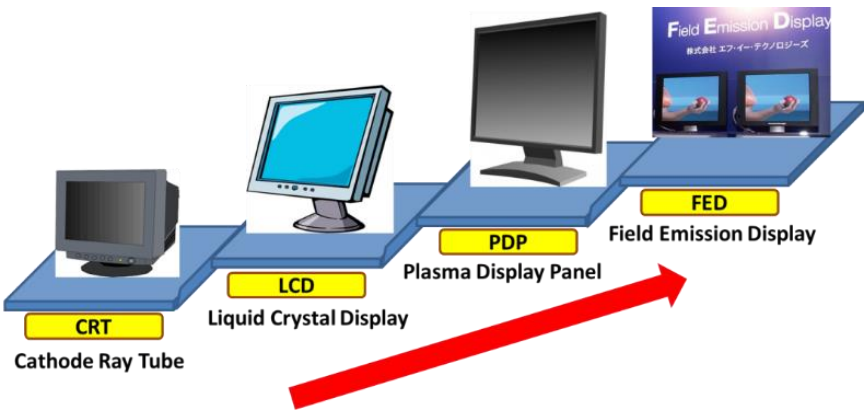

Figure 2-1: Development of display technology

2.1 Working mechanism of display technology

2.1.1 *Cathode ray tube*

Cathode ray tube (CRT) consists of electron guns which accelerate and deflect electron beams to display images, waveforms or radar targets on the screen. In a cathode ray tube, the cathode is a heated filament. The heated filament is inside the vacuum tube. Electrons from cathode are accelerating towards anode in the CRT and have been focused to hit the phosphor coated screen which turns glow as it being bombard by the beams. Due to the limitations of CRT such as bulky, heavy and take a lot of space, a flat panel display technology has been discovered.

2.1.2 *Liquid Crystal Display*

The technology so called liquid crystal display (LCD) discovered in 1888 had overcome some issues in CRT and fulfill a demand from consumers [2]. LCD is widely used as the laptop monitor screen, calculator display, digital clock and many others electronic devices. LCD works totally in different way with CRT. LCD consists of horizontal and vertical polarizing filter in which a pixel (red, blue or green) is located in between the two polarizing filters. Each pixel is control by a transistor that can be switch on and off electronically. When the transistor is switched off, horizontal polarizing filter will allow light to pass through it and being blocked by the vertical polarizing filter. Thus makes the pixel looks dark. When the transistor is switched on, it will rotate the light passing through it through 90˚ and thus makes a pixel looks bright. Even though LCD shows some advantages such as low power

consumption, energy efficient and safety than CRT, LCD also suffers from image persistence and very sensitive to temperature.

2.1.3 *Plasma display Panel*

Plasma display panel (PDP) is almost similar with LCD in terms of weight and having a flat panel screen. However, the working mechanism is completely different. Each pixel in plasma display is the fluorescence lamp glowing with plasma. Plasma screen used xenon and neon atoms [3]. When an electric supply is given, free electrons collide with those atoms. The atoms become unbalance due to the missing electrons from the collision. The atoms is now has net positive charge called ion. In a plasma with an electrical current run through it, the positively charge will go to the negatively charge area and vice versa. The collision between the particles excite gas atom in plasma to release photon of energy which is mostly ultraviolet light photons. The ultraviolet light photons can be used to excite visible light photons by hitting phosphor materials inside a plasma display [4]. Plasma may get hot and need fans to be cooled. Sometimes the fan make loud and interfering. This is the weakness of plasma display and it is also expensive compared to LCD.

2.1.4 *Field Emission Display*

Field emission (FE) technology is the most similar with CRT technology. FE can be obtained at low temperature as low as room temperature and thus it is sometimes known as cold-cathode emission. FE display (FED) consists of thousands sharp cathode tips as the emitter to accelerate electron and bombard phosphor layer at the screen display while CRT needs a single gun for all pixels as shown in Figure 2-2 [5].

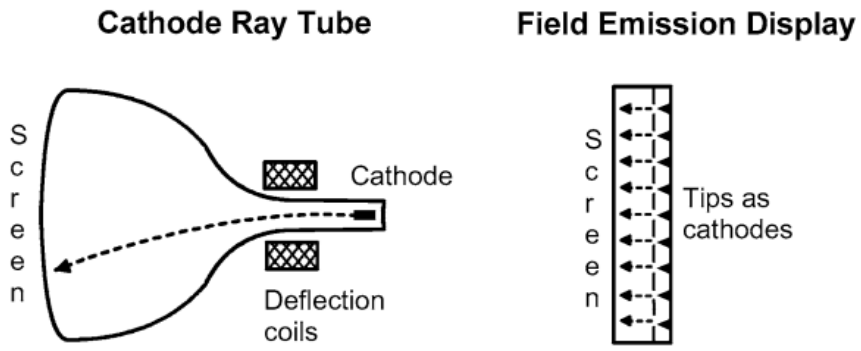

Figure 2-2: Comparison between CRT and FED

The FE concept is basically originate from the metal-insulator-metal behavior and now, semiconductor materials is being applied in FE fabrication [6]. When a positive potential is applied at the anode material of FED, an electric field induced at the emitter tip that allows electrons to tunnel from the solid surface to the vacuum area. The tunneling process of electron is highly depends on the work function (Φ) of the cathode materials. Work function is a minimum energy to remove electron from solid surface to a point in vacuum immediately outside the solid surface. The lower the work function the easier electrons to overcome the surface barrier. Figure 2-3 shows the schematic diagram of surface barrier with the comparison between planar and microtip emitter. Thermionic emission is unlike field emission where it needs higher local electric field to penetrate the vacuum area. A surface with planar emitter was normally does not have any emission property (no tunneling effect) but if the surface has microtip, it helps the electrons to penetrate vacuum at low electric field [7].

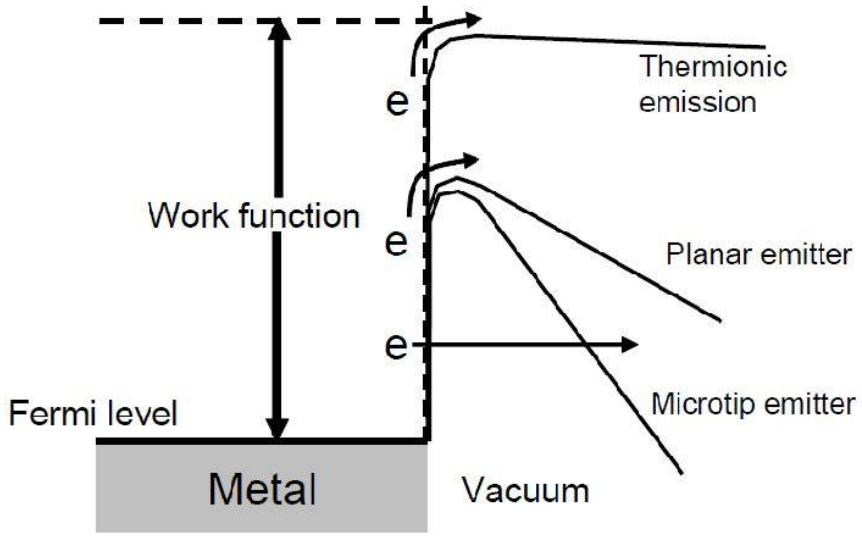

Figure 2-3: Surface barrier in field emission

In the field emission, there are three type of emission involved [8]. First, the internal emission in which the electron moves from valence band to conduction band. Next, the electron transport in which it is directly depends on the conductivity of the material use for the film. If the material use is low in conductivity, it will provide a poor path for electrons and thus degrade the emission property. The third emission is from the surface of film to the vacuum area. At this stage, the emission was depends on the field enhancement factor, β. β can be expressed as $\beta = h/r$, where h is the height and r is the radius of curvature of an emitting center. It is the ability of emitters to enhance local electric field.

2.2 Cathode and Phosphor materials of FED

There are many types of cathode materials for FED emitters such as CNTs, CNFs, silicon nanostructure, metal-based and semiconductor-based nanostructure [9-13]. Recently, graphene and hybrid structure are also employed as the emitters[14-16]. A thin film emission cathode was first fabricated by C.A.Spindt [17]. The materials with elongated geometry and

sharp tips will efficiently enhanced the emission current. However, for most of the materials, there are still lack of study on the stability test of the emitters in a long period of time.

High efficiency of phosphor at low electric field and longer life time with better brightness than CRT is highly dependent on the materials and the compounds used. Sulfide based materials is not preferable nowadays with respect to the hazardous materials. Thus, oxide based phosphor are currently being explore as it is comply with the environmental friendly materials. From the literature several phosphor materials such as $Y_2O_2S:Eu3^+$, ZnS:Cu,Al and ZnS:Ag, Al has been applied for red, green and blue, respectively [18], ZnO:Zn [19], ZnS:Ag, Cl blue phosphor coated with MgO and polyphosphate, and $SrGa_2S_4:Eu^{2+}$ green phosphor coated with MgO and In_2O_3 [20] and CaF_2 [21] was reported. As for commercialization of FED in the future, high efficiency, low cost and abundant material supply would be preferable to be chosen as the material for FED.

2.3 Zinc oxide (ZnO) and related doping materials

2.3.1 *General Properties of ZnO*

ZnO can be an alternative material for GaN in ultraviolet (UV) optoelectronic devices due to its high ground state exciton binding energy (60 meV) at room temperature compared to GaN. ZnO crystallizes in the hexagonal wurtzite-type structure as shown in Figure 2-4 and is characterized by two interconnecting sublattices of Zn^{2+} and O^{2-}. The lattice parameters of the hexagonal unit cell are a=3.2495Å and c=5.2069 Å [22].

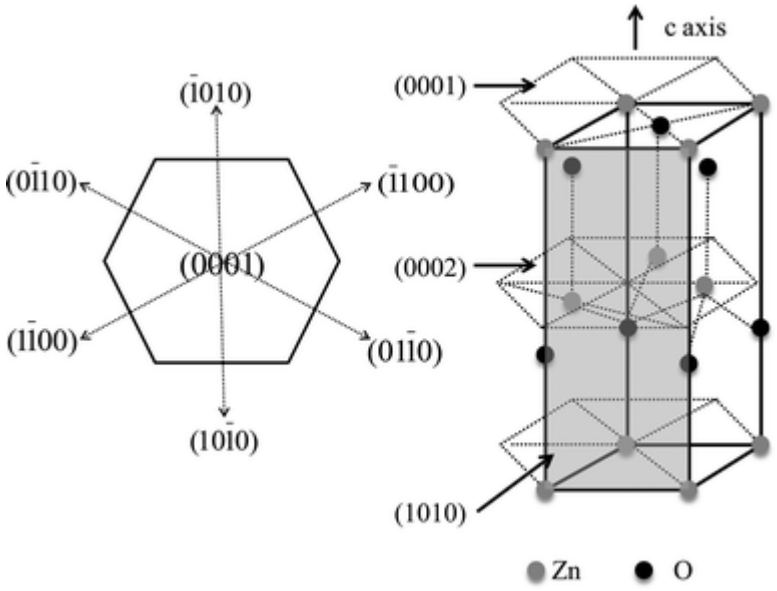

Figure 2-4: The crystal structure of ZnO [23]

Figure 2-5 shows the schematic diagram represent a direct band gap of ZnO. The figure shows a wide energy band gap of 3.4 eV which can be a potential material for transparent conductive oxide (TCO). Another merit of ZnO according to the property of direct band gap, based on the theory of charge carrier in semiconductor, a photon can provide the energy to produce electron-hole pair. In the ZnO material, an equal value of electron momentum occur at the top of valence band and at the bottom of conduction band. A photon with energy, E has a momentum p = E/c, where c is the velocity of light (3×10^8 ms^{-1}). An optical photon has energy in the order of 10^{-19} J. Thus, gives a very small momentum of a typical photon. Therefore, it is an advantage of employing ZnO in the optoelectronic application because a photon can produce electron-hole pair easily and the electrons does not need high momentum. Unlike indirect band gap, electrons moves at a slower rate and needs to interact not only with photon but also with phonon to gain energy. Hence, a transparent FED could be realized with ZnO material due to the above mention reasons.

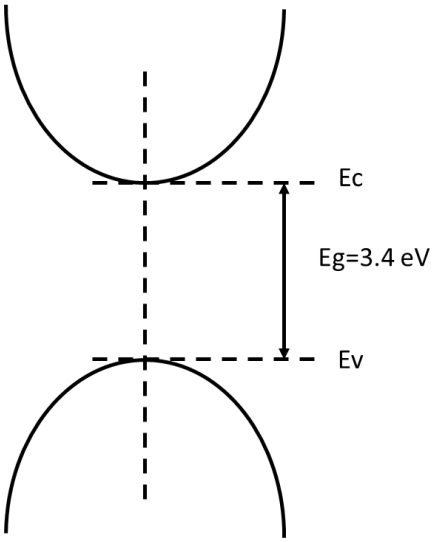

Figure 2-5: Schematic diagram of direct band gap ZnO material

2.3.2 *Doping materials*

Upon alloying with different materials such as MgO or CdO, the band gap of ZnO can be shifted to higher or lower energy [24,25]. The conductivity of unintentionally n-type ZnO also can be controlled by doping with Al or Ga [26-29]. P-type ZnO is remain a challenge. However, there are a lots of report can be found which claims on the successful of getting p-type ZnO with respect to their technique of fabrication and related doping materials [30,31].

Doping with some other materials such as Co, Ni and Fe with ZnO has enhanced the ferromagnetism property which can be applied in myriad potential applications (eg. Sensors, communication devices, data storage, and etc.) [32,33].

2.4 Growth Methods of ZnO Thin film

ZnO can be as in powder or as in solid physical structure. From that bulk target, it can be transformed to be a thin film with various fabrication methods. ZnO thin film can be

fabricated by dip-coating, spin coating [34,35], chemical vapor deposition (CVD) [36,37], pulse laser deposition (PLD) [38,39], RF sputtering[40,41], spray pyrolysis [42] and other methods. The property of deposited thin film varies with the parameters, fabrication condition and methods. Among the growth methods, RF sputtering is the most favorable because it is possible to obtain highly oriented crystalline quality of ZnO at c-axis (002) even on amorphous substrates.

2.5 ZnO nanostructures and growth mechanism

The formation of nanostructures could enhance efficiency of any electronic devices such as FED, solar cell and etc. High aspect ratio, strong adhesion on substrate, stable electrical and mechanical properties of nanostructures may improve life performance of any fabricated device. The shape of nanostructures can be fabricated in any forms depends on the growth parameters such as temperature, pressure, growth time, catalyst and others. For ZnO-based FED, ZnO nanostructures with high aspect ratio is indispensable to gain high emission current at low applied electric field. ZnO nanoneedles, nanopins, nanowire, nanocones, nanorods has been widely reported in the literature [43-47].

2.6 References

[1] B. R. Masters, "History of the Electron Microscopy in Cell Biology," *Encyclopedia of Life Sciences*. John Wiley & Sons, Ltd, Chichester, UK, pp. 1–9, 2001.

[2] K.-H. Kim and J.-K. Song, "Technical evolution of liquid crystal displays," *NPG Asia Mater.*, vol. **1**, no. 1, pp. 29–36, 2009.

[3] U. Kogelschatz, B. Eliasson, and W. Egli, "From ozone generators to flat television screens: history and future potential of dielectric-barrier discharges," *Pure Appl. Chem.*, vol. **71**, no. 10, pp. 1819–1828, 1999.

[4] J. Boeuf, "Plasma display panels: physics, recent developments and key issues," *J. Phys. D. Appl. Phys.*, vol. **53**, pp. 53–79, 2003.

[5] G. G. and H. W. P. K. K.Blankenbach, "Vacuum microelectronics," in *Vacuum Electronics: Components and Devices*, pp. 85–125, 2008.

[6] C. a. Mead, "Operation of Tunnel-Emission Devices," *J. Appl. Phys.*, vol. **32**, no. 4, pp. 646, 1961.

[7] B. K. Gupta, D. Haranath, S. Chawla, H. Chander, V. N. Singh, and V. Shanker, "Self-catalytic synthesis, structure and properties of ultra-fine luminescent ZnO nanostructures for field emission applications.," *Nanotechnology*, vol. **21**, no. 22, pp. 225709, 2010.

[8] J. B. You, X. W. Zhang, P. F. Cai, J. J. Dong, Y. Gao, Z. G. Yin, N. F. Chen, R. Z. Wang, and H. Yan, "Enhancement of field emission of the ZnO film by the reduced work function and the increased conductivity via hydrogen plasma treatment," *Appl. Phys. Lett.*, vol. **94**, no. 26, pp. 262105, 2009.

[9] X. Fang, Y. Bando, U. K. Gautam, C. Ye, and D. Golberg, "Inorganic semiconductor nanostructures and their field-emission applications," *J. Mater. Chem.*, vol. **18**, no. 5, pp. 509, 2008.

[10] J. M. Ha, H. J. Kim, H. S. Raza, and S. O. Cho, “Highly stable carbon nanotube field emitters on small metal tips against electrical arcing,” *Nanoscale Res. Lett.*, vol. **8**, no. 1, pp. 355, 2013.

[11] C.-C. Wu, K.-L. Ou, and C.-L. Tseng, “Fabrication and characterization of well-aligned and ultra-sharp silicon nanotip array,” *Nanoscale Res. Lett.*, vol. **7**, no. 1, pp. 120, 2012.

[12] M. E. Swanwick, P. D. Keathley, A. Fallahi, P. R. Krogen, G. Laurent, and F. X. Ka, “Nanostructured Ultrafast Silicon-Tip Optical Field-Emitter Arrays,” *Nano Lett.*, vol. **14**, pp. 5035–5043, 2014.

[13] a. C. Deshpande, P. M. Koinkar, S. S. Ashtaputre, M. a. More, S. W. Gosavi, P. D. Godbole, D. S. Joag, and S. K. Kulkarni, “Field emission from oriented tin oxide rods,” *Thin Solid Films*, vol. **515**, no. 4, pp. 1450–1454, 2006.

[14] S. Zhang, Y. Zhang, S. Huang, H. Liu, P. Wang, and H. Tian, “First-Principles Study of Field Emission Properties of Graphene-ZnO Nanocomposite,” *J. Phys. Chem. C*, vol. **114**, no. 45, pp. 19284–19288, 2010.

[15] R. Zou, G. He, K. Xu, Q. Liu, Z. Zhang, and J. Hu, “ZnO nanorods on reduced graphene sheets with excellent field emission, gas sensor and photocatalytic properties,” *J. Mater. Chem. A*, vol. **1**, no. 29, pp. 8445, 2013.

[16] D. Ye, S. Moussa, J. D. Ferguson, A. a Baski, and M. S. El-Shall, “Highly efficient electron field emission from graphene oxide sheets supported by nickel nanotip arrays,” *Nano Lett.*, vol. **12**, no. 3, pp. 1265–8, 2012.

[17] C. a. Spindt, “A Thin-Film Field-Emission Cathode,” *J. Appl. Phys.*, vol. **39**, no. 7, pp. 3504, 1968.

[18] Z. C. and J. L. Guogang Li, Xiao Zhang, Chong Peng, Mengmeng Shang, Dongling Geng, “Cyan-emitting Ti4+ - and Mn2+ -coactivated Mg2SnO4 as a potential

phosphor to enlarge the color gamut for field emission display," *J. Mater. Chem*, vol. **21**, no. 18, pp. 6477, 2011.

[19] S. Robert D. Herrick II, John L, "Phosphor FED," *J. SID*, vol. **6/3**, pp. 149–151, 1998.

[20] J. Souriau, Y. Dong, J. Penczek, H. G. Paris, and C. J. Summers, "Cathodoluminescent properties of coated SrGa 2 S 4 : Eu 2 + and ZnS : Ag , Cl phosphors for field emission display applications," *Mater. Sci. Eng. B*, vol. **76**, pp. 165–168, 2000.

[21] D. Ghosh, P. Ghosh, M. Tanemura, A. Haysahi, Y. Hayashi, K. Shinji, N. Miura, M. Z. Yusop, and T. Asaka, "Highly transparent and flexible field emission devices based on single-walled carbon nanotube films," *Chem. Commun. (Camb).*, vol. **47**, no. 17, pp. 4980–2, 2011.

[22] K. Ellmer and A. Klein, "ZnO and Its Applications," in Transparent Conductive Zinc Oxide: Basics and Applications in Thin Film Solar Cells, *Ed. Springer Science & Business Media*, pp. 460, 1990.

[23] S. Das and S. Ghosh, "Fabrication of different morphologies of ZnO superstructures in presence of synthesized ethylammonium nitrate (EAN) ionic liquid: synthesis, characterization and analysis," *Dalton Trans.*, vol. **42**, no. 5, pp. 1645–56, 2013.

[24] P. Bhattacharya, R. R. Das, and R. S. Katiyar, "Fabrication of stable wide-band-gap ZnO/MgO multilayer thin films," *Appl. Phys. Lett.*, vol. **83**, no. 10, pp. 2010, 2003.

[25] M. Yadav, M. Ghosh, R. Biswas, A. Raychaudhuri, A. Mookerjee, and S. Datta, "Band-gap variation in Mg- and Cd-doped ZnO nanostructures and molecular clusters," *Phys. Rev. B*, vol. **76**, no. 19, pp. 195450, 2007.

[26] T. Minami, T. Miyata, and Y. Ohtani, "Optimization of aluminum-doped ZnO thin-film deposition by magnetron sputtering for liquid crystal display applications," *Phys. Status Solidi*, vol. **204**, no. 9, pp. 3145–3151, 2007.

[27] P. J. Kelly, Y. Zhou, and a. Postill, "A novel technique for the deposition of aluminium-doped zinc oxide films," *Thin Solid Films*, vol. **426**, no. 1–2, pp. 111–116, 2003.

[28] B. Du Ahn, S. H. Oh, H. J. Kim, M. H. Jung, and Y. G. Ko, "Low temperature conduction and scattering behavior of Ga-doped ZnO," *Appl. Phys. Lett.*, vol. **91**, no. 25, pp. 252109, 2007.

[29] J. H. Kim, B. Du Ahn, C. H. Lee, K. A. Jeon, H. S. Kang, and S. Y. Lee, "Effect of rapid thermal annealing on electrical and optical properties of Ga doped ZnO thin films prepared at room temperature," *J. Appl. Phys.*, vol. **100**, no. 11, pp. 113515, 2006.

[30] S. Dhara and P. K. Giri, "Stable p-type conductivity and enhanced photoconductivity from nitrogen-doped annealed ZnO thin film," *Thin Solid Films*, vol. **520**, no. 15, pp. 5000–5006, 2012.

[31] A. Tsukazaki, A. Ohtomo, T. Onuma, M. Ohtani, T. Makino, M. Sumiya, K. Ohtani, S. F. Chichibu, S. Fuke, Y. Segawa, H. Ohno, H. Koinuma, and M. Kawasaki, "Repeated temperature modulation epitaxy for p-type doping and light-emitting diode based on ZnO," *Nat. Mater.*, vol. **4**, no. 1, pp. 42–46, 2004.

[32] P. Sharma, A. Gupta, K. V Rao, F. J. Owens, R. Sharma, R. Ahuja, J. M. O. Guillen, B. Johansson, and G. a Gehring, "Ferromagnetism above room temperature in bulk and transparent thin films of Mn-doped ZnO," *Nat. Mater.*, vol. **2**, no. 10, pp. 673–7, 2003.

[33] F. Pan, C. Song, X. J. Liu, Y. C. Yang, and F. Zeng, “Ferromagnetism and possible application in spintronics of transition-metal-doped ZnO films,” *Mater. Sci. Eng. R Reports*, vol. **62**, no. 1, pp. 1–35, 2008.

[34] J.-H. Lee, K.-H. Ko, and B.-O. Park, “Electrical and optical properties of ZnO transparent conducting films by the sol–gel method,” *J. Cryst. Growth*, vol. **247**, no. 1–2, pp. 119–125, 2003.

[35] R. E. Marotti, C. D. Bojorge, E. Broitman, H. R. Cánepa, J. a. Badán, E. a. Dalchiele, and a. J. Gellman, “Characterization of ZnO and ZnO:Al thin films deposited by the sol–gel dip-coating technique,” *Thin Solid Films*, vol. **517**, no. 3, pp. 1077–1080, 2008.

[36] M. Purica, E. Budianu, E. Rusu, M. Danila, and R. Gavrila, “Optical and structural investigation of ZnO thin films prepared by chemical vapor deposition (CVD),” *Thin Solid Films*, vol. **404**, pp. 485–488, 2002.

[37] J. L. Yang, S. J. An, W. I. Park, G.-C. Yi, and W. Choi, “Photocatalysis Using ZnO Thin Films and Nanoneedles Grown by Metal-Organic Chemical Vapor Deposition,” *Adv. Mater.*, vol. **16**, no. 18, pp. 1661–1664, 2004.

[38] E. Millon, O. Albert, J. C. Loulergue, J. Etchepare, D. Hulin, W. Seiler, and J. Perrière, “Growth of heteroepitaxial ZnO thin films by femtosecond pulsed-laser deposition,” *J. Appl. Phys.*, vol. **88**, no. 11, pp. 6937, 2000.

[39] F. Claeyssens, C. L. Freeman, N. L. Allan, Y. Sun, M. N. R. Ashfold, and J. H. Harding, “Growth of ZnO thin films-experiment and theory,” *J. Mater. Chem.*, vol. **15**, no. 1, pp. 139, 2005.

[40] S. Youssef, P. Combette, J. Podlecki, R. Al Asmar, and a. Foucaran, “Structural and Optical Characterization of ZnO Thin Films Deposited by Reactive rf Magnetron Sputtering,” *Cryst. Growth Des.*, vol. **9**, no. 2, pp. 1088–1094, 2009.

[41] W.-J. Yang, C.-C. Tsao, C.-Y. Hsu, H.-C. Chang, C.-P. Chou, and J.-Y. Kao, "Fabrication and Characterization of Transparent Conductive ZnO:Al Thin Films Deposited on Polyethylene Terephthalate Substrates," *J. Am. Ceram. Soc.*, vol. **95**, no. 7, pp. 2140–2147, 2012.

[42] M. Subramanian, M. Tanemura, T. Hihara, V. Ganesan, T. Soga, and T. Jimbo, "Magnetic anisotropy in nanocrystalline Co-doped ZnO thin films," *Chem. Phys. Lett.*, vol. **487**, no. 1–3, pp. 97–100, 2010.

[43] Y. W. Zhu, H. Z. Zhang, X. C. Sun, S. Q. Feng, J. Xu, Q. Zhao, B. Xiang, R. M. Wang, and D. P. Yu, "Efficient field emission from ZnO nanoneedle arrays," *Appl. Phys. Lett.*, vol. **83**, no. 1, pp. 144, 2003.

[44] L. Wei, X. Zhang, and Z. Zuoya, "Application of ZnO nanopins as field emitters in a field-emission-display device," *J. Vac. Sci. Technol. B Microelectron. Nanom. Struct.*, vol. **25**, no. 2, pp. 608, 2007.

[45] X. Qian, H. Liu, Y. Guo, Y. Song, and Y. Li, "Effect of Aspect Ratio on Field Emission Properties of ZnO Nanorod Arrays," *Nanoscale Res. Lett.*, vol. **3**, no. 8, pp. 303–7, 2008.

[46] D. Banerjee, S. H. Jo, and Z. F. Ren, "Enhanced Field Emission of ZnO Nanowires," *Adv. Mater.*, vol. **16**, no. 22, pp. 2028–2032, 2004.

[47] Y. Sun, K. E. Addison, and M. N. R. Ashfold, "Growth of arrays of Al-doped ZnO nanocones by pulsed laser deposition," *Nanotechnology*, vol. **18**, pp. 495601, 2007.

CHAPTER 3

Methodology and Characterizations

3.1 Introduction

This chapter will introduce radio frequency (RF) sputtering, ion beam irradiation and field emission technique which has been chosen as the method to fabricate ZnO thin films, ZnO nanostructured films and field emission display, respectively. The analysis method for samples characterizations are also being explained in this chapter. Samples were fabricated on glass and arylite substrate.

3.2 Preparation for ZnO thin film

ZnO thin films were deposited using an RF magnetron sputtering machine (ANELVA SPF-210HS). The machine is known as RF sputter machine as it use RF power as the source to generate plasma in the vacuum chamber. The schematic diagram of the magnetron sputter system is shown in Fig. 3-1.

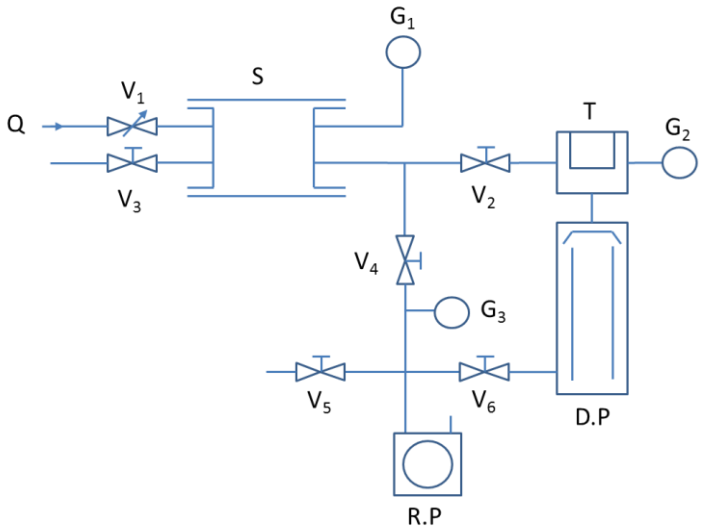

Figure 3-1: Schematic diagram of RF sputtering system

The sputtering machine has only one small chamber (S) with a single target. The size of chamber is 200 mm in diameter and 160 mm in height. ZnO ceramic with a purity of 99.99% and 101.6 mm in diameter was used as the target. The anode (substrate) and cathode (target) is fixed in parallel configuration with a distance of 5 cm between both electrodes as shown in Fig. 3-2.

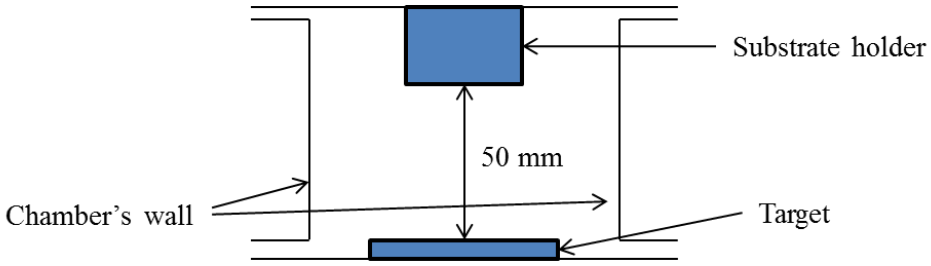

Figure 3-2: Schematic diagram of RF sputtering chamber

To load a sample inside the chamber, the chamber was vent by opening chamber vent valve (V3). Once the sample has been loaded into the chamber, it was then evacuated for 10 min to get for a rough vacuum (< 15 Pa). The low vacuum is to ensure that there are no outside particles that can contribute to contaminate the substrate which can result on producing a poor thin film. Besides that, it also helps for the diffusion pump to operate since

it cannot exhaust against atmospheric pressure. Next, to produce high vacuum level in the system, the foreline valve (V6) was opened and closed the rough valve (V4). The oil diffusion pump use silicon oil to be heated and produce evaporated oil vapor with high speed which moves to the jet stack. The evaporated oil vapor, collide with gas molecules and giving them moves downward direction to the foreline and pulled by rotary pump. Unlike using turbo pump, this chamber takes about 2 hours to reach high vacuum level with a background pressure of 3×10^{-5} Pa. Liquid nitrogen was used as the cold trap (T) to make oil molecules condense at the cooler wall and flow back to the oil pool.

Before sample deposition, the target was cleaned by pre-sputtering process for 10 min while keeping the shutter closed. The deposition rate can be calculated by using equation (1) as shown below

$$\text{Deposition rate} = \frac{\text{Film thickness (nm)}}{\text{deposition time (min)}} \quad (1)$$

3.3 Co-sputtering technique

Since there is only a single target source in this sputtering system, a doping process is done by placing any dopant materials on the ZnO target. This technique is known as co-sputtering technique. The targets were sputtered simultaneously during the deposition time. Figure 3-3(a) shows the top view of ZnO target that consist a permanent magnet located at below of the ZnO target. There are two permanent magnets, one is at center and another is at around the target. Figure 3-3(b) shows the high erosion area at where the magnetic flux exists. Before sample deposition, dopant material was placed at center position and at the high erosion area on the ZnO target. The effect of electrical and optical properties on ZnO thin films was investigated from the results obtained.

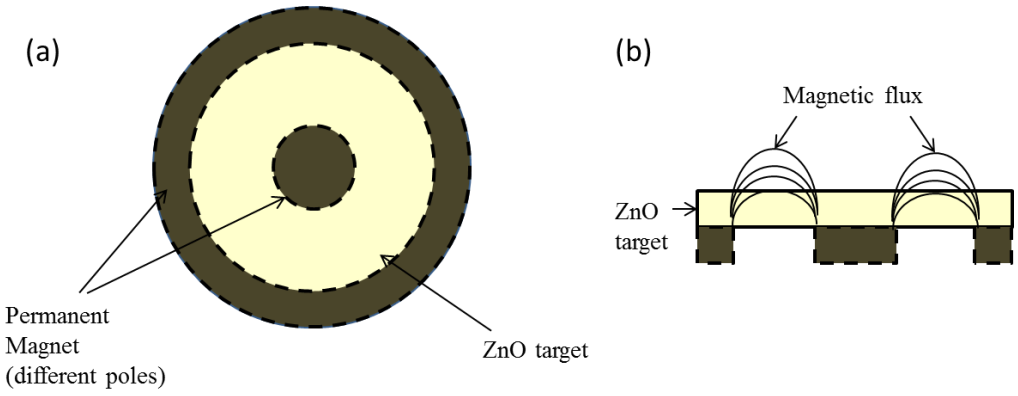

Figure 3-3: (a) Top and (b) side view of ZnO target

3.4 Preparation of nanostructured ZnO film

Fabrication of nanostructured ZnO films were done by ion beam irradiation technique at room temperature. This technique was found can induced conical protrusions and CNFs even at room temperature [1]. The same technique was applied for ZnO thin films. Argon gas was introduced in the chamber to produce ions which were accelerating to irradiate a sample and form nanostructures morphology. Before ion-irradiation, a thin layer of carbon was coated on the substrate to enhance surface diffusion during Ar^+ sputtering. The samples were ion-irradiated by a Kaufman-type ion gun. The acceleration of ions is depending on the given acceleration voltage. The basal and working pressures were 3×10^{-5} Pa and 2×10^{-2} Pa, respectively.

Figure 3-4 shows the incident angle of substrate from the normal to the surface. Ion incident angle can vary from 0 – 180˚. As shown in Fig. 3-4, if the substrate stage is moving towards in line with the beam source, it will give a larger incident angle (> 45˚). In another hand, moving the stage towards perpendicular with the beam source will give a smaller incident angle (< 45˚). Oblique Ar^+ bombardment seems to have the highest sputtering yield [2] as shown in Figure 3-5 and may induced cones morphology on the sample at room temperature.

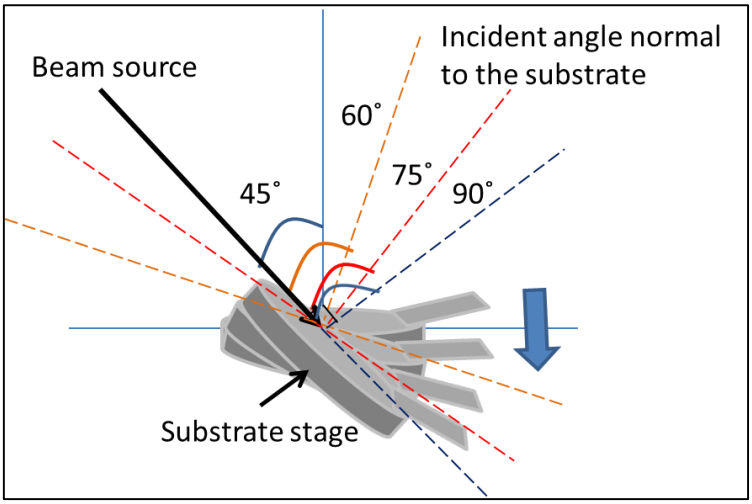

Figure 3-4: Schematic diagram of incident angle normal to the substrate

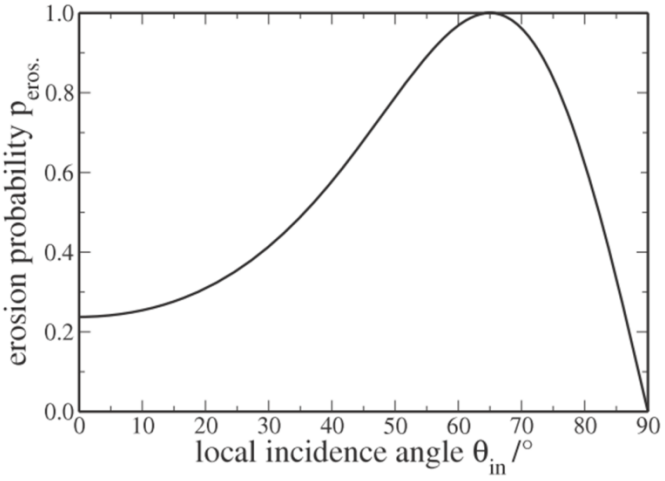

Figure 3-5: Sputtering yield curve

Sputtering yield can be calculated by using equation (2) as shown below.

$$Sputtering\ yield = \frac{Number\ of\ sputtered\ atoms}{Number\ of\ incident\ ions} \quad (2)$$

The amount of ion dose during irradiation process can be calculated by using equation (3) below.

$$\text{Ion dose} = \frac{\frac{Bem\ current\ (mA)}{1.6\ x\ 10^{-19}\ A/s} x\ irradiation\ time\ (s)}{Beam\ area\ (cm^2)} \quad (3)$$

3.5 Field Emission measurement

Field emission (FE) measurement was done to measure the efficiency of ZnO emitters and also to observe light emission from the thin film which act as a screen for field emission display (FED). A prototype of FED has been constructed as shown in Figure 3-6. Indium tin oxide (ITO) or ZnO thin film was used as the anode material (screen) while ZnO nanostructured film was used for the electron emitters (cathode). A layer of Teflon of 100 µm in thickness was used as the spacer. A current density was calculated thru an emission area of 2 x 5 mm (0.1 cm^2). High voltage was given to the anode material from 600 V up to 1500 V for ZnO emitters. The range of applied voltage supply can be lowered depends on the emission performance of the emitters such as carbon nanotubes (CNTs) or carbon nanofibers (CNFs).

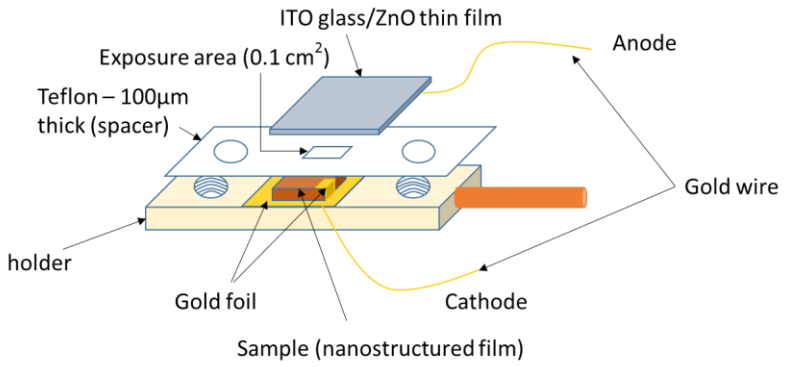

Figure 3-6: Schematic diagram of FED prototype

3.6 Electron emitters' efficiency

Geometrical structure of emitters plays an important role in producing high current density. Thus, during ion beam irradiation, all parameters that can change the morphological structure of thin film do needs an optimization. A good geometrical structure of emitters can

be defined by the value of field enhancement factor; β. β is equivalent to the emitter height divided by emitter tip radius. The larger the emitter tips, the lower the β and vice versa. If sharp tip of emitters can be achieved, high local electric field can be generated at the tips and decreased the FE barrier potential in which results in high FE current. FE was defined when strong electric field (i.e. high positive voltage) was applied at the surface of emitters which pulls the electrons out of the surface to a vacuum level due to an attraction of positive field. The stronger the electric field, the higher the electron emission. Field emission current exist when the emission current is exponentially increasing in a function of voltage [3]. It cannot be like a resistor where the current increase proportional with the voltage. The β can be calculated by using a Fowler-Nordheim (FN) Law which explains the quantum mechanics of tunneling electrons from the surface of the substance to the vacuum level. FN equation consists of work function of material, current and voltage of the field emission, and magnitude of electric field at the emitting surface as shown in equation (4).

$$\ln\left(\frac{J}{E^2}\right) = \ln\left(\frac{A\beta^2}{\Phi}\right) - \frac{B\Phi^{\frac{3}{2}}}{\beta E} \quad (4)$$

Where, J is current density (A/cm2), E is electric field (V/μm), A and B are constants with values of 1.54 x 10^{-6} A eV V^{-2} and 6.83 x 10^{-3} $eV^{-3/2}$ V μm^{-1}, respectively, Φ is the work function of material and β is the field enhancement factor [4]. In this experiment, the work function of ZnO was assumed as 5.3 eV. If a linear relation can be observed from the FN plot, it can be defined as the result of quantum tunneling. Otherwise, it may be due to some other physical phenomena such as thermal excitation or photoelectric effect which induced that emission current.

3.7 Sample characterizations and instrumentations

All samples were done for characterization in order to obtain for optimized properties of thin film and emitters that are suitable for FE display. The characterization techniques that was done throughout the experiment were explained in the following subchapter.

3.7.1 *Sheet resistance*

Sheet resistance can directly be measured using four point probe on the thin films surface without need any masking layer on the film. The width and length is equal as shown in Figure 3-7. Sheet resistance on thin film can only valid if the thickness of the thin film is less than probe spacing. If the thickness exceeds 0.1% than the probe spacing, it is known as bulk resistance. The objective to measure sheet resistance is to find the resistivity of the material and sheet resistance is depends on thin film thickness as shown in equation (5). The resistivity of the material will be the same regardless the geometrical size of the sample.

$$Rs = \frac{\rho}{d}(\Omega / sq) \tag{5}$$

Where d – thickness of the thin fillm (cm)

ρ - Resistivity of the material (Ω.cm)

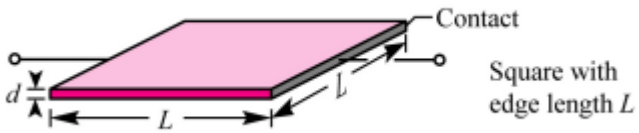

Figure 3-7: Sheet resistance measurement

Once the resistivity is known, the resistance of the sample can be calculated by using equation (6).

$$R = \frac{\rho}{t}\frac{L}{W} = \rho\frac{L}{A}(\Omega) \tag{6}$$

Where L – length

W – width

A – area (W x t)

T - thickness

Figure 3-8 shows the geometrical shape of resistance calculation.

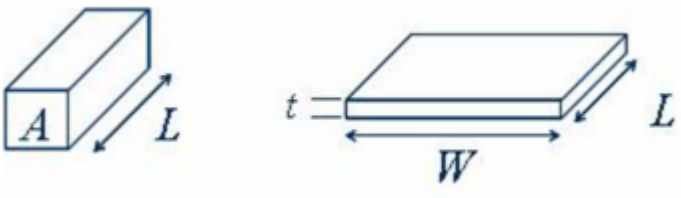

Figure 3-8: Resistance measurement

3.7.2 *Surface profiler*

Thickness of thin films can be measured by Dektak surface profiler and the average value of thickness was taken as the result of sample thickness in nanometer (nm).

3.7.3 *Scanning Electron Microscopy (SEM)*

Surface morphology of thin film, nanostructured film and the cross-section of the film are being measuring using SEM. The images were recorded in low and high magnification. SEM

is quite sensitive with non-conductive sample. The sample which is not conductive can easily get burned by the charging electron.

3.7.4 *UV-Vis Spectrometer*

The most important parameter need to be measured in this research work is the transmittance property of the thin film and nanostructured film. Ultraviolet-Visible (UV-Vis) spectrometer was used to measure the transparency in the visible wavelength from 300 nm to 800 nm.

3.7.5 *Atomic Force Microscopy (AFM)*

Roughness of thin film is measured by using AFM with a silicon cantilever. There are three types of roughness, arithmetic (Ra), root-mean square (Rq) and peak to valley roughness (Rt) as shown in Figure 3-9. Rt is the distance between the peak and valley, y_i is the height of an arbitrary point on the profile and $\bar{y}$ is the height of mid-line of the profile. Commonly, Rq value in nm is taken as the roughness of film surface. The value of Ra and Rq can be calculated using equation (7) and (8), respectively. A non-contact mode was used during the measurement. Besides the roughness of a thin film, thickness, 3D-view, homogeneity and size of nanostructure (i.e. height, diameter etc.) are also can be acquired by AFM measurement.

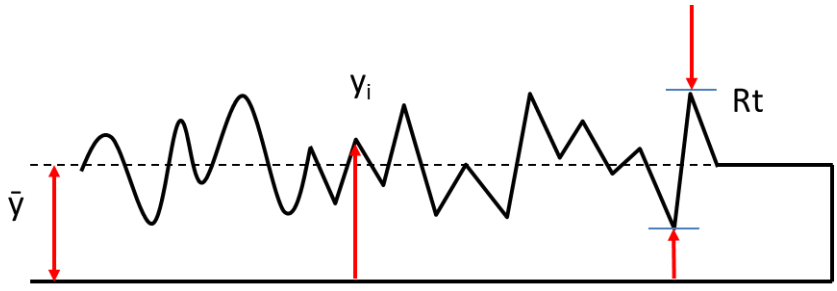

Figure 3-9: Definition of arithmetic, root mean square and peak to valley roughness in AFM measurement

$$\text{Ra} = \frac{1}{n}\sum_{i=1}^{n}|Yi - \bar{y}| \quad (7)$$

$$\text{Rq} = \sqrt{\frac{1}{n}\sum(yi - \bar{y})^2} \quad (8)$$

Where n is the number of data taken along the sampling length.

3.7.6 *X-Ray Diffraction (XRD)*

A crystallinity of deposited thin films can be analyzed from the XRD pattern. The crystallinity is depending on the crystal orientation of any materials that has been used in the film fabrication. ZnO was used as the material for thin film deposition in this experiment. Thus, a preferred orientation (002) at ~34.4˚ is indicating that the c-axis is perpendicular to the substrate. This peak was agreed with the standard in JCPDS (file no. 79=2205) for hexagonal wurtzite structure of ZnO.

3.7.7 *X-ray Photoelectron Spectroscopy (XPS)*

XPS which is also known as Electron Spectroscopy for Chemical Analysis (ESCA) is use to study the surface chemical on thin film. The XPS was used in order to measure the elemental compositions that exists within a material. XPS spectra are obtained when a beam of x-ray irradiate on a material surface and simultaneously measuring the kinetic energy and electrons that escape from the process of irradiation. This process is done in a very high vacuum condition.

3.7.8 *Raman Spectroscopy*

Raman spectroscopy is nondestructive measurement techniques that analyze chemicals for organic or inorganic sample. With Raman measurement, vibrational, rotational and other low frequency modes of molecules can be detected. A green laser at a wavelength of 532.08 nm was employed as the source of the incident light during Raman measurement. For ZnO sample, a peak at Raman shift in the range of 437 ~ 444 cm^{-1} is belongs to c-axis of wurtzite ZnO [5] . This peak is known as nonpolar phonon modes of Raman frequency, E_2 (high) which is associated with oxygen atoms. The study of Raman peaks and intensity had also revealed the defect formation in ZnO film.

3.8 References

[1] M. Tanemura and T. Okita, “Room-temperature growth of a carbon nanofiber on the tip of conical carbon protrusions,” *Appl. Phys. Lett.*, vol. **84**, no. 19, pp. 3831–3833, 2004.

[2] Q. Wei, K. Li, J. Lian, and L. Wang, “Angular dependence of sputtering yield of amorphous and polycrystalline materials,” *J. Phys. D. Appl. Phys.*, vol. **41**, pp. 172002, 2008.

[3] P. Rumbach and D. Go, “Fundamental properties of field emission-driven direct current microdischarges,” *J. Appl. Phys.*, vol. **112**, pp. 103302, 2012.

[4] D. Banerjee, S. H. Jo, and Z. F. Ren, “Enhanced Field Emission of ZnO Nanowires,” *Adv. Mater.*, vol. **16**, no. 22, pp. 2028–2032, 2004.

[5] K. a. Alim, V. a. Fonoberov, M. Shamsa, and A. a. Balandin, “Micro-Raman investigation of optical phonons in ZnO nanocrystals,” *J. Appl. Phys.*, vol. **97**, no. 12, pp. 124313, 2005.

CHAPTER 4

Fabrication of Nanostructured ZnO Films for Transparent Field Emission Displays

4.0 Introduction

Nanocarbons, such as carbon nanotubes (CNTs) and carbon nanofibers (CNFs), have been widely reported as promising materials for high-performance field emission (FE) devices owing to their high aspect ratio and low turn-on field [1-5]. However, the fabrication of a nanocarbon-based transparent and flexible FE devices is still challenging owing to their low transparency and high sheet resistance. If a highly transparent emitter material is available, are the transparent FE devices readily achievable? The answer is not so simple because of the difficulty specific to the FE phenomenon; the flat surface is suitable for transparency, but not for FE.

ZnO field emitters have also been reported [6-8]. Although they showed good FE properties, unfortunately they were not transparent owing to the visible light scattering by nanostructures [9,10]. In this chapter, the development of transparent FE emitters with good FE properties for transparent and conductive ZnO films with nanostructures induced by ion irradiation was reported.

4.1 Experimental Procedure

ZnO thin films were deposited on glass substrates for 30 min at 300 ˚C substrate temperature by RF magnetron sputtering, using a high-purity ZnO target (99.99%). Ar gas at a flow rate of 4.5 sccm was introduced into the chamber, and pressure was maintained at 0.5 Pa. RF power was kept constant at 100 W for the deposition of ZnO films.

The ZnO nanostructures were fabricated by the ion beam irradiation technique. The technique allows us to control the length and density of the nanostructures by optimizing the ion beam incident angle, beam current, and voltage. Ar^+ ion was irradiated on the ZnO thin film for 3 min at room temperature to fabricate the nanostructures. The ion incidence angles were 30˚, 45˚ and 60˚. The energy of the ion beam used was 600 eV at a working pressure of $5.0x10^{-2}$ Pa. The film thickness and sheet resistance before and after ion irradiation were measured using a surface profiler and 4-point probes, respectively. The surface morphology was characterized by SEM (JEOL JSM-5600). The crystallinity of the ZnO thin film before and after the fabrication of nanostructures was analyzed by X-ray diffraction (XRD; Rigaku Smartlab). The transparency of the films was measured using UV-vis spectrophotometer (Shimadzu UV-800). FE properties were measured with a parallel plate configuration at 3 $x10^{-4}$ Pa. In the FE measurements, an indium–tin oxide (ITO)-coated glass was used as the anode and the fabricated nanostructured ZnO film was used as the cathode. Current density was calculated at an emission area of 0.1 cm^2 and the gap distance between the anode and the cathode was 100 μm.

4.2 Results and Discussion

The thickness of ZnO thin films was 1.2 μm and the obtained average sheet resistance was about 186 Ω/□. After the ion irradiation, the sheet resistance slightly increased to 240-375 Ω/□, may be owing to the ion-induced defect formation. Figure 4-1 shows a SEM image of the as-deposited ZnO thin film on the glass substrate showing an almost flat surface. Figure 4-2 shows typical SEM images of the ZnO film surface after ion irradiation at 30° normal to the surface. Conical nanostructures can be observed throughout the surface of ZnO film. As seen in Fig. 4-2, the nanocones were 4-6 μm^{-2} in number density and about 180-250 nm in height. The SEM images also show that the nanocones were formed on top of the original ZnO thin films with the remaining bottom layer acting as the platform that connects the nanocones together and provides the path for electron transport.

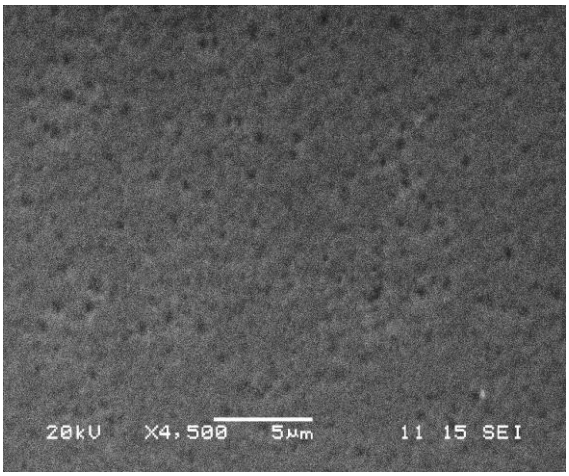

Figure 4-1: SEM image of as-deposited ZnO on glass substrate.

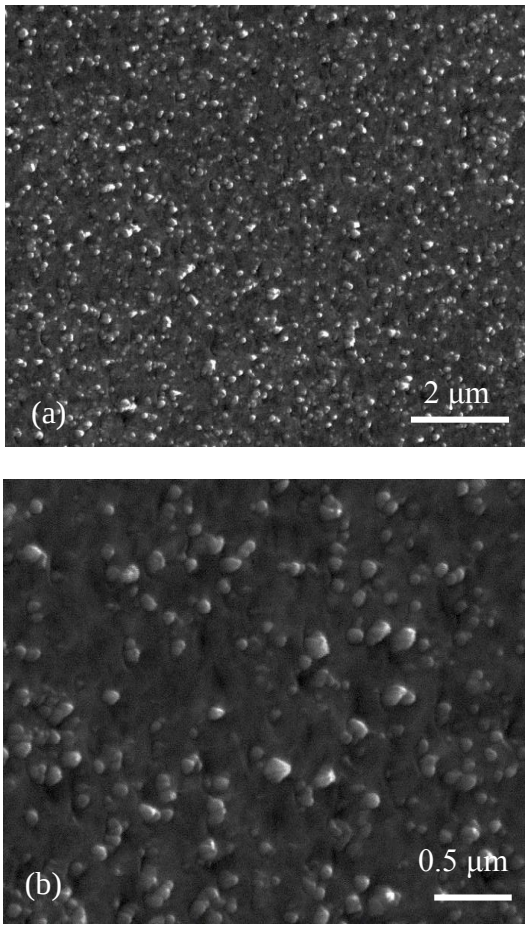

Figure 4-2: SEM images of ZnO nanocones fabricated by Ar^+ ion irradiation at ion-incidence angle of 30°. (a) Low- and (b) high-magnification SEM images.

The TEM image in Fig. 4-3 shows high crystalline quality of as-deposited ZnO thin film. The calculation by Bragg's Law equation as shown in equation (9) prove the thin film growth at preferable orientation of (002) along c-axis.

$$\lambda = 2\mathrm{d}\sin\theta \tag{9}$$

$$\sin\theta = \frac{\lambda}{2d}$$

$$= \frac{1.5402\mathrm{x}10^{-10}}{2(0.26\,nm)}$$

$$= 0.296$$

$$\theta = 17.23°$$

$$\mathbf{2\theta = 34.46°\ (002)}$$

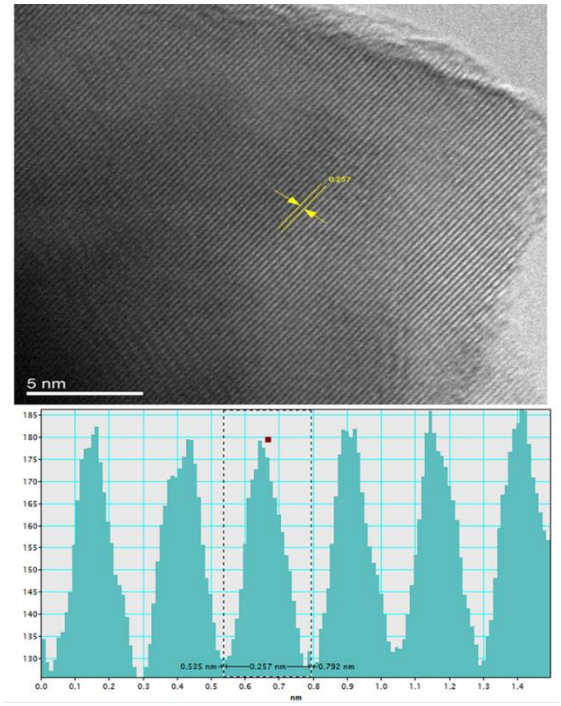

Figure 4-3: TEM image of ZnO thin film

Figure 4-4 shows the XRD patterns of as-deposited ZnO thin film, and nanostructured ZnO film irradiated at ion incidence angles of 30˚, and 45˚ were agreed with the result obtained from TEM measurement. All samples exhibited high crystalline quality at preferable growth along the c-axis orientation (002). The peak intensity of the ion-irradiated samples was slightly lower than that of the as-deposited ZnO film. This would be due to the decrease in ZnO thin film thickness during ion irradiation. Note that there was no significant change in the peak width or position. Thus, from the XRD patterns, it is revealed that the formation of ZnO nanocones did not seriously affect the crystalline quality of the ZnO thin films.

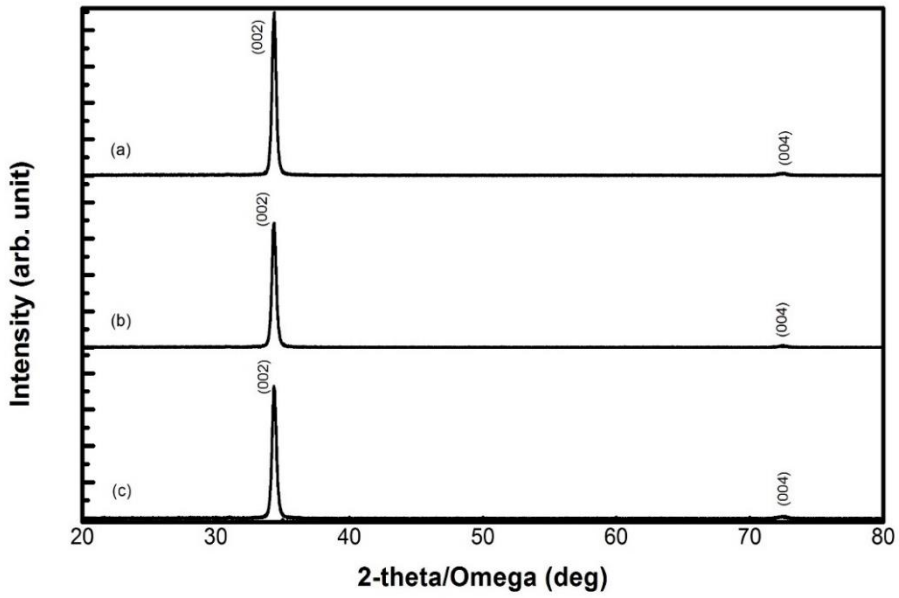

Figure 4-4: XRD patterns of (a) as-deposited ZnO film, and nanostructured ZnO film ion-irradiated at ion-incidence angles of (b) 30˚and (c) 45˚.

The transmittance of the as-deposited ZnO films showed a high transparency of about 90% at a wavelength of 550 nm. After the ion irradiation, the transmittance remained very high, about 85%, for the sample shown in Fig. 4-2. A key factor is the size of the nanocones. Light scattering occurs at the interface where refractive index changes abruptly, namely, at the surface of the ZnO film in this study. For a rough surface, the wavelength region of light scattering is known to strongly depend on the roughness of the surface [11]. If the roughness is smaller than the wavelength in the visible light region, the refractive index in the visible light region changes gradually; thus, no reflection occurs, and hence, the transparency in the visible light region is achievable. For good FE performance, a rough surface is necessary, as mentioned above. In fact, no field emission current was attained up to 15 V μm^{-1} for the as-deposited flat ZnO film in the present study. Therefore, conducting materials with surface nanocones smaller than the wavelength of visible light will be the answer for transparent field emitters.

On the basis of the above concept, the FE properties of the nanostructured ZnO films thus prepared was measured. ZnO is suitable for this purpose, because ZnO nanocones are known to provide high FE current as their sharp tips could accelerate electrons better than other forms of nanostructures [12-15]. Figure 4-5 shows the FE property of the ZnO nanocones shown in Fig. 4-2. By applying voltage at the anode material (ITO glass), the electric field required to obtain a current density of 1 μA cm^{-2} was achieved at 8 V μm^{-1} and the achievable current density was 1.14 μA cm^{-2} at 10 V μm^{-1}.

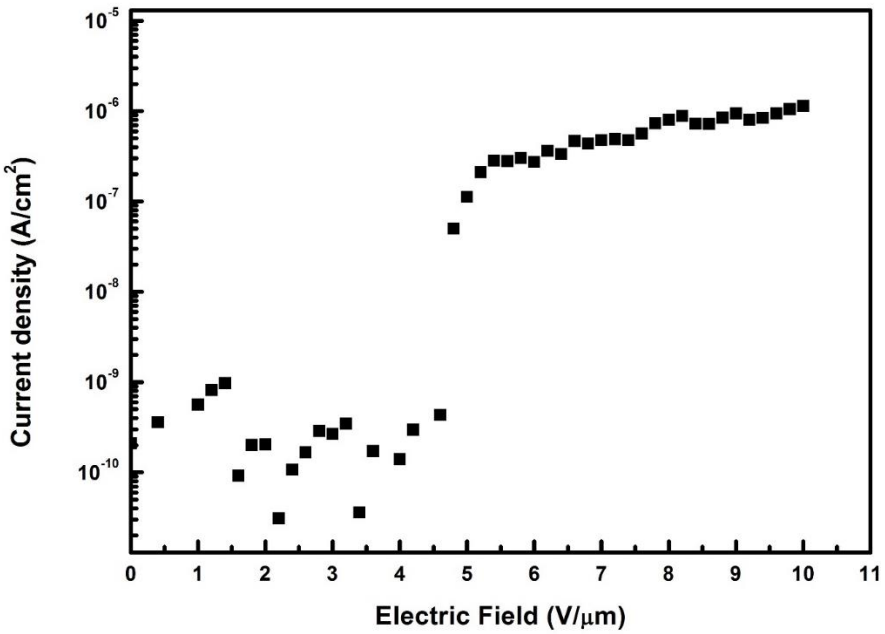

Figure 4-5: Field emission property of ZnO nanocones irradiated at ion-incidence angle of 30˚.

The size and number density of ZnO nanostructures are the key factors in generating high FE properties. To achieve better FE properties, conical nanostructures with larger size and higher number density than those shown in Fig. 4-2 were fabricated. A typical example is shown in Fig. 4-6. The ion beam parameters employed were identical to those shown in Fig. 4-2 except for the ion incidence angle, 45˚, normal to the surface. As seen in Fig. 4-6, the size and number density of nanocones were 200-400 nm and 6-8 μm^{-2}, respectively. Owing to the nanocones being smaller than the wavelength of visible light, transmittance was kept high enough, about 86% at a wavelength of 550 nm.

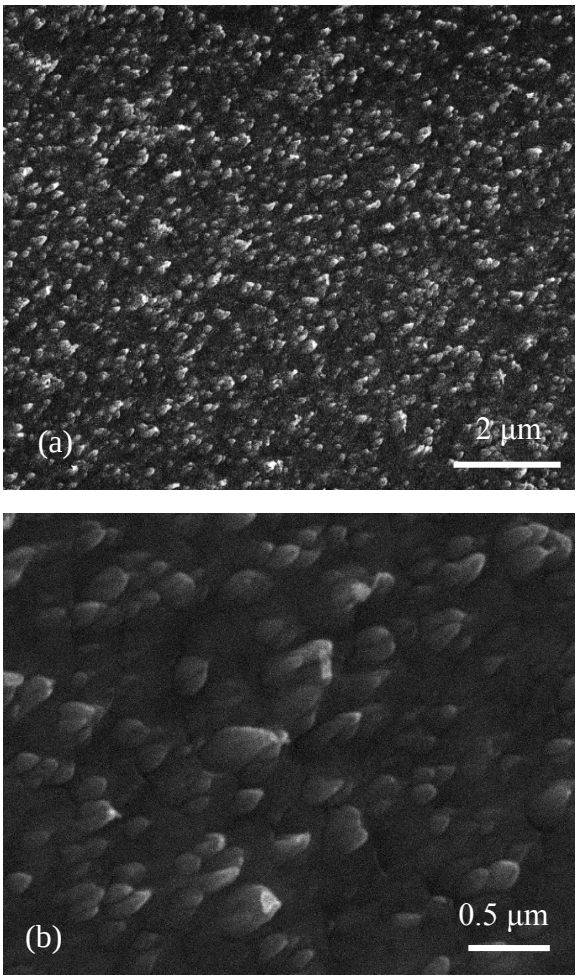

Figure 4-6: SEM images of ZnO nanocones fabricated by Ar+ ion irradiation at ion-incidence angle of 45˚. (a) Low- and (b) high-magnification SEM images.

Figure 4-7 shows the FE properties of the ZnO nanocones, disclosing that the electric field required to obtain a current density of 1 μA cm^{-2} was achieved at 6.2 V μm^{-1}. The current density continuously increased to more than $2x10^{-5}$ A cm^{-2}, as observed at 10 V μm^{-1}. The inset figure shows a current-voltage (I-V) plot that has been converted to a Fowler-Nordheim (FN) plot by expressing ln (I/E^2) vs 1/E. The FN plot exhibits a linear behavior, which is in agreement with the typical FN equation as shown in chapter 3. Work function for ZnO field emitters is assumed to be 5.3 eV [16,17]. β is the field enhancement factor, which can be calculated from the slope of the linear line of the FN plot. The β calculated from the inset figure is 2252, which is high enough for field-emission applications and comparable to those of other types of ZnO nanostructure [18-20].

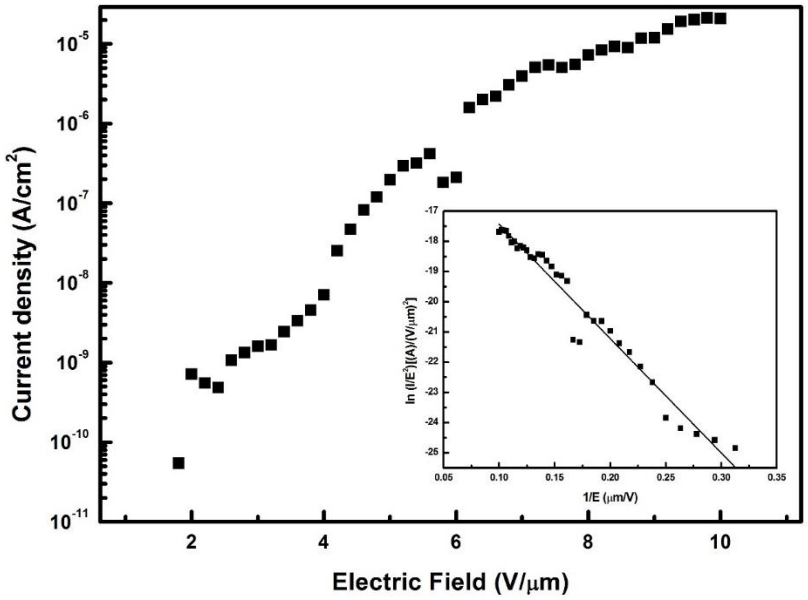

Figure 4-7: Field emission property of ZnO nanocones irradiated at ion-incidence angle of 45°. The inset figure is the corresponding FN plot.

A better surface morphology in terms of the nanocones shape was obtained when the ion incident angle was increased at 60°. The nanocones structures showed 7-10 μm^{-2} in number density with height in about 400 nm. Nanocones tips fabricated at 60° is the sharpest compared to 30° and 45° as shown in Fig.4-8. The transmittance of the nanocones film was achieved about 80% at a wavelength of 550 nm.

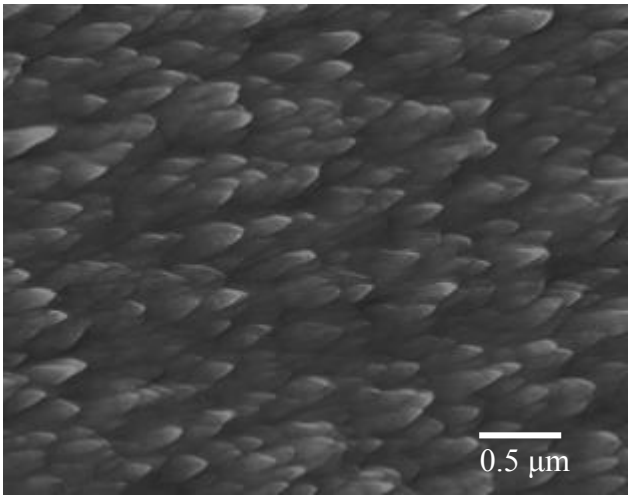

Figure 4-8: SEM image of ZnO nanocones fabricated by Ar$^+$ ion irradiation at ion-incidence angle of 60°

Figure 4-9 shows the FE properties of nanocones at ion-incident angle of 60˚. The electric field required to obtain a current density of 1 μA cm^{-2} was achieved at 4.3 V μm^{-1} which is the lowest among the other two ion-incident angles. The current density continuously increased to more than $6.5x10^{-5}$ A cm^{-2}, as observed at 10 V μm^{-1}. Larger value of β was obtained with the sharp tips of the nanocones. The calculated β from the inset figure is 3333.

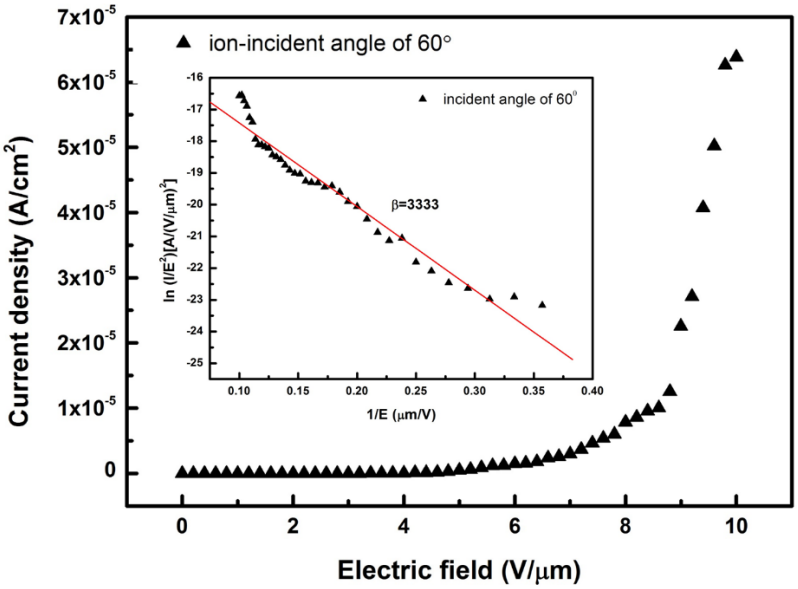

Figure 4-9: Field emission property of ZnO nanocones irradiated at ion-incidence angle of 60˚. The inset figure is the corresponding FN plot.

This simple and cost-effective fabrication technique is comparable to nontransparent techniques that used Au as the catalyst or silicon as the substrate. The highly transparent nanostructured ZnO film fabricated without a catalyst exhibited a large field enhancement factor and a high field emission current. The simple technique of forming ZnO nanocones at room temperature is believed to drive the fabrication of upcoming transparent ZnO FE devices on flexible substrates.

4.3 Conclusions

A highly transparent and conductive field emitter with high field emission properties was achieved on highly transparent and conductive ZnO thin films. For as-deposited flat ZnO films, no field emission current was obtained. The transmittance of the as-deposited ZnO films of 90% remained very high, about 80%, after the ion irradiation. The heights of the ZnO nanocones were about 400 nm for an ion-incident angle of 60˚. The size of ZnO nanocones being smaller than the wavelength of visible light was the key factor for maintaining the high transmittance. The ZnO nanocones induced at an ion-incidence angle of 60˚ exhibited better field emission properties owing to their larger size and the higher number density than those induced at 30˚ and 45˚. The electric field required to obtain a current density of 1 μA cm^{-2} was achieved at 4.3 V μm^{-1}, and a large field enhancement factor of 3333 was calculated from the FN plot. The field emission properties of transparent nanoconed ZnO were comparable to those of other nontransparent nanostructured ZnO. Thus, it is believed that nanoconed ZnO films are promising transparent field emitters for FE devices.

4.4 References

[1] H. J. Jeong, H. D. Jeong, H. Y. Kim, J. S. Kim, S. Y. Jeong, J. T. Han, D. S. Bang, and G.-W. Lee, "All-Carbon Nanotube-Based Flexible Field-Emission Devices: From Cathode to Anode," *Adv. Funct. Mater.*, vol. **21**, no. 8, pp. 1526–1532, 2011.

[2] P. Ghosh, M. Z. Yusop, S. Satoh, M. Subramanian, A. Hayashi, Y. Hayashi, and M. Tanemura, "Transparent and flexible field electron emitters based on the conical nanocarbon structures.," *J. Am. Chem. Soc.*, vol. **132**, no. 12, pp. 4034–5, 2010.

[3] H. S. Sim, S. P. Lau, L. K. Ang, G. F. You, M. Tanemura, K. Yamaguchi, M. Zamri, and M. Yusop, "Field emission from a single carbon nanofiber at sub 100 nm gap," *Appl. Phys. Lett.*, vol. **93**, no. 2, pp. 023131, 2008.

[4] D. Ghosh, P. Ghosh, M. Tanemura, A. Haysahi, Y. Hayashi, K. Shinji, N. Miura, M. Z. Yusop, and T. Asaka, "Highly transparent and flexible field emission devices based on single-walled carbon nanotube films.," *Chem. Commun. (Camb).*, vol. **47**, no. 17, pp. 4980–2, 2011.

[5] P. Ghosh, M. Zamri, D. Ghosh, T. Soga, T. Jimbo, S. Hashimoto, S. Ohashi, and M. Tanemura, "Improvement in Field Electron Emission Performance of Natural-Precursor-Grown Carbon Nanofibers by Thermal Annealing in Argon Atmosphere," *Jpn. J. Appl. Phys.*, vol. **50**, pp. 01AF09, 2011.

[6] J. Song, S. a. Kulinich, J. Yan, Z. Li, J. He, C. Kan, and H. Zeng, "Epitaxial ZnO nanowire-on-nanoplate structures as efficient and transferable field emitters," *Adv. Mater.*, vol. **25**, pp. 5750–5755, 2013.

[7] C. Li, C. Li, Y. Di, W. Lei, J. Chen, and Y. Cui, “ZnO Electron Field Emitters on Three-Dimensional Patterned Carbon Nanotube Framework,” *ACS Appl. Mater. Interfaces*, vol. **5**, pp. 9194–9198, 2013.

[8] Z. Zhang, G. Meng, Q. Xu, Y. Hu, Q. Wu, and Z. Hu, “Aligned ZnO nanorods with tunable size and field emission on native si substrate achieved via simple electrodeposition,” *J. Phys. Chem. C*, vol. **114**, pp. 189–193, 2010.

[9] Z. Zhang, G. Meng, Q. Wu, Z. Hu, J. Chen, Q. Xu, and F. Zhou, “Enhanced Cold Field Emission of Large-area Arrays of Vertically Aligned ZnO-nanotapers via Sharpening: Experiment and Theory.,” *Sci. Rep.*, vol. **4**, pp. 4676, 2014.

[10] X. Fan, W. Zheng, and D. J. Singh, “Light scattering and surface plasmons on small spherical particles,” *Light Sci. Appl.*, vol. **3**, pp. e179, 2014.

[11] P. Ghosh, S. Satou, T. Tsuchiya, Y. Hayashi, and M. Tanemura, “Controllable fabrication and characterization of conical nanocarbon structures on polymer substrate for transparent and flexible field emission displays,” *Phys. status solidi - Rapid Res. Lett.*, vol. **6**, no. 4, pp. 184–186, 2012.

[12] C. Ye, Y. Bando, X. Fang, G. Shen, and D. Golberg, “Enhanced Field Emission Performance of ZnO Nanorods by Two Alternative Approaches,” *J. Phys. Chem. C*, vol. **111**, no. 34, pp. 12673–12676, 2007.

[13] L. Wei, X. Zhang, and Z. Zuoya, “Application of ZnO nanopins as field emitters in a field-emission-display device,” *J. Vac. Sci. Technol. B Microelectron. Nanom. Struct.*, vol. **25**, no. 2, pp. 608, 2007.

[14] J. Bae, J.-I. Hong, W. H. Han, Y. J. Choi, and R. L. Snyder, “Superior field emission properties of ZnO nanocones synthesized by pulsed laser deposition,” *Chem. Phys. Lett.*, vol. **475**, no. 4–6, pp. 260–263, 2009.

[15] X. Fang, Y. Bando, U. K. Gautam, C. Ye, and D. Golberg, “Inorganic semiconductor nanostructures and their field-emission applications,” *J. Mater. Chem.*, vol. **18**, no. 5, pp. 509, 2008.

[16] J. Singh, S. S. Patil, M. a. More, D. S. Joag, R. S. Tiwari, and O. N. Srivastava, “Formation of aligned ZnO nanorods on self-grown ZnO template and its enhanced field emission characteristics,” *Appl. Surf. Sci.*, vol. **256**, no. 21, pp. 6157–6163, 2010.

[17] Y. K. Tseng, C. J. Huang, H. M. Cheng, I. N. Lin, K. S. Liu, and I. C. Chen, “Characterization and Field-Emission Properties of Needle-like Zinc Oxide Nanowires Grown Vertically on Conductive Zinc Oxide Films,” *Adv. Funct. Mater.*, vol. **13**, no. 10, pp. 811–814, 2003.

[18] D. Banerjee, S. H. Jo, and Z. F. Ren, “Enhanced Field Emission of ZnO Nanowires,” *Adv. Mater.*, vol. **16**, no. 22, pp. 2028–2032, 2004.

[19] F. Xu, K. Yu, G. Li, Q. Li, and Z. Zhu, “Synthesis and field emission of four kinds of ZnO nanostructures: nanosleeve-fishes, radial nanowire arrays, nanocombs and nanoflowers,” *Nanotechnology*, vol. **17**, no. 12, pp. 2855–2859, 2006.

[20] C. X. Xu and X. W. Sun, “Field emission from zinc oxide nanopins,” *Appl. Phys. Lett.*, vol. **83**, no. 18, pp. 3806, 2003.

CHAPTER 5

Effect of surface morphology on the field emission property for ZnO films

5.0 Introduction

In the previous work, highly transparent ZnO nanocone as field emitters on glass substrate and owned large field enhancement factor was successfully fabricated [1]. Many efforts have been reported to achieve high aspect ratio and large field enhancement factor in order to obtain low turn-on electric field with high emission current [2-5]. However, only few efforts have been devoted to study the morphological change of field emitters due to the stability test [6,7]. For a better performance of FE devices, the stability of the emitters is an important criterion [8]. Unintentional heating of the cathodes (field emitter) during field emission process as the transport of electrons, may possible to change the ZnO emitters' morphology. Joule heating may be serious due to a small cross section area of emitter tips [9,10]. Nevertheless, owing to a high thermal stability of ZnO material, it will be expected that ZnO field emitter may sustain high field emission property during field emission measurement even for a longer duration. Thus, in what follows, one hour stability test was done and the surface morphology of ZnO field emitters and field emission properties was investigated in detail.

5.1 Experimental Details

5.1.1 *Sample preparations*

ZnO thin film was deposited on glass substrate by RF sputtering at substrate temperature of 300˚C for 30 minutes. Argon gas at a flow rate of 4.5 sccm was introduced into the chamber and the RF power was kept constant at 100W during the deposition of ZnO film. The base pressure was 3 x 10^{-5} Pa and the working pressure was maintained at 0.5 Pa during sample deposition. ZnO nanostructure was induced onto the ZnO films by Ar^{+} during ion beam irradiation in 3 min at room temperature. After the 3 min irradiation, ZnO nanocones of 200-400 nm in length were formed. Ion beam current and voltage was maintained at 6 mA and 600 eV, respectively during the irradiation.

5.1.2 *Sample Characterizations*

Morphology of ZnO films was observed by SEM (JEOL JSM-5600). Sheet resistance of ZnO thin film was measured using four point probes and film thickness was determined using a surface profiler. The crystalline quality of ZnO film was analysed by X-ray diffraction (XRD; Rigaku Smartlab) patterns. For field emission measurement, a parallel plate configuration was used in a vacuum condition with pressure at 3 x 10^{-4} Pa. Indium-tin oxide (ITO)-coated glass was used as the anode and ZnO nanocones as the field emitter (cathode). A Teflon sheet 100 μm in thickness was used as the spacer between anode and cathode. Current density was calculated at an emission area of 0.1 cm^2. The emission current stability test was conducted continuously for one hour at constant electric field of 12 V/μm after the measurement of the initial FE property.

5.2 Result and Discussion

Figure 5-1(a) shows a flat surface morphology of an as-deposited ZnO thin film. The thickness of ZnO thin film was 1.3 μm and a high transparency of 86% at a visible wavelength of 550 nm was obtained. The ZnO thin film shows high crystalline quality as the dominant peak of the XRD pattern was at (002) c-axis orientation. As was demonstrated in the previous chapter, the flat surface morphology of ZnO film did not show any electron emission. By contrast, ZnO nanocones was readily induced by Ar^+ after 3 min as shown in Figure 5-1(b). The density of ZnO nanocones calculated from the SEM figure was about 8-15 μm^{-2} with irregular distance between one and another nanocones. The length of ZnO nanocones was 200-400 nm which is smaller than the wavelength of visible light and thus maintained the high transparency of ZnO film.

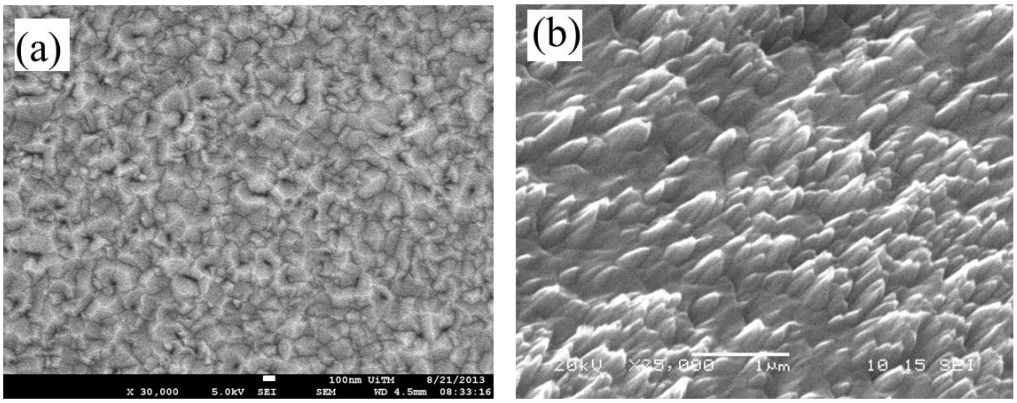

Figure 5-1: SEM images of (a) as-deposited ZnO thin film and (b) ZnO nanocones induced on the film surface by ion irradiation after 3 min.

Figure 5-2 shows the initial FE property of ZnO nanocones before the stability test. The current density of 1 μA cm^{-2} was achieved at 9.8 V/μm and the achievable current density was 15.7 μA cm^{-2} at 12 V/μm. The inset figure shows the FN plot which follows a linear behavior, indicating that the electron emission from ZnO nanocones was controlled by a barrier tunneling quantum-mechanical process, namely FE process. The calculated field

enhancement factor (β) from the slope of the linear line of the FN plot was 906. The β of ZnO nanocones in this work was better and comparable with other types of ZnO nanostructures such as ZnO nanowire by vapor phase growth (847) [11], ZnO-spheroid (699) [12], CNFs on polyimide (850) [13] and silicon emitters (455-700) [14,15]. The difference in β is due to the geometrical structure of field emitters which has been prepared in various methods. Fabricating nanocones field emitter would enhance the field emission compared to nanowire, nanorods and other blunt tips of nanostructures.

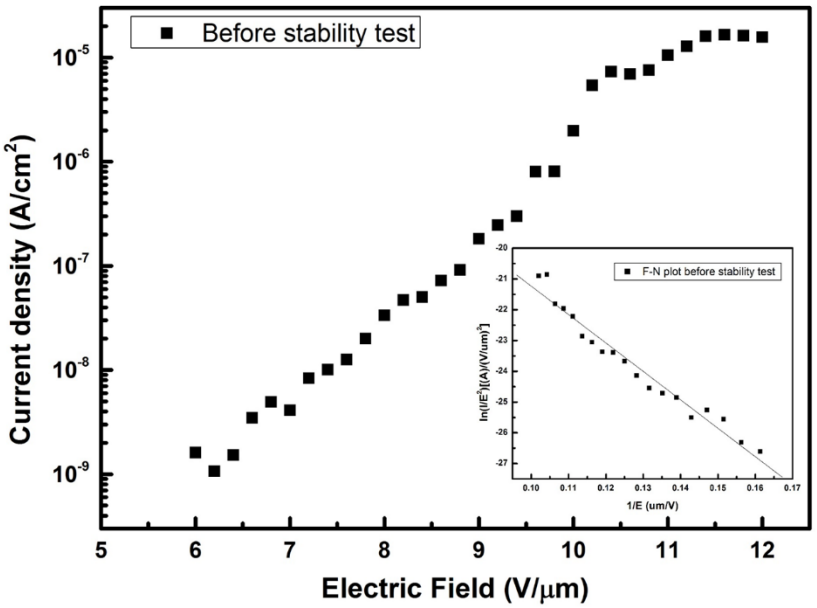

Figure 5-2: Initial FE property of ZnO nanocones before the stability test.

In order to study the FE performance of ZnO nanocones, a stability test was done for 60 min at fixed electric field of 12 V/μm. Figure 5-3 shows the emission current – time (I-T) plot during the stability test which reveals a high performance of ZnO nanocones as field emitters after the steep increase and decrease in emission current at the very initial stage (in 2 min) of the I-T test. No violent fluctuation in emission current can be seen after 2 min and the current gradually decreased from ~4.5 μA to ~2 μA.

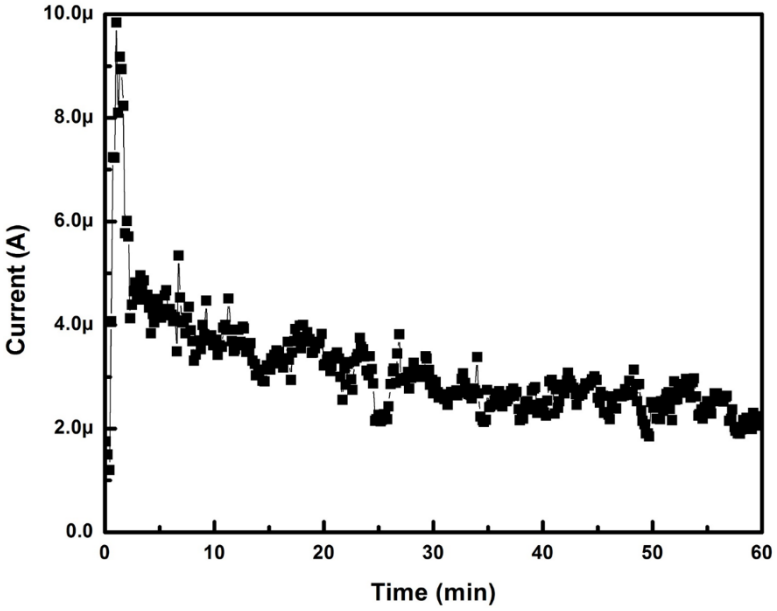

Figure 5-3: Stability test at electric field of 12 V/μm for 60 minutes in a vacuum condition.

Figure 5-4 shows the FE property of the ZnO nanocones after the stability test. The current density of 1 μA cm^{-2} was achieved at about 7.8 V/μm. The achievable current density of 26.3 μA cm^{-2} at 12 V/μm was higher than that before the stability test. However, the FN plot in the inset of Fig. 5-4 discloses two linear lines with different slope. The calculated values of β1 and β2 from the slopes for high and low electric fields were 2314 and 794, respectively. Despite the difference in β, the enhancement factor was still high compared to other types of nanostructures which have been stated above. The FE behavior would strongly depend on the morphological change of the emitter. Thus the detailed SEM observation was carried out.

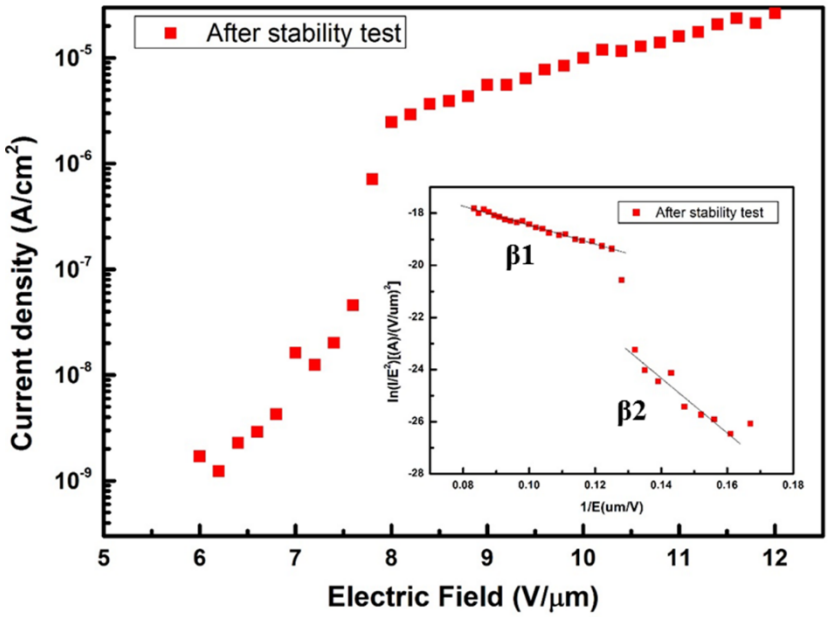

Figure 5-4: Field emission properties of ZnO nanocones after the stability test.

Figure 5-5 shows the surface morphology of ZnO nanocones at the emission area after the measurement of FE property shown in Fig. 5-4. In some part in the emission area nanocones seem to melt at the tip region. Inhomogeneous surface morphology of ZnO nanocones should result in a difference intensity of electric field on the tips of ZnO nanocones. The longer ZnO nanocones should possess higher intensity of electric field compared to the shorter ZnO nanocones. Thus, during the field emission, electrons would have a tendency to emit through an emitter with a higher electric field. Consequently, the resistance at the tips of the longer ZnO nanocones may increase due to Joule heating effect and the tips would have higher possibilities to be damaged or melt [16]. This drawback can be over-come if a homogeneous surface morphology can be fabricated [17]. However, as seen in Fig. 5-5, besides the melted ZnO nanocones, there would be still high number density of ZnO nanocones which are not being affected by the occurrences of local heat resistance and are accountable for the transport of electron emission after the stability test.

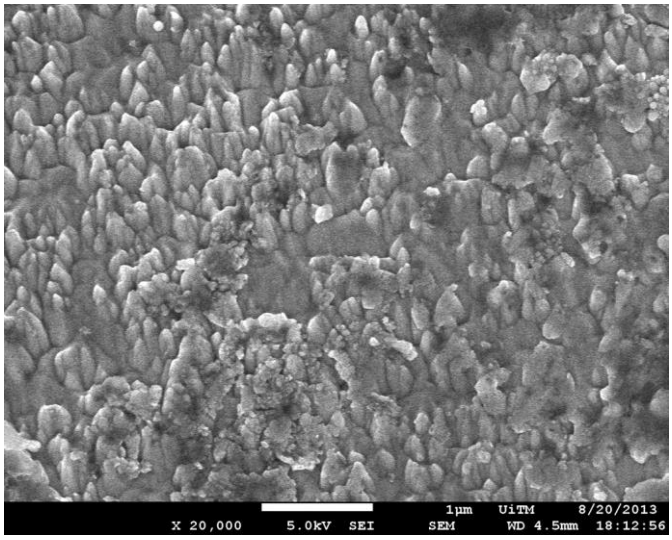

Figure 5-5: Surface morphology of ZnO nanocones at the emission area

Figure 5-6 shows the surface morphology of ZnO nanocones at out of the emission area. It can be observed that, the surface morphology was not being affected by the high electric field due to no electrons could emit at the tips of the field emitters. This area was covered by a teflon sheet which act as an insulator between the cathode and the anode.

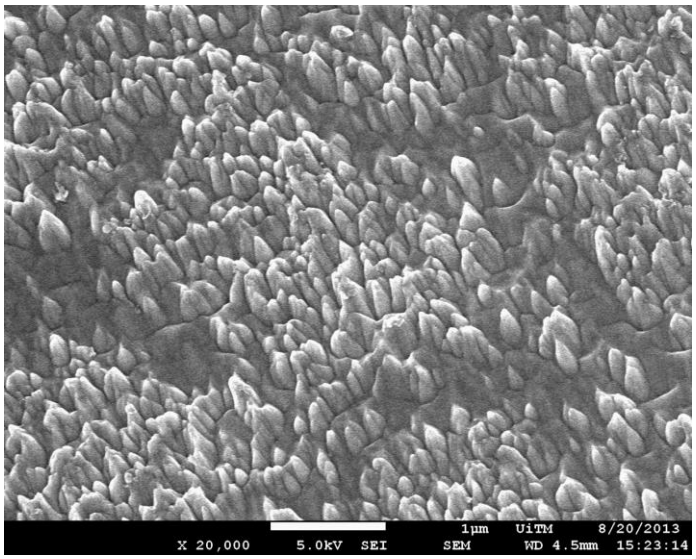

Figure 5-6: Surface morphology of ZnO nanocones at out of the emission area

5.3 Conclusion

In summary, with a simple ion beam irradiation in a very short time, ZnO nanocones field emitter was fabricated. From a view point of stability, ZnO can be a promising field emitter for transparent field emission device. As proven, ZnO nanocones were relatively tolerant against the high electric field of 12 V/μm. However, longer ZnO nanocones tip tended to melt due to local Joule heating induced by high emission current. In addition, inhomogeneous surface morphology also may be a factor of the melting tips at a longer nanocones. If homogeneous nanocones film and highly conductive of field emitter can be fabricated, this problem would be eliminated and would exhibit higher field emission current. ZnO nanocones are also comparable with other types of field emitters and even better in working with high thermal condition.

5.4 References

[1] Z. Zulkifli, S. Munisamy, M. Zamri, M. Yusop, G. Kalita, and M. Tanemura, "Fabrication of Nanostructured ZnO Films for Transparent Field Emission Displays Fabrication of Nanostructured ZnO Films for Transparent Field Emission Displays," *Jpn. J. Appl. Phys.*, vol. **52**, pp. 11NJ07, 2013.

[2] E. Le Shim, J. Bae, E. Yoo, C. Kang, and Y. J. Choi, "Large Enhancement of Field Emission from ZnO Nanocone Arrays via Patterning Process," *Jpn. J. Appl. Phys.*, vol. **49**, no. 11, pp. 115001, 2010.

[3] J. Bae, J.-I. Hong, W. H. Han, Y. J. Choi, and R. L. Snyder, "Superior field emission properties of ZnO nanocones synthesized by pulsed laser deposition," *Chem. Phys. Lett.*, vol. **475**, no. 4–6, pp. 260–263, 2009.

[4] Q. Zhao, J. Xu, X. Y. Xu, Z. Wang, and D. P. Yu, "Field emission from AlN nanoneedle arrays," *Appl. Phys. Lett.*, vol. **85**, no. 22, pp. 5331, 2004.

[5] Y. J. Zeng, S. S. Lin, a. Volodin, Y. F. Lu, Z. Z. Ye, and C. Van Haesendonck, "Zero-dimensional field emitter based on ZnO quantum dots," *Appl. Phys. Lett.*, vol. **97**, no. 14, pp. 143102, 2010.

[6] Q. Zhao, H. Z. Zhang, Y. W. Zhu, S. Q. Feng, X. C. Sun, J. Xu, and D. P. Yu, "Morphological effects on the field emission of ZnO nanorod arrays," *Appl. Phys. Lett.*, vol. **86**, no. 2005, pp. 1–3, 2005.

[7] N. S. Ramgir, D. J. Late, A. B. Bhise, I. S. Mulla, M. a More, D. S. Joag, and V. K. Pillai, "Field emission studies of novel ZnO nanostructures in high and low field regions," *Nanotechnology*, vol. **17**, pp. 2730–2735, 2006.

[8] P. Feng, X. Q. Fu, S. Q. Li, Y. G. Wang, and T. H. Wang, "Stable electron field emission from triangular-shaped ZnO nanoplate arrays with low local heating effects," *Nanotechnology*, vol. **18**, pp. 165704, 2007.

[9] K. Higa and T. Asano, "Joule Heating of Field EmitterTip Fabricated on Glass Substrate," *Jpn. J. Appl. Phys.*, vol. **43**, pp. 2749–2750, 2004.

[10] H. J. Kim, J. M. Ha, S. H. Heo, and S. O. Cho, "Small-sized flat-tip cnt emitters for miniaturized X-ray tubes," *J. Nanomater.*, vol. **2012**, pp. 1–6, 2012.

[11] C. J. Lee, T. J. Lee, S. C. Lyu, Y. Zhang, H. Ruh, and H. J. Lee, "Field emission from well-aligned zinc oxide nanowires grown at low temperature," *Appl. Phys. Lett.*, vol. **81**, no. 19, pp. 3648, 2002.

[12] B. K. Gupta, D. Haranath, S. Chawla, H. Chander, V. N. Singh, and V. Shanker, "Self-catalytic synthesis, structure and properties of ultra-fine luminescent ZnO nanostructures for field emission applications.," *Nanotechnology*, vol. **21**, no. 22, pp. 225709, 2010.

[13] S. Hofmann, C. Ducati, B. Kleinsorge, and J. Robertson, "Direct growth of aligned carbon nanotube field emitter arrays onto plastic substrates," *Appl. Phys. Lett.*, vol. **83**, no. 22, pp. 4661, 2003.

[14] X. Fang, Y. Bando, C. Ye, G. Shen, U. K. Gautam, C. Tang, and D. Golberg, "Si nanowire semisphere-like ensembles as field emitters.," *Chem. Commun. (Camb).*, vol. **7345**, no. 40, pp. 4093–5, 2007.

[15] C.-M. Lu, H.-F. Hsu, and K.-C. Lu, “Growth of single-crystalline cobalt silicide nanowires and their field emission property.,” *Nanoscale Res. Lett.*, vol. **8**, no. 1, pp. 308, 2013.

[16] S. Dardona, A. Peles, G. Wrobel, M. Piech, and P.-X. Gao, “Gas adsorption and high-emission current induced degradation of field emission characteristics in solution-processed ZnO nanoneedles,” *J. Appl. Phys.*, vol. **108**, no. 12, pp. 124318, 2010.

[17] M. E. Swanwick, P. D. Keathley, A. Fallahi, P. R. Krogen, G. Laurent, and F. X. Ka, “Nanostructured Ultrafast Silicon-Tip Optical Field-Emitter Arrays,” *Nano Lett.*, vol. **14**, pp. 5035–5043, 2014.

CHAPTER 6

Highly transparent and conducting C:ZnO thin film for field emission display

6.0 Introduction

In present state of art, a screen display normally coated with a phosphor material, such as, $ZnGa_2O_4$, ZnS, Y_2O_3:Eu, CdSe and several others, however these materials significantly may reduce the transparency of display screen [1-3]. Thus, a potential material for phosphor film which possess a high transmittance property and possible to emit light by itself can be most suitable. ZnO is one of the promising materials for transparent thin film application, as well as, widely known for green light emission due to presence of native defects [4-6]. However, undoped ZnO thin film has a limitation in the conductivity even though the highly transmittance can be achieved. In many reports, trivalent metal ions (Al^{3+}, Ga^{3+} and In^{3+}) has been employed into ZnO wurtzite crystal to increase the free carrier concentration and consequently improving the conductivity of ZnO thin film [7-10]. However, even the conductivity and transparency could be achieved for the metal doped ZnO thin film; the light emission property is still being an issue. Thus, the aim of this work is to improve the conductivity of highly transparent ZnO thin film by doping a non-metal element, which also contributes to modify the intrinsic defects. Graphite plate was used as the carbon source which was co-sputtered with ZnO by RF sputtering at a low temperature. Sputtering method could be a reliable method to fabricate a thin film without forming any agglomeration of doping material. The fine distribution of particles on the thin film would help to avoid a coulombic degradation which has been one of the problems in a phosphor screen [11].

The effect on transparency and conductivity of C:ZnO thin film with the variation of number, sizes and position of graphite plate used as carbon source along with ZnO target were investigated. C:ZnO has been widely reported on their ferromagnetism [12,13] or the p-type properties [14,15] and yet there is no report on the optical properties of the thin film. Carbon is an amphoteric impurity in II-IV compound semiconductor which could improve the electrical properties of ZnO thin film by defect formation such as oxygen vacancies or Zn interstitial. If a higher transparency and conductivity can be achieved, the thin film can be one of the promising TCO film for myriad applications in electronic industries. Besides the advantages of cheap, non-oxidation and abundant material, the ability to emit light emission from carbon doped thin film can be one of the merits of C:ZnO film to be applied as a transparent phosphor screen for field emission display.

6.1 Experimental details

6.1.1 *Thin film preparation*

Highly pure ZnO ceramic target (99.99%) and graphite plate (1x1x0.1 and 1.5x1.5x0.1 cm) were used as the source for ZnO and carbon, respectively. The size of ZnO target is 101.6 mm in diameter and 5 mm in thickness. The substrate was a 1x1 cm corning glass which was first cleaned with ethanol for 10 min and followed by rinsed in distilled water for another 10 min in ultrasonic bath. Then, the glass substrate was blow dried with air using a squeezer hand pump. C:ZnO thin film was deposited by RF sputtering (ANELVA SPF-210HS) for 20 min using a RF power supply (13.56 MHz) with Ar as the sputtering gas under the sputtering condition as shown in Table 6-1.

Table 6-1: Sputtering condition of C:ZnO thin film

Condition	Value
Ar flow rate	1 sccm
Background pressure	3 x 10^{-5} Pa
Working pressure	0.5 Pa
Substrate temperature	200˚C
RF power	200 W

The glass substrate was placed at substrate holder with a fixed distance of 5 cm facing the target. Prior to the film deposition, surface of the targets was cleaned for 10 min by pre-sputtering process using the same condition as given in Table 6-1 while keeping the shutter closed. The schematic of sputtering process was shown in Fig.6-1. Carbon concentration of C:ZnO thin films was calculated as the nominal dopant concentration based on the percentage of total area of the graphite plate on the ZnO target as illustrated in Fig. 6-2.

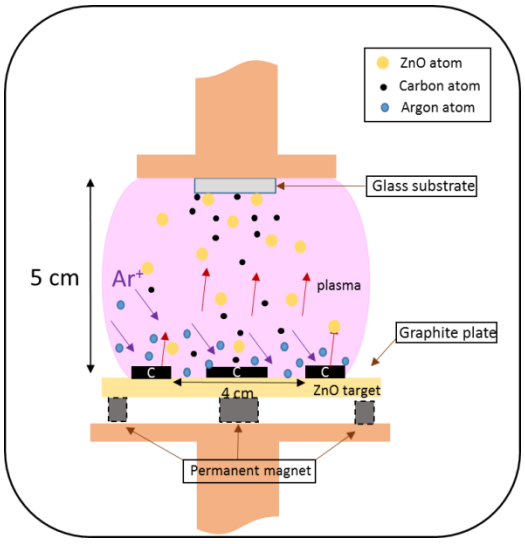

Figure 6-1: RF Sputtering schematic diagram

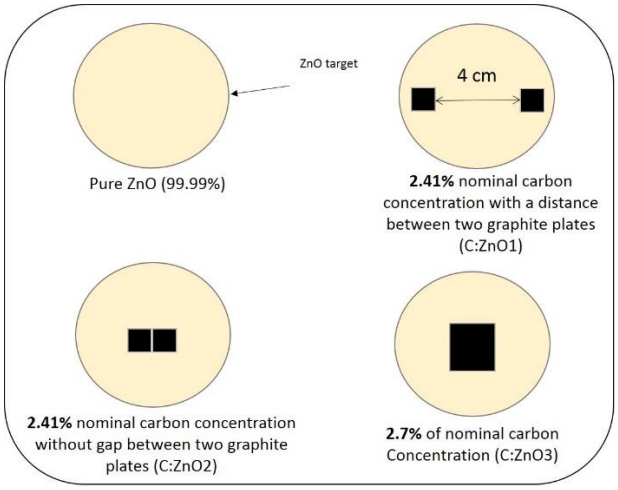

Figure 6-2: Top view of graphite plate position on the ZnO target

Naturally, carbon cannot be avoided during sample fabrication even for undoped thin film. It can easily be detected from analysis such as x-ray photoelectron and energy dispersed x-ray. However, unlike other materials, the difficulty in quantify an atomic percentage of pure carbon concentration in the thin films by co-sputtering process had driven to the calculation of nominal carbon concentration. The percentage of nominal carbon concentration will be used throughout this paper as the carbon composition in C:ZnO thin film. It seems difficult to reproduce the doped thin film without introducing an accurate concentration that corresponding to the atomic percentage of doping material. However, with the same experimental setup, background pressure, and experimental parameters, doped thin film with almost the same film properties is reproducible. There are three samples of C:ZnO thin film prepared in this experiment in which the calculated percentage of graphite area are 2.41%; with distance about 4 cm between the two 1x1 cm graphite plates and was placed at high erosion area of the ZnO target (denoted as C:ZnO1), 2.41%; without distance between two 1x1 cm graphite plates and was placed at the center of ZnO target (denoted as C:ZnO2), and 2.7%; a single 1.5x1.5 cm graphite plate at the center of the ZnO target (denoted as C:ZnO3), respectively. As a reference to study the concentration of carbon in ZnO thin films, an undoped ZnO thin film was prepared with the same condition of that C:ZnO thin films.

6.1.2 *Characterization*

Surface morphology and the roughness of undoped and carbon doped ZnO thin film was characterized by scanning probe microscope (JEOL JSPM-5200TM). Sheet resistance was measured by 4 point probes (Napson RT-70V/RG-7C) without deposited contact on the thin films. The measurement was done at 10 random points on each of the thin film and the average sheet resistance was taken as the result. Raman spectra were measured by Raman spectroscopy (Jasco NRS-3300) with an excitation wavelength of 534.08 nm. The average thickness of the thin films was measured by Dektak profilometer at two different edges for each thin film. Transmittance property was analyzed by UV-vis spectrophotometer (Jasco V-670K) and the film transparency was defined at visible wavelength of 550 nm. The X-ray photoelectron spectroscopy (XPS) of the thin films was analyzed using a focused monochromatized Mg-Kα X-ray source (1253.6 eV) in the XPS instrument (Shimadzu ESCA-3300KM). Luminescence property of the thin films was measured using SEM-CL spectroscopy (JEOL JSM 7800F) at room temperature with an accelerating voltage of 5kV. The field emission property was measured by using a parallel plate configuration in which the C:ZnO thin film was used as an anode material while the cathode is a single wall carbon nanotube (SWCNT) thin film. The size of emission area was 0.1 cm^2 and the spacer was a layer of Teflon in 100 µm thickness. The measurement was done in a vacuum condition when the background pressure reached at 3×10^{-4} Pa and was carried out in a dark room to observe for a light emission.

6.2 Results and Discussion

6.2.1 *Morphology, electrical and optical properties*

Surface homogeneity of ZnO thin film was improved with C doping. AFM image in Fig. 6-3 (a) shows ZnO particles of undoped ZnO thin film. The surface roughness of that 5x5 μm^2 scanning area was 41 nm. Non-homogeneous surface of undoped ZnO film was due to a large distance between the top and valley area. With the incorporation of carbon, the distance measured between the top and valley area was smaller compared to that of undoped film. Surface roughness of C:ZnO1, C:ZnO2 and C:ZnO3 as shown in Fig. 6-3 (b-d) was 35.1 nm, 29.4 nm and 25.6 nm, respectively. The higher concentration of carbon introduced in the thin film, the more homogenous film morphology was fabricated. The result indicates carbon atom in ZnO thin film has contribute to improve surface homogeneity of deposited films by the formation of homogenous coalescence structure that can be clearly seen from the AFM images. Due to that reason, C:ZnO thin film surface could provide a smoother electrons path since the grain boundary decreased and attributed to the lower sheet resistance of C:ZnO film.

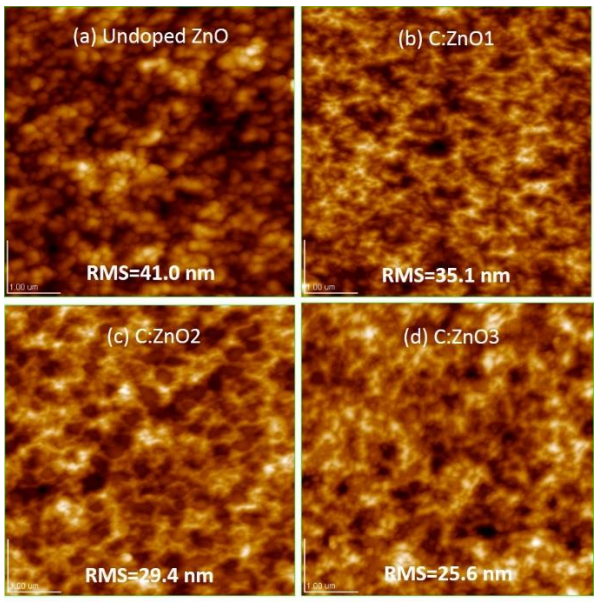

Figure 6-3: AFM images of undoped and carbon doped ZnO thin film

Sheet resistance of ZnO thin films decreases when carbon was introduced in the thin film as shown in Table 6-2. Undoped ZnO thin film showed very high sheet resistance indicates the property of an insulator.

Table 6-2: Electrical and transmittance property of undoped and C:ZnO thin films

Sample	Electrical and Optical Properties		
	Sheet resistance (Ω/□)	%T	Thickness (μm)
undoped ZnO	Very high	77	1.3
C:ZnO1	1.4k	78	1.52
C:ZnO2	646	78	1.5
C:ZnO3	37	84	1.5

As mention in the introduction section, the conductivity of undoped ZnO thin film can be improved by doping with trivalent metal materials such as Al and Ga. To achieve for a phosphor and conductive screen film, carbon material can be the best candidate of non-metal doping material in this experiment due to its properties to tune the film conductivity with a very low doping concentration. According to the literature, incorporation of carbon atoms in ZnO thin film could modified the intrinsic native deep levels in ZnO i.e. oxygen vacancy (Vo), Zn interstitial (Vzni), oxygen interstitial (Oi), Zn vacancy (Vzn), oxygen anti-site (Ozn) and zinc anti-site (Zno). These native point defects often control doping and luminescence efficiency of ZnO directly or indirectly. The ZnO thin film with higher Vo is said to possess a higher conductivity [16,17]. Raman spectra shown in Fig. 6-4 revealed the higher Vo in ZnO thin film determined by A1 (LO) intensity peak. There are two dominant peaks can be observed from the Raman spectra. The peak of E2 (high) mode at 435-437 cm^{-1} was

attributed to wurtzite lattice of ZnO with high crystallinity and peak A1 (LO) mode at 570 cm^{-1} can be associated with oxygen deficiency in the matrix of ZnO. The E2 (high) is often related to oxygen atoms. The undoped ZnO film, peak E2 (high) and A1 (LO) shows almost the same intensity indicates for a stoichiometry of undoped ZnO film. As the carbon was introduced in ZnO film, sample C:ZnO1, C:ZnO2 and C:ZnO3 shows higher intensity of A1 (LO) mode compared to the E2 (high) mode. The higher intensity peak of A1 (LO) mode for carbon doped ZnO film indicates higher oxygen deficiency in that films [18].

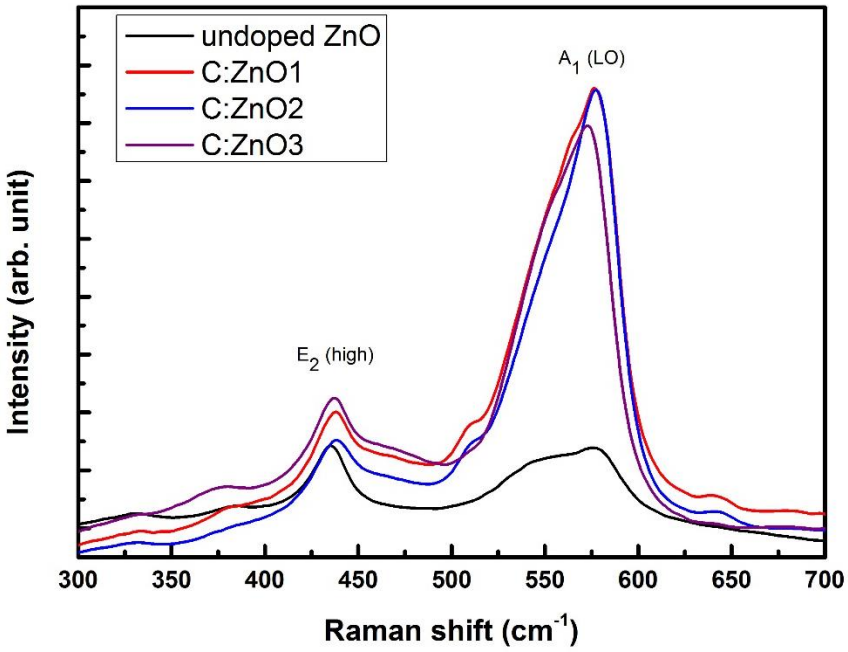

Figure 6-4: Raman spectra of undoped and C doped ZnO thin film

Sheet resistance can also be affected by a thickness of thin film. In this experiment, the film showed almost the same thickness regardless the position of the graphite plate. All carbon doped samples showed the average thicknesses of 1.5 μm except for the undoped ZnO film which has 1.3 μm. The thickness result shows that the low sheet resistance of carbon doped thin films is not directly related with the film thickness. It can be assumed that, the

contribution of carbon atoms in the ZnO film could be responsible to the modification in the conductivity of ZnO thin film.

The position of the graphite plate can also be a factor of the difference in sheet resistance due to the number of sputtered atoms condenses on the substrate. C:ZnO1 and C:ZnO2 thin film was deposited with the same nominal carbon concentration of 2.41% with a different position of graphite plate on the ZnO target. The different in sheet resistance of these two samples can be attributed to the different in scattering effect inside the sputter chamber during the deposition process. C:ZnO1 thin film showed 1.4 kΩ/□ in a sheet resistance while C:ZnO2 thin film showed a lower value at 646 Ω/□. Higher scattering effect can be occurred at the higher erosion area i.e. between the two permanent magnets at the sputter target. Due to this high scattering effect, the number of sputtered carbon atoms to be condensed on the substrate could be less because the atoms would lose their energy due to the impact of collision with other particles inside the chamber. Graphite plate at the center of ZnO target could have a lower collision thus resulted for the good quality of carbon doped thin film. C:ZnO3 thin film with the highest nominal carbon concentration at 2.7% showed the lowest value of sheet resistance at 37 Ω/□. The lowest in sheet resistance of C:ZnO3 thin film could be due to high probability of more carbon atoms possible to condense on the substrate. Since the larger size of graphite plate was located at the center of ZnO target, less collision is expected and thus supports the reason of more number of carbon atoms in C:ZnO3 thin film.

The optical property was measured in the wavelength range of 300-800 nm and the percentage of transmittance was taken at the visible wavelength of 550 nm. A transparency property can be affected by the surface morphology of a thin film. A smoother surface morphology of thin film will give higher transmittance property due to less reflection of light scattering from the thin film surface [19]. Figure 6-5 shows the transmittance of undoped and

C:ZnO doped thin film. The wavy curve of the transmittance spectra is because of the interference in light propagation during the measurement between the thick ZnO-based film and the glass substrate. If the thickness of the deposited thin film is less than 500 nm, the wavy curve could not be observed. Undoped ZnO film possess a transmittance of 77% which is lower than the C:ZnO thin films. C:ZnO3 thin film shows the higher transmittance property of 84%, yet the appearance color of the thin film become slightly brownish. C:ZnO1 and C:ZnO2 thin film having the same value of transmittance at 78%. The result shows that, the same area of graphite plates which was located at a different position on the ZnO target did not give significant effect to the transparency of C:ZnO thin film.

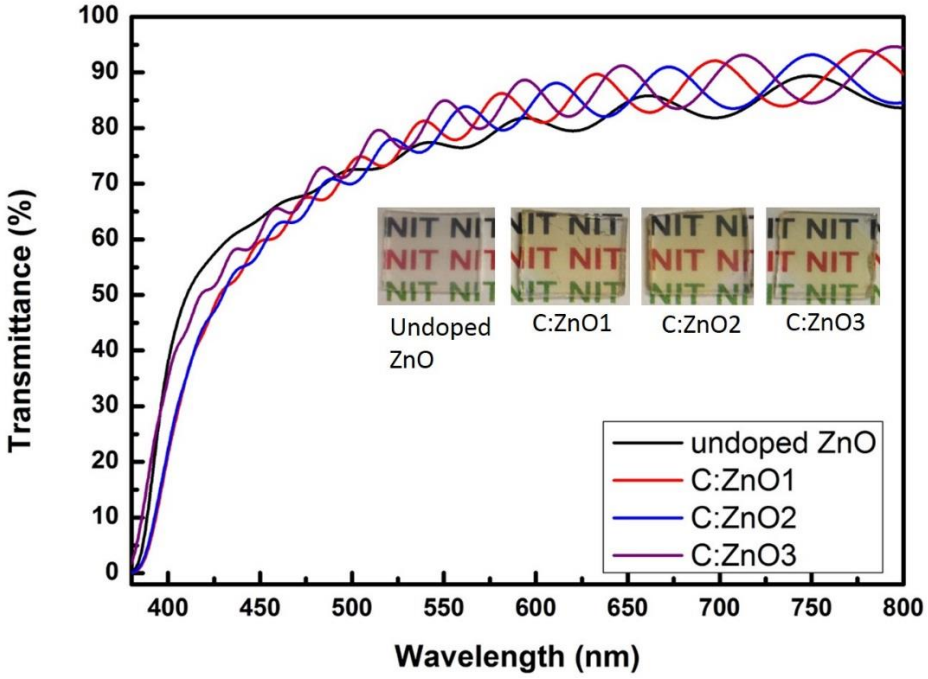

Figure 6-5: Transmittance spectra of undoped and carbon doped ZnO thin films

6.2.2 *X-ray Photoelectron spectrometer (XPS)*

The chemical state and surface composition of C:ZnO thin film were determined by XPS spectrum. All thin films were etched for 1 min by Ar to remove any contamination on the thin film surface. For that 1 min etched, about 10 nm in thickness of the thin film surface

was removed. There is no C1s peak can be found after the etching process in the survey spectrum. ZnO related peaks can clearly been observed from the survey spectrum as shown in Figure 6-6 (a). The peak at ~531 eV from O1s spectrum of ZnO, C:ZnO1, C:ZnO2 and C:ZnO3 as shown in Figure 6-6 (b) was attributed to O^{2-} ions in wurtzite structure of ZnO [20]. The result of Zn2p core level revealed the doublet spectral line of ZnO at 1022 eV ($Zn2p_{3/2}$) and 1045 eV ($Zn2p_{1/2}$) with spin-orbit splitting of 23 eV as depicted in Figure 6-6 (c). Only one result of the XPS analysis was represented in which it was taken from sample C:ZnO3. This is because all samples showed the same peak at the same binding energy as agreed in the XPS handbook for ZnO [21]. In this case, the chemical bonding between ZnO and C cannot be revealed since the concentration of C was too small and was not detected by the XPS characterization.

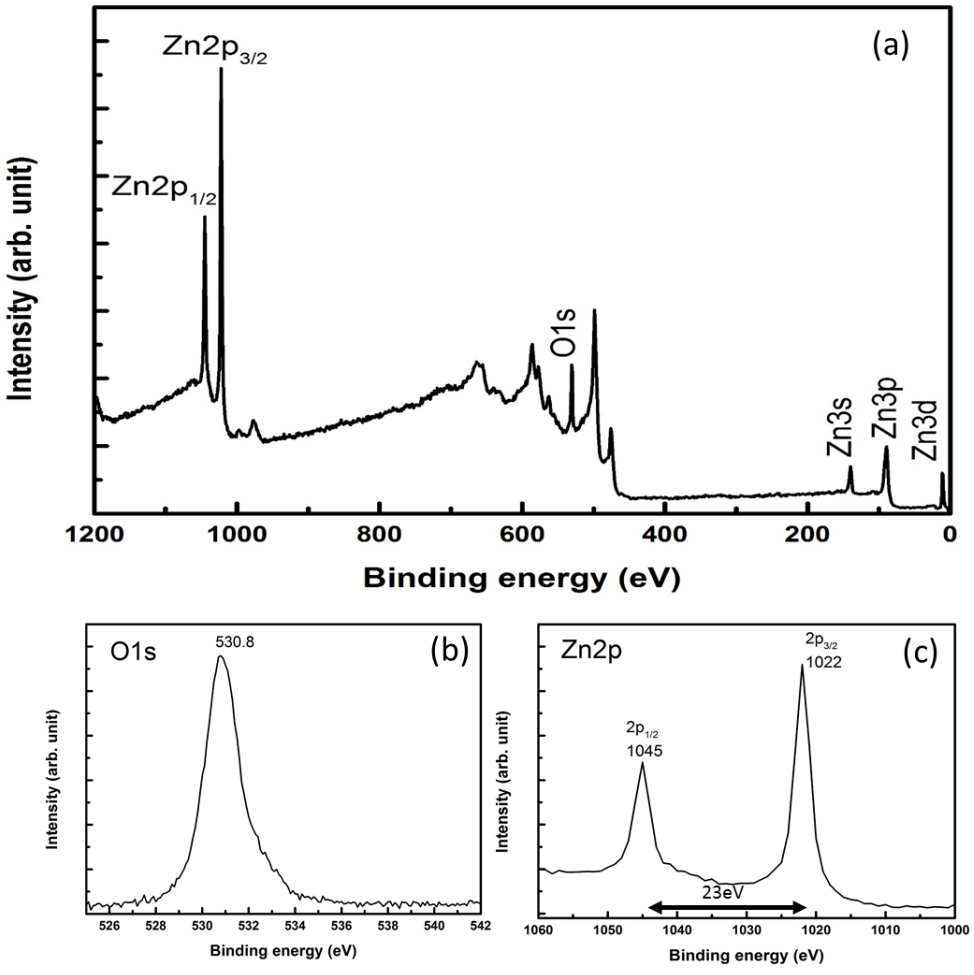

Figure 6-6: XPS spectrum of C doped ZnO

6.2.3 *Luminescence emission properties*

Figure 6-7 shows cathodoluminescence (CL) spectra of undoped and carbon doped ZnO thin film (C:ZnO1) analyzed in the range of 250-900 nm. The luminescence emission properties are strongly related with the defect states in ZnO. The observed CL spectra of both undoped and C:ZnO1 samples exhibit the band-edge position at 378 nm (3.28 eV) and 384 nm (3.25 eV), respectively. These peaks are attributed to the UV emission originated from recombination of free excitons from conduction band (CB) to valence band (VB). The peak observed at 752 nm of undoped ZnO sample is attributed to the infra-red (IR) wavelength. A significant difference of CL spectra was observed from the carbon doped ZnO thin film. The broad peak centered at 646 nm (1.92 eV) indicated a complex defects of substitutional carbon (Co), oxygen vacancy and interstitial Zn (2Co-Vo-Zni) which responsible for red-orange emission [22].

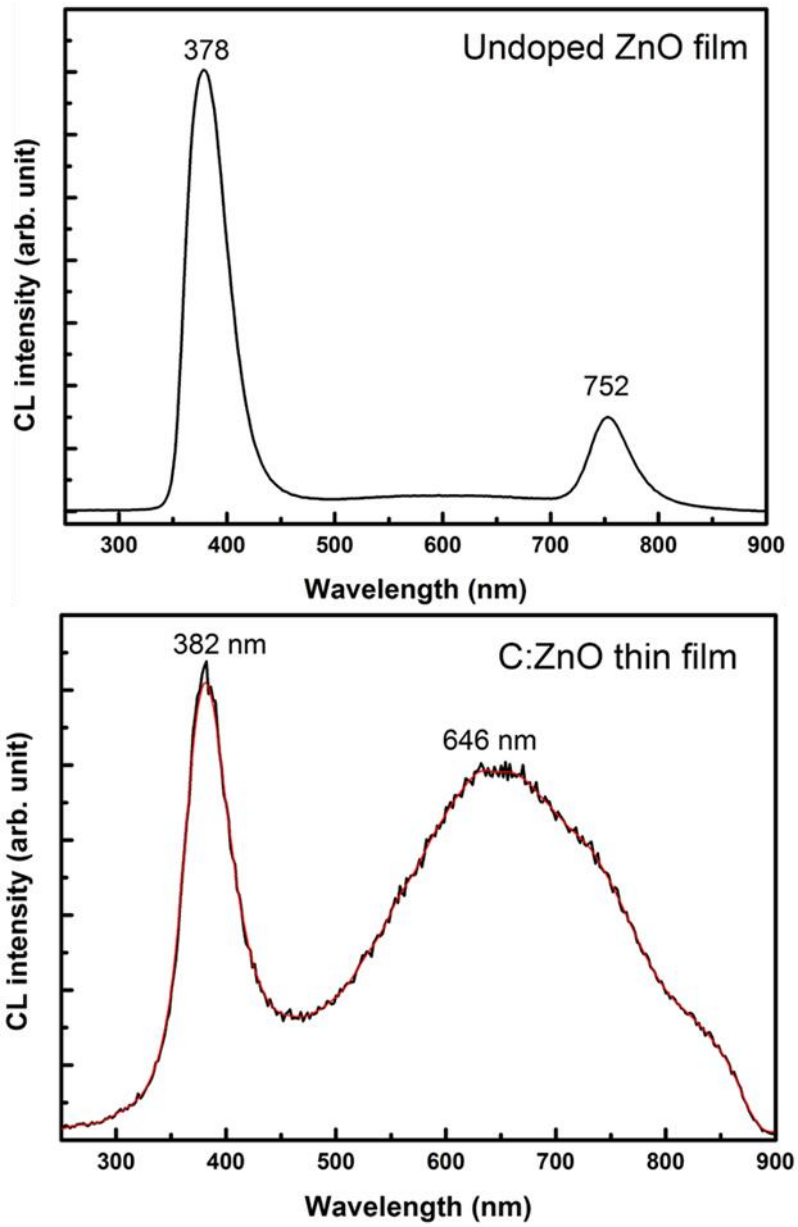

Figure 6-7: CL spectra of undoped and carbon doped ZnO thin film

6.2.4 *Field emission application*

In the field emission measurement, C:ZnO1 film was employed as the phosphor film to observe light emission. The measurement was done by using two parallel electrodes in which a SWCNTs film was used as the field emitter. Preparation of SWCNT as the field emitter was explained elsewhere [23]. Figure 6-8 shows the FE property of carbon doped ZnO film. The SWCNT emitter possess an excellent efficiency owing to the high field

enhancement factor of 4492 calculated from the linear behavior of FN plot shown in inset of Fig. 6-8 (a). High emission current was also achieved at lower threshold voltage. The electric field at current density of 1 mA/cm^2 was achieved at 5 V/μm. The experimental result of light emission is shown in inset of Fig. 6-8 (b). It shows a UV-violet emission. The mechanism can be explained by the typical exciton emission when photo-generated electron recombines with holes in the valence band. The light emission became brighter as the electric field increased with a higher current density for more than 1 mA/cm^2. The presence of carbon in ZnO thin film may modify the intrinsic defects and contributed for the light emission [24].

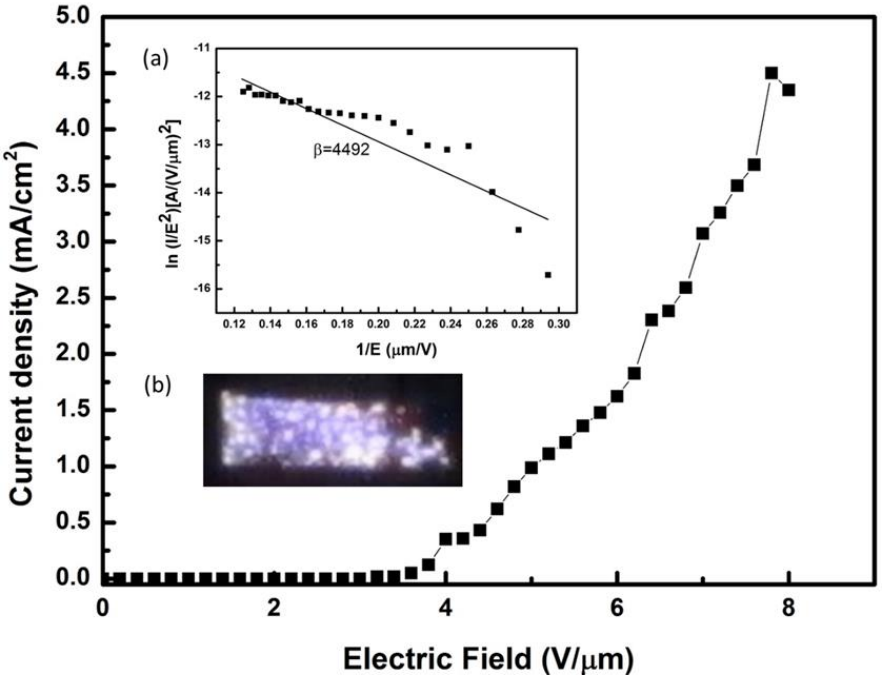

Figure 6-8: FE property of C doped ZnO film as the phosphor layer and SWCNT as the field emitter. Inset figures are (a) the FN plot and (b) light emission from C doped ZnO film

6.3 Conclusion

Highly transparent and conductive C:ZnO thin film was successfully fabricated and was employed as the phosphor screen of field emission display. The position, sizes and number of graphite plates which act as carbon source played a crucial role in a co-sputtering

technique to fabricate the conductive and transparent C:ZnO thin film. Lower sheet resistance of carbon doped ZnO thin film was achieved for sample C:ZnO3 which having the higher nominal carbon concentration of 2.7%. Carbon atoms could be condensed more on glass substrate from graphite plate position at the center of ZnO target. Due to less collision of particles in the plasma at the center of ZnO target compared to the high erosion area, resulted in a low sheet resistance of C:ZnO2 thin film even though the same nominal concentration was introduced in the chamber. All carbon doped ZnO thin films did not show significant difference in the transmittance properties. A CL spectrum shows a broad peak centered at 646 nm indicating red-orange luminescence emission from the carbon doped ZnO film (C:ZnO1). The experimental result shows UV-violet light emission and brighter when the current density increased more than 1 mA/cm^2. Thus, depending on the doping and deposition conditions, highly conductive and transparent C:ZnO thin film can be obtained, which also act as a promising material for a phosphor screen of transparent field emission display.

6.4 References

[1] P. F. Smet, I. Moreels, Z. Hens, and D. Poelman, "Luminescence in Sulfides: A Rich History and a Bright Future," *Materials*, vol. **3**, no. 4, pp. 2834–2883, 2010.

[2] P. Thiyagarajan, M. Kottaisamy, N. Rama, and M. S. Ramachandra Rao, "Study of pulsed laser deposited ZnGa 2 O 4 : Mn phosphor thin films in an oxygen controlled environment," *J. Phys. D. Appl. Phys.*, vol. **42**, no. 15, pp. 155301, 2009.

[3] M. a. Schreuder, J. D. Gosnell, N. J. Smith, M. R. Warnement, S. M. Weiss, and S. J. Rosenthal, "Encapsulated white-light CdSe nanocrystals as nanophosphors for solid-state lighting," *J. Mater. Chem.*, vol. **18**, no. 9, pp. 970, 2008.

[4] Y. Gong, T. Andelman, G. F. Neumark, S. O'Brien, and I. L. Kuskovsky, "Origin of defect-related green emission from ZnO nanoparticles: effect of surface modification," *Nanoscale Res. Lett.*, vol. **2**, no. 6, pp. 297–302, 2007.

[5] H. S. Kang, "Annealing effect on the property of ultraviolet and green emissions of ZnO thin films," *J. Appl. Phys.*, vol. **95**, no. 3, pp. 1246, 2004.

[6] H. Faber, J. Hirschmann, M. Klaumu, B. Braunschweig, W. Peukert, and M. Halik, "Impact of Oxygen Plasma Treatment on the Device Performance of Zinc Oxide Nanoparticle-Based Thin-Film Transistors," *ACS Appl. Mater. Interfaces*, vol. **4**, pp. 1693–1696, 2012.

[7] M.-C. Jun, S.-U. Park, and J.-H. Koh, "Comparative studies of Al-doped ZnO and Ga-doped ZnO transparent conducting oxide thin films.," *Nanoscale Res. Lett.*, vol. **7**, no. 1, pp. 639, 2012.

[8] J. Sun, Y. Huang, and H. Gong, "Improved mobility and conductivity of an Al2O3 incorporated indium zinc oxide system," *J. Appl. Phys.*, vol. **110**, no. 2, pp. 023709, 2011.

[9] J. Jia, A. Takasaki, N. Oka, and Y. Shigesato, “Experimental observation on the Fermi level shift in polycrystalline Al-doped ZnO films,” *J. Appl. Phys.*, vol. **112**, no. 1, pp. 013718, 2012.

[10] A. K. Srivastava and J. Kumar, “Effect of zinc addition and vacuum annealing time on the properties of spin-coated low-cost transparent conducting 1 at% Ga–ZnO thin films,” *Sci. Technol. Adv. Mater.*, vol. **14**, no. 6, pp. 065002, 2013.

[11] S. a. Bukesov, D. Y. Jeon, and B. I. Lee, “Enhanced stability of light-emitting performances of phosphors under low energy electrons,” *Appl. Phys. Lett.*, vol. **87**, no. 25, pp. 253503, 2005.

[12] B. J. Nagare, S. Chacko, and D. G. Kanhere, “Ferromagnetism in carbon-doped zinc oxide systems.,” *J. Phys. Chem. A*, vol. **114**, no. 7, pp. 2689–96, 2010.

[13] M. Subramanian, Y. Akaike, Y. Hayashi, M. Tanemura, H. Ebisu, and D. L. S. Ping, “Effect of defects in ferromagnetic C doped ZnO thin films,” *Phys. Status Solidi B*, vol. **249**, no. 6, pp. 1254–1257, 2012.

[14] S. T. Tan, X. W. Sun, Z. G. Yu, P. Wu, G. Q. Lo, and D. L. Kwong, “p-type conduction in unintentional carbon-doped ZnO thin films,” *Appl. Phys. Lett.*, vol. **91**, no. 7, pp. 072101, 2007.

[15] T. S. Herng, S. P. Lau, L. Wang, B. C. Zhao, S. F. Yu, M. Tanemura, a. Akaike, and K. S. Teng, “Magnetotransport properties of p-type carbon-doped ZnO thin films,” *Appl. Phys. Lett.*, vol. **95**, no. 1, pp. 012505, 2009.

[16] C.-F. Yu, C.-W. Sung, S.-H. Chen, and S.-J. Sun, “Relationship between the photoluminescence and conductivity of undoped ZnO thin films grown with various oxygen pressures,” *Appl. Surf. Sci.*, vol. **256**, no. 3, pp. 792–796, 2009.

[17] M. S. Arnold, P. Avouris, Z. W. Pan, and Z. L. Wang, “Field-Effect Transistors Based on Single Semiconducting Oxide Nanobelts,” *J. Phys. Chem. B*, vol. **107**, no. 3, pp. 659–663, 2003.

[18] D. Das and P. Mondal, “Photoluminescence phenomena prevailing in c-axis oriented intrinsic ZnO thin films prepared by RF magnetron sputtering,” *RSC Adv.*, vol. **4**, no. 67, pp. 35735, 2014.

[19] P. Ghosh, S. Satou, T. Tsuchiya, Y. Hayashi, and M. Tanemura, “Controllable fabrication and characterization of conical nanocarbon structures on polymer substrate for transparent and flexible field emission displays,” *Phys. status solidi - Rapid Res. Lett.*, vol. **6**, no. 4, pp. 184–186, 2012.

[20] J. Ding, M. Wang, X. Zhang, and C. Ran, “Field emission mechanism insights of graphene decorated with ZnO nanoparticles,” *RSC Adv.*, vol. **3**, no. 33, pp. 14073, 2013.

[21] P. E. Sobol and J. Chastain, "Handbook of X-ray Photoelectron Spectroscopy", pp. 260, 1992.

[22] L. T. Tseng, J. B. Yi, X. Y. Zhang, G. Z. Xing, H. M. Fan, T. S. Herng, X. Luo, M. Ionescu, J. Ding, and S. Li, “Green emission in carbon doped ZnO films,” *AIP Adv.*, vol. **4**, no. 6, pp. 067117, 2014.

[23] D. Ghosh, P. Ghosh, G. Kalita, T. Noda, C. Takahashi, and M. Tanemura, “Conducting polymer based hybrid structure as transparent and flexible field electron emitter,” *Phys. status solidi - Rapid Res. Lett.*, vol. **7**, no. 7, pp. 489–492, 2013.

[24] Z. G. Wang and X. T. Zu, “Blue luminescence from carbon modified ZnO nanoparticles-summary,” *J Mater Sci*, vol. **41**, pp. 3729, 2006.

CHAPTER 7

Fabrication of transparent graphene-ZnO nanocone based field emission display

7.0 Introduction

A highly transparent ZnO nanocones film was fabricated at room temperature and their stability was reported in chapter 5. However, the intrinsic ZnO film has a limitation in their conductivity which can increase the joule heating effect at the tips of field emission (FE) [1]. Thus, a material with excellent electron transport is capable of enhancing the electron emission. In conjunction of that reason, C:ZnO nanocones film was fabricated to improve the conductivity, which revealed a sheet resistance of less than 100 Ω/□. Carbon was chosen as the dopant, since it can modify the electrical property of ZnO by defect formation such as oxygen vacancy or Zn interstitial [2]. Although C:ZnO has significantly improve the conductivity, the high and stable emission current is still remain a challenge.

Hybrid structure such as CNT-ZnO FE device has been reported can improved the FE property [3-5]. However there is an issue on the transmittance property. In this prospect, graphene based materials with presence of rich edges have been significantly investigated for high performance FE devices [6-10]. The two dimensional (2D) graphene sheet shows ballistics transport in submicron scale approaching relativistic speeds, with intrinsic mobility as high as 200,000 cm2 $V^{-1}s^{-1}$[11]. Graphene also possess excellent mechanical properties with breaking strength of ~40 N/m and Young's modulus of ~1.0 TPa [12]. A single graphene layer absorb ~2.3% of the incident light with a negligible reflectance of <0.1%, where the absorbance and transparency are independent of wavelength [13]. Therefore,

graphene can maintain the transparency of the C:ZnO nanocone film for the hybrid structure. Graphene sheet can provide high mechanical robustness and chemical inertness to withstand the intense electric field induced mechanical stress [14]. If high and stable emission current can be achieved with the ability to be as phosphor screen, a promising transparent and conductive C:ZnO-based FED could be realized.

7.1 Experimental details

7.1.1 *Thin film preparation*

Highly pure ZnO ceramic target (99.99%) and three sizes of graphite plate were used as the source for ZnO and carbon, respectively. The size of graphite plate used was 1x1 cm^2 (2 pieces) and 1.5x1.5 cm^2. C:ZnO thin film was deposited by RF sputtering for 30 min using a RF power supply (13.56 MHz) with Ar as the sputtering gas under the sputtering condition as shown in Table 7-1. Prior to the film deposition, surface of the targets was cleaned for 10 min by pre-sputtering process using the same condition as given in Table 7-1 while keeping the shutter closed.

Table 7-1: Sputtering condition of C:ZnO thin film

Condition	Value
Ar flow rate	5 sccm
Background pressure	3×10^{-5} Pa
Working pressure	0.5 Pa
Substrate temperature	300˚C
RF power	100 W

7.1.2 *C:ZnO nanocones film preparation*

C:ZnO nanocones was fabricated by using ion beam irradiation technique at room temperature. The sample was loaded into a chamber and evacuated until the background pressure reached $3x10^{-4}$ Pa. Next, argon gas was introduced in the chamber as the sputter ions with the working pressure of $5x10^{-2}$ Pa. The beam current and beam voltage was set at 6 mA and 1000 eV, respectively during the irradiation process. Ion incident angle was set at 60° to obtain a sharp tips of nanocones. The sample was irradiated for 10 min to gain an appropriate number density of nanocones (6-8 μm^{-2}).

7.1.3 *Synthesis of graphene and transfer process*

Graphene synthesized by atmospheric pressure chemical vapour deposition (CVD) technique was transferred on the ZnO nanocones for fabrication of the heterostructure FE device. High quality large-area graphene film was growth on Cu foil [15]. Commercially available Cu foil with a thickness of 20 μm and purity of 99.99% (Nilaco Pvt. Ltd) was used. The graphene was cleaned in acetone by sonication and directly used without further treatment. To synthesize graphene, solid camphor powder with a vapor pressure and molar mass of 0.65 mmHg at 25°C and 152.23 $gmol^{-1}$, respectively, was used. In the experiment, 0.5 mg of solid camphor was used to achieve for individual graphene formation on the Cu foil. The Cu foil was heated at 1020°C and annealed in H_2 for 15 min a flow rate of 100 sccm. H_2 quantity was significantly reduced and Ar was introduced in the growth zone along with H_2. Solid camphor was slowly evaporated and pushed to the growth zone by the 100 sccm of Ar and H_2 (98:2 sccm) gas mixture for 10 minute and then the growth furnace was cooled down to room temperature. The graphene film was transferred on the C:ZnO nanocones

structure by conventional chemical etching process of Cu. The cleaning process was important to make sure only highly transmittance graphene was transferred without any contamination. Few drops of PMMA solution was deposited on the graphene film. Next the film was immersed in the iron nitrate nonaydrate until the Cu foil dissolved and leave it graphene in the solution. The graphene was transferred on C:ZnO nanocones and heated for a few minutes. The sample was then immersed in the acetone to remove PMMA. After removing the PMMA layer, the sample was rinsed in DI water and ready to be characterized.

7.1.4 *Sample characterizations*

Scanning electron microcopy (SEM) and Raman studies were performed to confirm the structure and morphology of transferred graphene film on C:ZnO nanocones. UV-Vis spectrometer was used to measure the transmittance property of hybrid graphene-C:ZnO nanocones film. The field emission property was measured by using a parallel plate configuration in which the C:ZnO thin film was used as an anode material while the cathode is the graphene-C:ZnO nanocones film. The size of emission area was 0.1 cm^2 and the spacer used was a layer of Teflon in 100 µm thickness. The measurement was done in a vacuum condition when the background pressure reached at 3×10^{-4} Pa. To analyze the stability of the hybrid structure, a 50 min test was carried out with the same condition as the FE measurement.

7.2 Results and Discussion

Figure 7-1 (a) shows the transmittance property of synthesized C:ZnO nanocones film which is around 70-80% at wavelength of 550 nm. Initially the C:ZnO thin film has a

transmittance of ~85%. Since, the wavelength region of light scattering is highly dependent on the roughness of the thin film, the changes of the C:ZnO thin film surface morphology after the formation of nanocone structure, had slightly reduced the film transparency. Fig. 7-1 (b) shows a SEM image of the nanocones fabricated on the glass substrate with a density of 6 μm^{-2} and average height of 500 nm. The nanocones formed uniformly thru out the substrate by ion irradiant with homogenous morphology. The average sheet resistance for the C:ZnO nanocone film was found to be 80 Ω/□. The fabricated nanocone substrate was taken as base for transferring the CVD graphene film and thereby creating a heterostructure.

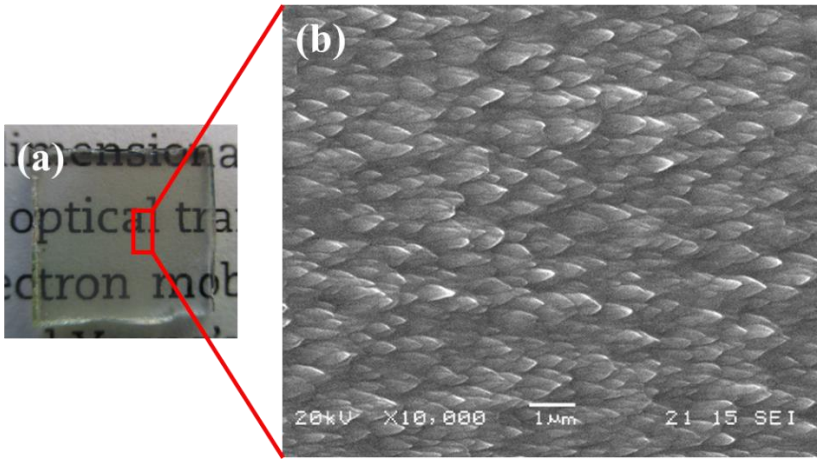

Figure 7-1: (a) Highly transparent pristine C:ZnO nanocone film and (b) SEM image of C:ZnO nanocones on the glass substrate after 10 min ion beam irradiation at RT.

Figure 7-2 (a) shows a low magnification SEM image of graphene-C:ZnO nanocones film. The C:ZnO nanocones is well covered with transferred graphene film. Fig. 7-2 (b) shows a higher magnified view of the graphene-C:ZnO nanocones structure. Owing to a thin layer of graphene, the tips of nanocones still can be observed as well as transferred graphene film was optically homogenous. Thus, there is no noticeable changes in the transmittance of the hybrid graphene-C:ZnO nanocones film compared to pristine C:ZnO nanocones film as shown in the transmittance spectra in Fig. 7-3. The pristine C:ZnO and hybrid graphene-C:ZnO film shows 74% and 72% of film transmittance, respectively at 550 nm in visible wavelength.

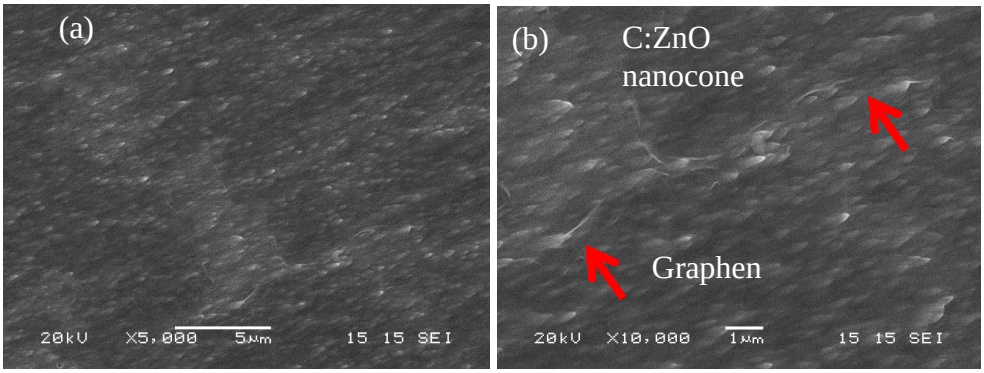

Figure 7-2: (a) A low magnification and (b) high magnification of SEM images of hybrid graphene-C:ZnO nanocones film (red arrows shows the fold of graphene).

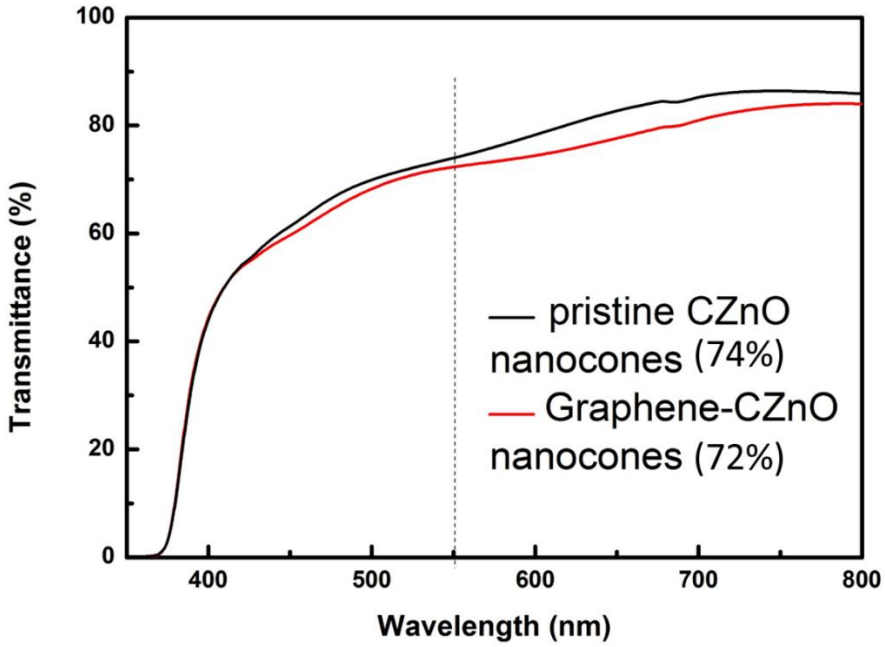

Figure 7-3: Transmittance spectra of pristine C:ZnO nanocones and graphene-C:ZnO nanocones film.

The Raman spectra as depicted in Fig. 7-4 (a), shows Raman active E_2 mode at 442 cm^{-1} and IR active A1 mode (LO) at 578 cm^{-1} for C:ZnO nanocones. The peak at 1106 cm^{-1} is from the glass substrate. Fig. 7-4 (b) shows the Raman spectra of hybrid graphene-C:ZnO film. The disorder (D) peak was observed at 1341 cm^{-1}. The graphitic (G) and second disorder (2D) peak were observed at 1587 cm^{-1} and 2675 cm^{-1}, respectively. The higher intensity of 2D peak than that of G peak, present a single layer graphene [16]. The result

shows that the graphene was covered at almost all surface area of C:ZnO nanocones based on the existing of D, G and 2D peak on several areas on the measured hybrid film. It shows that the graphene was uniformly transferred on the nanocones. Since graphene has no band gap, it acts like a metal [17]. The single layer of graphene may provide a good path for electron transport. Thus, by transferred graphene on top of the nanocones, resistance at the nanocone tips may reduce and consequently reduce the local joule heating and prevent the C:ZnO nanocones from damage.

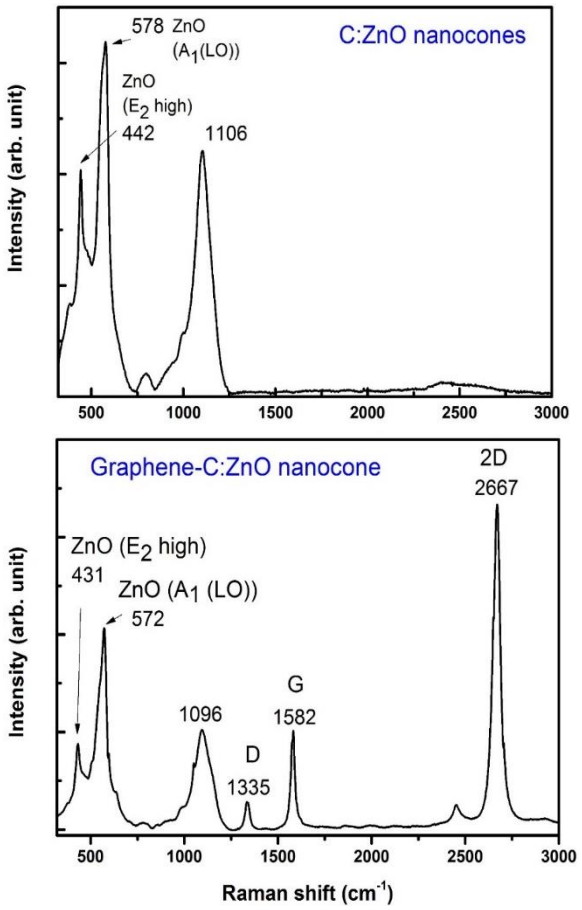

Figure 7-4: (a) Raman spectra of pristine C:ZnO nanocones and (b) hybrid graphene-C:ZnO nanonocones film.

Fig. 7-5 shows the FE properties of pristine C:ZnO nanocones and the modified surface C:ZnO nanocones by graphene film. It can be seen that the threshold field at current density of 1 μAcm^{-2} was obtained at 6.5 V μm^{-1} and 4.3 V μm^{-1} for pristine C:ZnO nanocones and graphene coated C:ZnO nanocones film, respectively. Sharp edge of single layer of

graphene had enhanced the emission current thus, the lower threshold field was obtained for that hybrid graphene-C:ZnO nanocones film. Using Fowler-Nordheim (FN) equation [18], the field enhancement factor (β) can be calculated from the approximate linearity of FN plot as shown in the inset figure of Fig. 7-5. By assuming the work function (ϕ) is ~4.5 eV [19] for graphene and 5.3 eV for C:ZnO [20], β was calculated as 2525 and 1603 for the hybrid graphene-C:ZnO and pristine C:ZnO film, respectively. The key factor of high emission current is depending on the aspect ratio and the work function of the electron emitters. Low emission current was observed if only graphene film or pristine C:ZnO nanocones was used as the emitters. In fact, in this experiment the bare graphene film does not show any emission current up to 10 V um^{-1} given electric field. The reason is because of low aspect ratio of graphene and high work function of C:ZnO material. However, higher emission current at a lower threshold field was obtained for the transparent hybrid structure of graphene-C:ZnO nanocones film. The higher β obtained for transparent hybrid graphene-C:ZnO nanocones film than the pristine C:ZnO nanocones was attributed by the improvement in high aspect ratio of C:ZnO nanocones with a sheet of graphene on top of the nanocones.

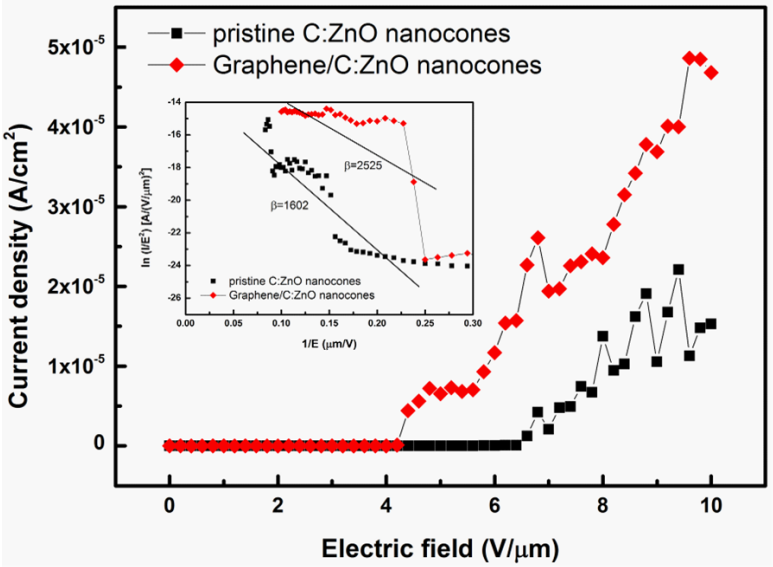

Figure 7-5: FE properties of pristine C:ZnO and hybrid graphene-C:ZnO nanocones film. Inset indicates the F-N plot for field enhancement factor of the emitters.

Fig. 7-6 depicted the stability test of graphene-C:ZnO nanocones film. It shows an average stability around 10 μA in 50 minute with few spikes observed from the stability plotted graph. The stability test was done at a fixed voltage of 1200V.

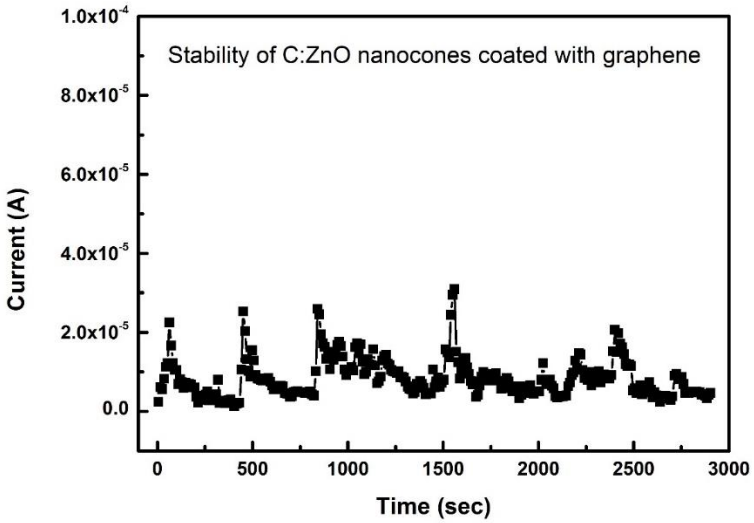

Figure 7-6: Stability test for graphene-C:ZnO nanocones film in 50 min at 1200V

7.3 Conclusion

In summary, the fabrication of graphene-C:ZnO nanocones hybridized transparent field emission device with significantly enhance emission properties was demonstrated. The threshold field for hybrid and pristine C:ZnO nanocones film at current density of 1 μA/cm^2 was obtained at 4.3 V/μm and 6.5 V/μm, respectively. The graphene-C:ZnO nanocones showed a large field enhancement factor of 2525 calculated from Fowler-Nordheim plot. The improved field emission with low turn-on fields for the graphene-C:ZnO nanocone is attributed to the locally enhance electric field. The hybrid structure film is fabricated on a high quality substrate, the emission current could be increased higher than the existing one and will adequate to excite electrons to emit light at the phosphor screen. This will also open up for flexible device applications by creating hybrid graphene-C:ZnO nanocones structure on plastic substrate. Thus, a promising transparent and flexible ZnO-based FED can be achieved.

7.4 References

[1] Z. Zulkifli, S. Munisamy, M. Z. M. Yusop, and M. Tanemura, "Effect of surface morphology on the field emission property of ZnO films," *Phys. Status Solidi*, vol. **11**, no. 7–8, pp. 1349–1352, 2014.

[2] Y. H. Lu, Z. X. Hong, Y. P. Feng, and S. P. Russo, "Roles of carbon in light emission of ZnO," *Appl. Phys. Lett.*, vol. **96**, no. 9, pp. 091914, 2010.

[3] Y. M. Ho, W. T. Zheng, Y. A. Li, J. W. Liu, and J. L. Qi, "Field emission properties of hybrid carbon nanotube-zno nanoparticles," *J. Phys. Chem. C*, vol. **112**, pp. 17702–17708, 2008.

[4] R. N. Gayen and a. K. Pal, "Growth of carbon nanofibers on aligned zinc oxide nanorods and their field emission properties," *Appl. Surf. Sci.*, vol. **256**, no. 21, pp. 6172–6178, 2010.

[5] Y. M. Ho, G. M. Yang, W. T. Zheng, X. Wang, H. W. Tian, Q. Xu, H. B. Li, J. W. Liu, J. L. Qi, and Q. Jiang, "Synthesis and field electron emission properties of hybrid carbon nanotubes and nanoparticles.," *Nanotechnology*, vol. **19**, pp. 065710, 2008.

[6] D. Ye, S. Moussa, J. D. Ferguson, A. a Baski, and M. S. El-Shall, "Highly efficient electron field emission from graphene oxide sheets supported by nickel nanotip arrays.," *Nano Lett.*, vol. **12**, no. 3, pp. 1265–8, 2012.

[7] A. Geim and K. Novoselov, "The rise of graphene," *Nat. Mater.*, vol. **6**, pp. 183–191, 2007.

[8] M. Zamri Yusop, G. Kalita, Y. Yaakob, C. Takahashi, and M. Tanemura, "Field emission properties of chemical vapor deposited individual graphene," *Appl. Phys. Lett.*, vol. **104**, no. 9, pp. 093501, 2014.

[9] Z.-S. Wu, S. Pei, W. Ren, D. Tang, L. Gao, B. Liu, F. Li, C. Liu, and H.-M. Cheng, "Field Emission of Single-Layer Graphene Films Prepared by Electrophoretic

Deposition," *Adv. Mater.*, vol. **21**, no. 17, pp. 1756–1760, 2009.

[10] S. Santandrea, F. Giubileo, V. Grossi, S. Santucci, M. Passacantando, T. Schroeder, G. Lupina, and a. Di Bartolomeo, "Field emission from single and few-layer graphene flakes," *Appl. Phys. Lett.*, vol. **98**, no. 16, pp. 163109, 2011.

[11] S. Morozov, K. Novoselov, M. Katsnelson, F. Schedin, D. Elias, J. Jaszczak, and a. Geim, "Giant Intrinsic Carrier Mobilities in Graphene and Its Bilayer," *Phys. Rev. Lett.*, vol. **100**, no. 1, pp. 016602, 2008.

[12] C. Lee, X. Wei, J. W. Kysar, and J. Hone, "Measurement of the Elastic Properties and Intrinsic Strength of Monolayer Graphene," *Science*, vol. **321**, pp. 385–388, 2008.

[13] R. R. Nair, P. Blake, A. N. Grigorenko, K. S. Novoselov, T. J. Booth, T. Stauber, N. M. R. Peres, and A. K. Geim, "Fine Structure Constant Defines Visual Transparency of Graphene," *Science*, vol. **320**, pp. 1308, 2008.

[14] a. V. Krasheninnikov and K. Nordlund, "Ion and electron irradiation-induced effects in nanostructured materials," *J. Appl. Phys.*, vol. **107**, no. 7, pp. 071301, 2010.

[15] X. Li, W. Cai, J. An, S. Kim, J. Nah, D. Yang, R. Piner, A. Velamakanni, I. Jung, E. Tutuc, S. K. Banerjee, L. Colombo, and R. S. Ruoff, "Large-area synthesis of high-quality and uniform graphene films on copper foils.," *Science*, vol. **324**, no. 5932, pp. 1312–4, 2009.

[16] S. Sharma, G. Kalita, R. Hirano, S. M. Shinde, R. Papon, H. Ohtani, and M. Tanemura, "Synthesis of graphene crystals from solid waste plastic by chemical vapor deposition," *Carbon N. Y.*, vol. **72,** pp. 66–73, 2014.

[17] M. Peplow, "Graphene: The quest for supercarbon.," *Nature*, vol. **503**, pp. 327–9, 2013.

[18] Z. Zulkifli, S. Munisamy, M. Zamri, M. Yusop, G. Kalita, and M. Tanemura, "Fabrication of Nanostructured ZnO Films for Transparent Field Emission Displays

Fabrication of Nanostructured ZnO Films for Transparent Field Emission Displays," *Jpn. J. Appl. Phys.*, vol. **52**, pp. 11NJ07, 2013.

[19] J.-H. Kim, J. H. Hwang, J. Suh, S. Tongay, S. Kwon, C. C. Hwang, J. Wu, and J. Young Park, "Work function engineering of single layer graphene by irradiation-induced defects," *Appl. Phys. Lett.*, vol. **103**, no. 17, pp. 171604, 2013.

[20] A. Al-Tabbakh, M. More, and D. Joag, "The Fowler−Nordheim Plot Behavior and Mechanism of Field Electron Emission from ZnO Tetrapod Structures," *ACS Nano*, vol. **4**, no. 10, pp. 5585–5590, 2010.

CHAPTER 8

Fabrication of transparent and flexible carbon doped ZnO field emission display on plastic substrate

8.0 Introduction

Slim design, mechanical robustness, light in weight, flexible, transparent and yet cheap electronic gadgets including the future display technology are becomes a demand in nowadays global electronic industry [1-3]. It can only be implemented if the current circuitry, electrodes can be minimized and fabricated on the flexible substrate [4]. Polyethylene terephthalate (PET) is among the most flexible substrate that has been used in this research field [5-8]. Besides PET, there are several types of flexible substrate such as Polyethylene Naphthalate (PEN), flexible polycarbonate (PC) and arylite. The melting temperature for PET, PEN, PC and Arylite is 258˚C, 269˚C, 225˚C and 300˚C, respectively. The main issue in fabricating flexible substrate is the adhesion between the thin film and the substrate and the sensitivity of the substrate towards temperature. In the recent literature, UV-light decomposition process has been employed to deposit nanoparticle on the flexible substrate [9]. With an appropriate surface treatment on the flexible substrate, the issue of adhesion is possible to overcome. As reported by Park et al., low surface energy of polymeric materials was the factor that attributed to the poor surface adhesion [10]. There are several techniques of surface treatment which have also been reported to improvise the adhesion between film and substrate such as air–plasma discharge [11] and treatment of the substrate in oxygen atmosphere [12]. In recent development of transparent and flexible display technology of field emission display (FED), many researchers have comes with their experimental works to

fulfill the market needs. Yet, until now, there is no report on fully transparent and flexible FED. Few reports on transparent field emitters could be found, however it is not flexible [13], flexible emitters but not transparent [14], transparent and flexible field emitter but the anode screen is not flexible thus restrict the fabrication of flexible display [15,16], fully flexible based FED but not transparent [17,18] and most of the fabrications were used carbon nanotubes (CNTs) as the materials which is costly even though it can provide a good electron transport to produce high emission current. In addition, a phosphor layer is needed to be coated for that CNTs FED structure. The phosphor layer will increase the thickness of anode film and might reduce the transmittance property. Thus, to tackle the limitations in fabricating transparent and flexible FED, ZnO based film was employed as the device material owing to the advantages of high transmittance property, wide (3.3 eV) and direct band gap, abundant materials and yet is cheap compared to indium tin-oxide (ITO). In addition, ZnO material has an ability to emit light emission [19]. As it has been reported in the existing FED fabrication, most of the researchers deposit a layer of phosphor materials to exhibit for the light emission [20]. If the fabrication process can be reduced, the cost of the final product also could be cheaper. In chapter 6, transparent C:ZnO film on glass substrate was successfully fabricated which can be applied for phosphor screen as well as the emitters of FED [21]. To achieve a flexible FED, the fabrication of C:ZnO film was done on an arylite substrate. The high transmittance property of C:ZnO thin film was achieved. Thus, for the first time, a promising fully transparent and flexible FED using ZnO film is demonstrated in this chapter.

8.1 Experimental details

8.1.1 *C:ZnO thin and nanostructured film preparations*

C:ZnO thin film was deposited on 100 μm thick arylite substrate (Ferrania Technologies, AryLite™ A100HC) by RF sputtering at 200˚C for 20 min. Low argon flow rate and RF power were introduced during the deposition at 1 sccm and 50 W, respectively. These lower values of argon flow rate and RF power can avoid the surface of C:ZnO thin film from crack. The bare arylite substrate has an optical transmittance of 90.4%. Firstly, a 1.5 x 1.5 cm size of arylite was attached on a glass substrate which has a bigger size than that arylite. All four sides of arylite substrate were stuck on the glass substrate by Kapton tape to prevent the flexible substrate from bending during film deposition process. Next, the prepared flexible substrate was placed on the substrate holder in the sputtering machine which is located in parallel with the target. Deposition process can only be started when the background pressure showed high vacuum level around 3 x 10^{-5} Pa. The same preparation of deposited C:ZnO thin films was employed for both cathode (emitter) and anode material (phosphor screen) of the FED. A single piece of graphite plate with the size of 1.5 x 1.5 cm^2 was used as the carbon source in the co-sputtering process. The size of graphite plate contributed 0.1 at% of carbon concentration in ZnO thin film measured by secondary ion mass spectroscopy (SIMS) with concentration calibration using standard specimens. Both cathode and anode films having the same concentration of carbon. The fabrication for nanocones field emitters was done by Ar^+ ions irradiation using a Kaufman type ion gun (ION TECH. INC.Ltd., model 3-1500-100FC) on the transparent and flexible deposited C:ZnO thin film at room temperature for 5 min. The working pressure in the beam chamber was 5 x 10^{-2} Pa. The energy and current beam used were 1000 eV and 6 mA, respectively. The incidence angle was at 60˚ from normal to the surface.

8.1.2 *C:ZnO films characterizations*

The morphology of irradiated C:ZnO film was observed by scanning electron microscopy (SEM; JEOL JSM-5600). The transmittance of both C:ZnO thin film and nanostructured film were characterized by UV-Vis spectrometer (Jasco V-670K). Sheet resistance value was measured from the four point probes (Napson RT-70V/RG-7C) without deposited contact on the thin film and the field emission property was measured from 0-1300V under a parallel plate configuration. A spacer used in this measurement was 50 μm thick Teflon and the emission area was 0.1 cm^2. During the observation for light property, the cathode material was changed to single wall carbon nanotubes thin film and the light emission was taken by a digital camera from the O-ring-shield glass at the chamber. To support the experimental result of light emission property, a cathodoluminescence (CL) spectrum was taken using scanning electron microscopy-cathodoluminescence spectroscopy (SEM-CL; JEOL JSM 7800F).

8.2 Results and Discussion

Initially 100W of RF power was applied during the deposition process. However, many cracks were found on the C:ZnO thin film as shown in Fig.8-1.

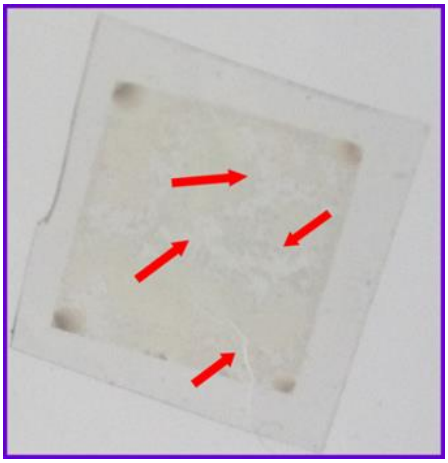

Figure 8-1: C:ZnO thin film deposited at high RF power

The SEM image shown in Fig.8-2 emphasizes the cracked and peel off C:ZnO film on the arylite substrate. Due to this reason, lower RF power at 50W was applied as it can reduce the scattered particles during the deposition process. This condition gave less stress on the thin film and resulted in good adhesion between C:ZnO film and the substrate.

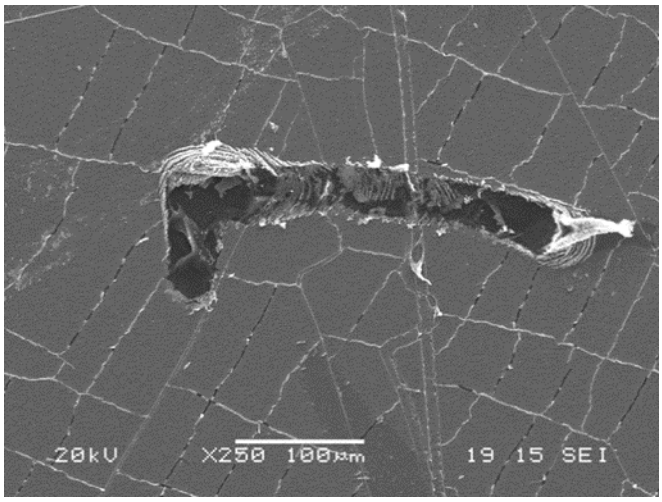

Figure 8-2: SEM image of C:ZnO on arylite substrate deposited at high RF power

As shown in Fig. 8-3, no crack can be observed after applied the lower RF power. Thus, the lower RF power was maintained the optimum parameter for the next fabricated flexible C:ZnO nanocones film.

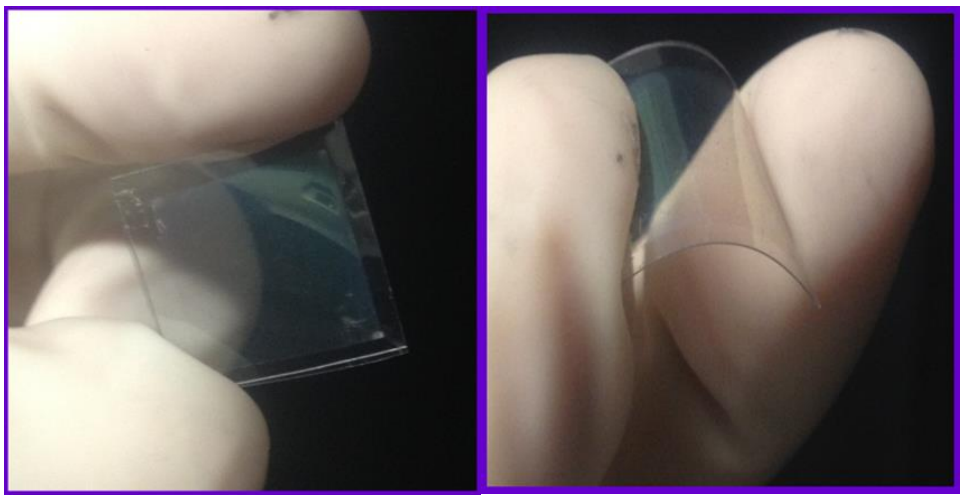

Figure 8-3: C:ZnO thin film on arylite substrate deposited at low RF power

Figure 8-4 shows the surface morphology of C:ZnO nanostructured film from the typical SEM images at low and high magnification. From the low magnification image (Fig. 8-4 (a)), the nanocones formation can be observed at the whole area of the arylite substrate. The high magnification SEM image (Fig. 8-4 (b)) revealed the C:ZnO nanocones were about 6-7 μm^{-2} in number density and in a few hundreds nanometer in height. Sharp tips of the C:ZnO nanocones was attributed to the higher energy beam employed during ions irradiation.

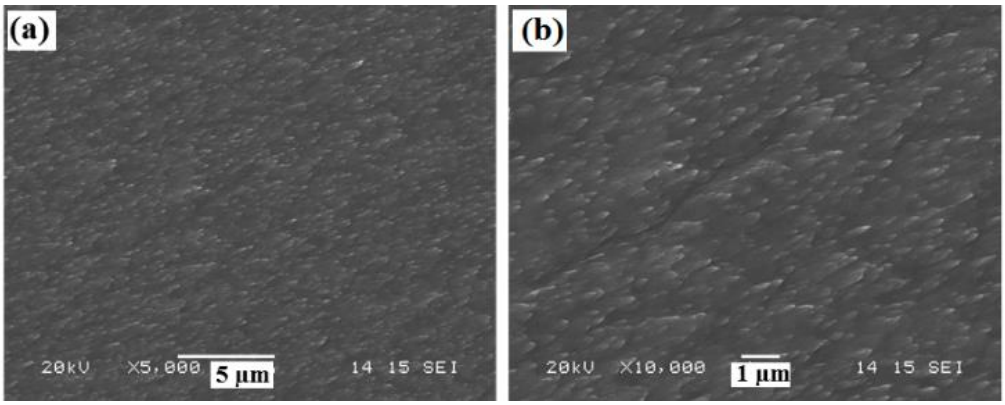

Figure 8-4: **Typical SEM images of C:ZnO nanocone emitters on an arylite substrate at (a) low magnification and (b) high magnification.**

Figure 8-5 (a) shows the transmittance property of the flexible C:ZnO nanocone emitters and the phosphor screen. The C:ZnO phosphor screen film shows 80% transmittance at 550 nm wavelength while for the nanocones shows at 77%. In general, there was no significant difference can be observed in the transmittance property for both films. The wavy transmittance spectra was due to the interference between the substrate and C:ZnO film. Fig. 8-5 (b) and (c) demonstrate the text behind the films were clearly can be seen and a bending behaviour of anode and cathode of C:ZnO FED without showing any crack on the surface of the films. The result obtained suggest that a lower RF power during film deposition exhibit good adhesion between C:ZnO film and arylite substrate. The measured average sheet resistance of C:ZnO thin film was 1.96 kΩ/□.

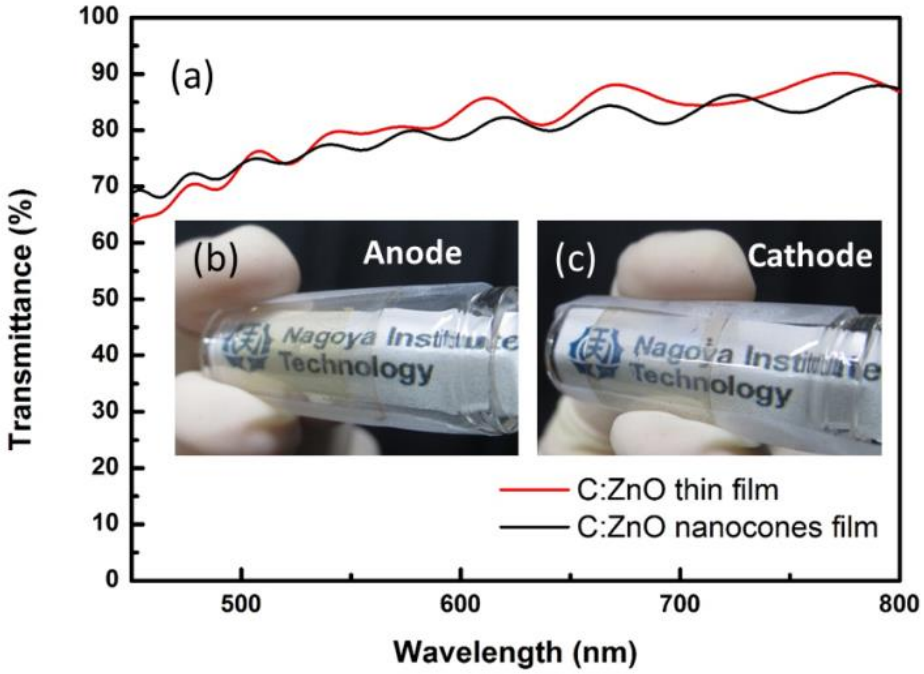

Figure 8-5: (a) The transmittance spectra of C:ZnO thin and nanoconces film. Transparent and flexible C:ZnO (b) anode film and (c) nanocone emitters.

Figure 8-6 (a) shows the field emission (FE) property of the transparent and flexible C:ZnO FED. The electric field required to obtain current density at 1 μA cm^{-2} was achieved at 18 V μm^{-1}. FE measurement was carried out up to 1300 V and the maximum current density was obtained at 16 μA cm^{-2}. Inset figure shows the FN plot which exhibit a linear behaviour correspond to the typical FN equation as discussed in the previous publication [22]. The field enhancement factor, (β), was calculated from the slope of linear line and was found to be 474. Figure 8-6 (b) shows the stability test of the transparent and flexible C:ZnO nanocone emitters for 1 hr. As seen in the life test, the result shows almost stable emission current at 2 μA in average at a fixed voltage of 1200 V.

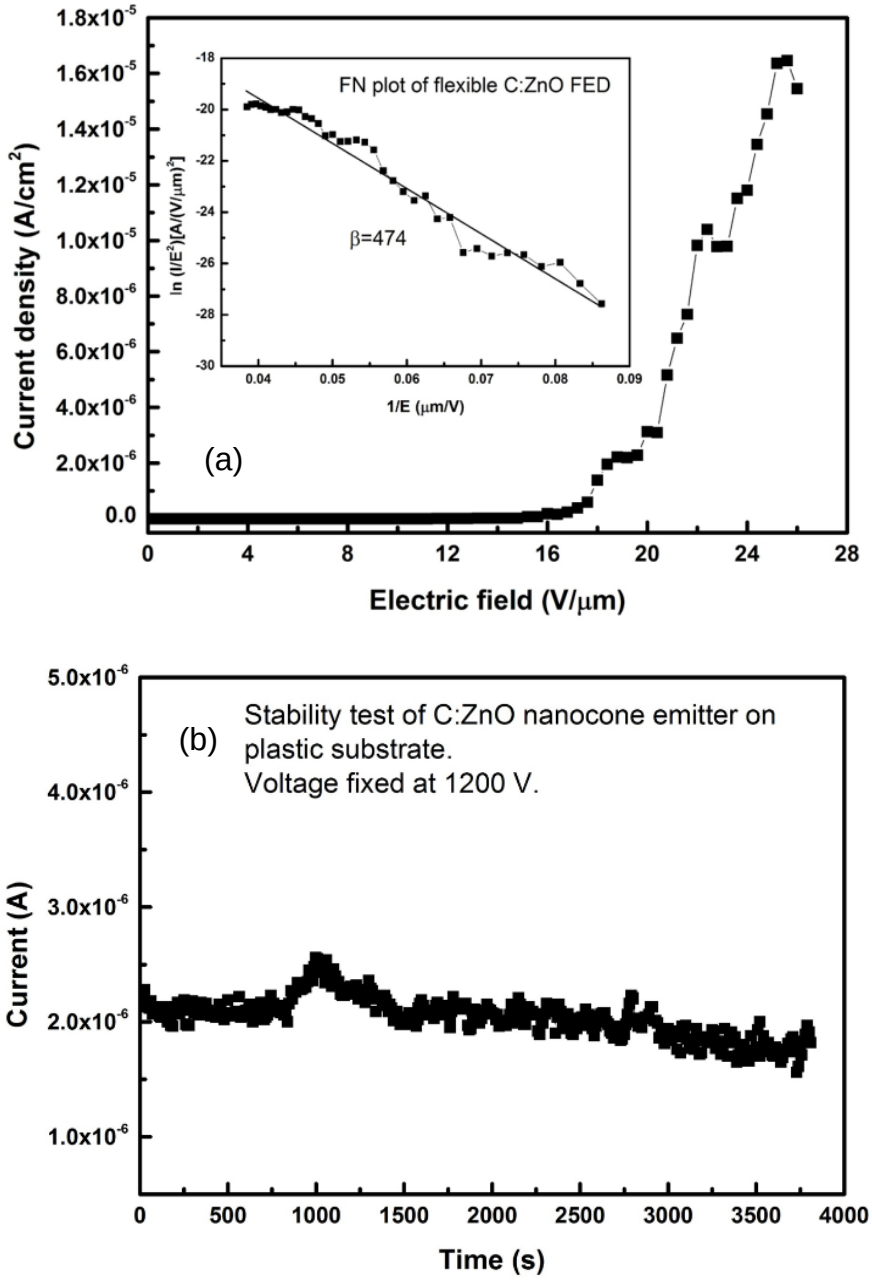

Figure 8-6: (a) FE properties of transparent and flexible C:ZnO FED and the inset figure is the corresponding FN plot. (b) Stability test of transparent and flexible C:ZnO nanocones emitters for 1 hr.

To investigate a light emission property, the C:ZnO film which was employed as the phosphor screen was measured with the single wall carbon nanotube (SWCNT) as the cathode material. At this stage, electron emission from the fabricated C:ZnO nanocone emitters was not enough to yield the intense light emission of the phosphor. The light emission of the phosphor using C:ZnO nanocone emitters can be seen by naked eyes, but the

light intensity was not enough to be captured by digital camera. This might be due to low aspect ratio of C:ZnO emitters. Thus, to investigate a phosphor property from the C:ZnO thin film (anode), transparent SWCNT film was employed as the cathode since it is a stable electron transport and can produce high emission current. The preparation of transparent and flexible SWCNT film can be explained elsewhere [23]. The distance between that phosphor screen and SWCNT film was 100 μm. Same emission area of 0.1 cm^2 was applied in this measurement. From the measurement, the light emission can be observed when the current density reached more than 20 μA cm^{-2}. When higher electric field was applied as shown in Fig. 8-7 (a), the brightness of light emission increased until it can be fully observed in the emission area as depicted in Fig. 8-7 (b). To confirm that the red light emission captured by a digital camera is not due to spark, the C:ZnO thin film was characterized by CL spectroscopy. From CL spectrum as shown in Fig. 8-7 (c), a defect peak was observed at 646 nm in which it is corresponding to the red light wavelength. The observed red light emission showed the phosphor property of C:ZnO film in which it was agreed by that CL spectrum. Red phosphor screen has been achieved by other materials such as $Y_2O_3:Eu^+$ and $AIN:Mn^{2+}$ [24]. This finding exhibited the ability of transparent C:ZnO film to be as an alternative of red phosphor screen. Yet, further improvement is still needed to compare with the existing red phosphor material.

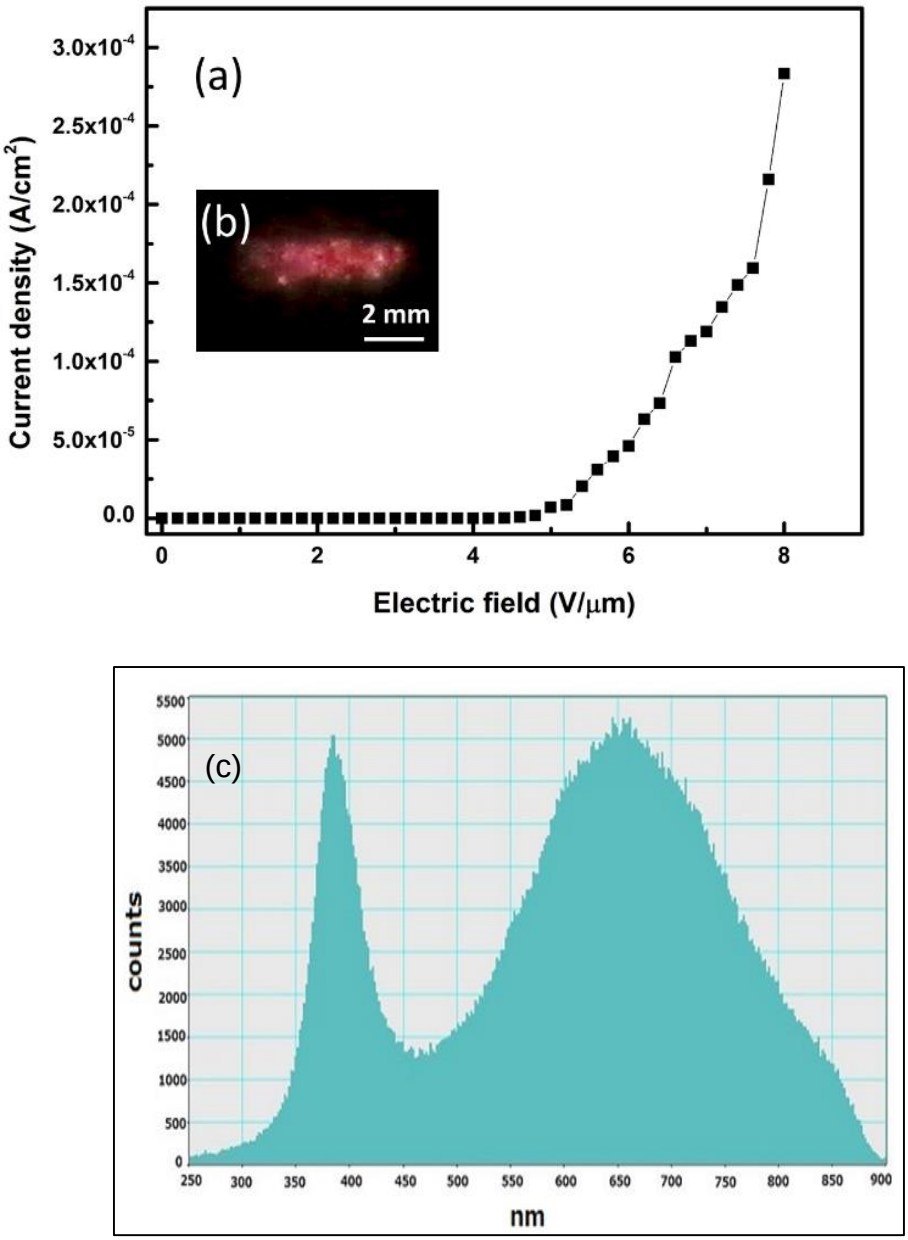

Figure 8-7: **(a) FE property of transparent and flexible C:ZnO anode film with CNT as the cathode material. (b) Red light emission observed from FE measurement and (c) CL spectra shows the dominant peak at 646 nm at the visible wavelength which is corresponding to the red colour wavelength.**

8.3 Conclusion

In conclusion, the transparent and flexible C:ZnO thin and nanocones films can be easily fabricated at low temperature by RF sputtering and ion beam irradiation, respectively without damaging the flexible substrate. Influence of carbon in the ZnO film is not only to improve the film conductivity but also form an oxygen-related defect. The defect peak can be

observed in the visible wavelength from CL spectrum which is directly attributed to the red light emission property of C:ZnO thin film. With this achievement, ZnO based material can be a promising transparent and flexible FED. Due to the unique property of ZnO to be as the transparent and flexible phosphor screen, the next goal is to tune the defect formation from the ZnO based film to exhibit several different light emission. So that, with only use ZnO material, different emission colour could be obtained for a transparent and flexible FED application. Transparent and flexible ZnO based FED could open a revolution in electronic industry of the future low cost, light weight, transparent and flexible display with a simple fabrication process.

8.4 References

[1] G. Zhou, F. Li, and H.-M. Cheng, "Progress in flexible lithium batteries and future prospects," *Energy Environ. Sci.*, vol. **7**, no. 4, pp. 1307, 2014.

[2] S. Berchmans, A. J. Bandodkar, W. Jia, J. Ramírez, Y. S. Meng, and J. Wang, "An epidermal alkaline rechargeable Ag–Zn printable tattoo battery for wearable electronics," *J. Mater. Chem. A*, vol. **2**, no. 38, pp. 15788–15795, 2014.

[3] P. Hosseini, C. D. Wright, and H. Bhaskaran, "An optoelectronic framework enabled by low-dimensional phase-change films," *Nature*, vol. **511**, no. 7508, pp. 206–211, 2014.

[4] S. Das, R. Gulotty, A. V Sumant, and A. Roelofs, "All two-dimensional, flexible, transparent, and thinnest thin film transistor.," *Nano Lett.*, vol. **14**, no. 5, pp. 2861–6, 2014.

[5] H. Su, M. Zhang, Y. Chang, P. Zhai, N. Y. Hau, Y. Huang, C. Liu, A. K. Soh, and S. Feng, "Highly Conductive and Low Cost Ni-PET Flexible Substrate for E ffi cient Dye-Sensitized Solar Cells," *ACS Appl. Mater. Interfaces*, vol. **6**, pp. 5577–5584, 2014.

[6] N. Saran, K. Parikh, and D. Suh, "Fabrication and characterization of thin films of single-walled carbon nanotube bundles on flexible plastic substrates," *J. Am. Chem. Soc.*, vol. **126**, pp. 4462–4463, 2004.

[7] S. Fernández and F. B. Naranjo, "Optimization of aluminum-doped zinc oxide films deposited at low temperature by radio-frequency sputtering on flexible substrates for solar cell applications," *Sol. Energy Mater. Sol. Cells*, vol. **94**, no. 2, pp. 157–163, 2010.

[8] A. R. Madaria, A. Kumar, F. N. Ishikawa, and C. Zhou, "Uniform, highly conductive, and patterned transparent films of a percolating silver nanowire network

on rigid and flexible substrates using a dry transfer technique," *Nano Res.*, vol. **3**, no. 8, pp. 564–573, 2010.

[9] B. Sun, Y.-Z. Long, Z.-J. Chen, S.-L. Liu, H.-D. Zhang, J.-C. Zhang, and W.-P. Han, "Recent advances in flexible and stretchable electronic devices via electrospinning," *J. Mater. Chem. C*, vol. **2**, no. 7, pp. 1209, 2014.

[10] J.-S. Park, T.-W. Kim, D. Stryakhilev, J.-S. Lee, S.-G. An, Y.-S. Pyo, D.-B. Lee, Y. G. Mo, D.-U. Jin, and H. K. Chung, "Flexible full color organic light-emitting diode display on polyimide plastic substrate driven by amorphous indium gallium zinc oxide thin-film transistors," *Appl. Phys. Lett.*, vol. **95**, no. 1, pp. 013503, 2009.

[11] D. R. Iii, A. Parness, and M. Spenko, "Improving controllable adhesion on both rough and smooth surfaces with a hybrid electrostatic / gecko-like adhesive Improving controllable adhesion on both rough and smooth surfaces with a hybrid electrostatic / gecko-like adhesive," *J. R. Soc. Interface*, vol. **11**, pp. 1-10, 2014.

[12] S. H. Kim, S. W. Na, N.-E. Lee, Y. W. Nam, and Y.-H. Kim, "Effect of surface roughness on the adhesion properties of Cu/Cr films on polyimide substrate treated by inductively coupled oxygen plasma," *Surf. Coatings Technol.*, vol. **200**, no. 7, pp. 2072–2079, 2005.

[13] A. a. Kuznetzov, S. B. Lee, M. Zhang, R. H. Baughman, and A. a. Zakhidov, "Electron field emission from transparent multiwalled carbon nanotube sheets for inverted field emission displays," *Carbon*, vol. **48**, no. 1, pp. 41–46, 2010.

[14] X. Zhang, L. Gong, K. Liu, Y. Cao, X. Xiao, W. Sun, X. Hu, Y. Gao, J. Chen, J. Zhou, and Z. L. Wang, "Tungsten oxide nanowires grown on carbon cloth as a flexible cold cathode.," *Adv. Mater.*, vol. **22**, no. 46, pp. 5292–6, 2010.

[15] D. Ghosh, P. Ghosh, G. Kalita, T. Noda, C. Takahashi, and M. Tanemura, "Conducting polymer based hybrid structure as transparent and flexible field

electron emitter," *Phys. status solidi - Rapid Res. Lett.*, vol. **7**, no. 7, pp. 489–492, 2013.

[16] P. Ghosh, M. Z. Yusop, S. Satoh, M. Subramanian, A. Hayashi, Y. Hayashi, and M. Tanemura, "Transparent and flexible field electron emitters based on the conical nanocarbon structures.," *J. Am. Chem. Soc.*, vol. **132**, no. 12, pp. 4034–5, 2010.

[17] H. J. Jeong, H. D. Jeong, H. Y. Kim, J. S. Kim, S. Y. Jeong, J. T. Han, D. S. Bang, and G.-W. Lee, "All-Carbon Nanotube-Based Flexible Field-Emission Devices: From Cathode to Anode," *Adv. Funct. Mater.*, vol. **21**, no. 8, pp. 1526–1532, 2011.

[18] D. H. Shin, S. Il Jung, K. N. Yun, G. Chen, Y. Song, Y. Saito, W. I. Milne, D. H. Shin, I. Jung, N. Yun, G. Chen, and Y. Song, "Field emission properties from flexible field emitters using carbon nanotube film Field emission properties from flexible field emitters using carbon nanotube film," *Appl. Phys. Lett.*, vol. **105**, pp. 033110, 2014.

[19] J. E. Stehr, S. L. Chen, N. K. Reddy, C. W. Tu, W. M. Chen, and I. a. Buyanova, "Turning ZnO into an efficient energy upconversion material by defect engineering," *Adv. Funct. Mater.*, vol. **24**, pp. 3760–3764, 2014.

[20] V. P. Verma, S. Das, I. Lahiri, and W. Choi, "Large-area graphene on polymer film for flexible and transparent anode in field emission device," *Appl. Phys. Lett.*, vol. **96**, no. 20, pp. 203108, 2010.

[21] Z. Zulkifli, M. Subramanian, T. Tsuchiya, M. S. Rosmi, P. Ghosh, G. Kalita, and M. Tanemura, "Highly transparent and conducting C:ZnO thin film for field emission displays," *RSC Adv.*, vol. **4**, no. 110, pp. 64763–64770, 2014.

[22] Z. Zulkifli, S. Munisamy, M. Zamri, M. Yusop, G. Kalita, and M. Tanemura, "Fabrication of Nanostructured ZnO Films for Transparent Field Emission Displays

Fabrication of Nanostructured ZnO Films for Transparent Field Emission Displays," *Jpn. J. Appl. Phys.*, vol. **52**, pp. 11NJ07, 2013.

[23] D. Ghosh, P. Ghosh, M. Z. Yusop, M. Tanemura, Y. Hayashi, T. Tsuchiya, and T. Nakajima, "Transparent and flexible field emission display device based on single-walled carbon nanotubes," *Phys. status solidi - Rapid Res. Lett.*, vol. **6**, no. 7, pp. 303–305, 2012.

[24] X.-J. Wang, R.-J. Xie, B. Dierre, T. Takeda, T. Suehiro, N. Hirosaki, T. Sekiguchi, H. Li, and Z. Sun, "A novel and high brightness AlN:Mn2+ red phosphor for field emission displays.," *Dalton Trans.*, vol. **43**, no. 16, pp. 6120–7, 2014.

CHAPTER 9

Conclusion and Future Development

9.0 Conclusions

Highly transparent and conducting ZnO-based thin film by RF sputtering at low temperature for FED screen was successfully fabricated. The ZnO-based thin film was also successfully fabricated on the flexible substrate. Thus, with the simple deposition method and catalyst-free, ZnO-based thin film can be a potential candidate to replace ITO as the anode layer for transparent FED in the future. A low concentration of C in ZnO thin film had changed a lot of ZnO property and make it interesting to explore and understand the process occurred during the deposition. C doped ZnO film exhibited light emission during the field emission measurement. However, the brightness of that light emission could not be measured due to the limitation of FE instrument.

Sharp tips of transparent ZnO-based nanocones film was achieved in 10 min irradiation time. The height of nanocones was obtained around 400 -700 nm. The transmittance of ZnO thin film decreased due to the increasing of surface roughness. The best ion incident angle was achieved at 60° for a sharp tip of ZnO-based nanocones. ZnO-based nanocones demonstrate a stable morphology even though after being exposed to high electric field for about 60 min. The result concluded that ZnO had a good mechanical properties.

A hybrid structure of graphene-C:ZnO nanocones had enhanced higher emission current at low electric field. The higher transmittance property of graphene was a factor that the hybrid structure possesses the same transmittance property even after the graphene

transfer process. Graphene transfer process was done at room temperature and need intensively cleaning process to remove PMMA.

Even though high transmittance and conductive thin and nanocones film was successfully achievable, the flexible film remain challenging and needs a lot of improvements. The proposed ZnO-based transparent and flexible FED shows low emission current at high electric field. Nevertheless, it is the first reported transparent and flexible ZnO-based FED in which this achievement could lead to fabricate low cost, light weight, flexible and transparent display in the future.

9.1 Future development

The light emission from ZnO-based thin film could be varied according to the defect formation of ZnO. It can produce more than one emission color and that ZnO thin film can be a potential source of color pixel for a color display. Since most of the defect in ZnO that attribute to the color of light emission was reported by a calculation from density functional theory, it would be great if the color of light emission can also be proved by FE experiment to agree with the calculation. In addition, an improvement on the FE instrument to measure the emission power and brightness of the light emission has to be catered in the future.

Fabrication of p-type ZnO can develop highly transparent and flexible ZnO emitters which can emit light from the emitter itself without the needs of phosphor layer in future display technology. This can be realized due to the property of recombination behavior from the heterojunction of n- and p-type ZnO materials. The fabrication of nanocones on high crystalline quality substrate such as sapphire can enhance an emission current due to the excess electrons from the substrate. The existing sapphire substrate has only one side polished surface thus make the substrate less transparent. If both sides of the sapphire surface could be polished, a high quality substrate can be used for the transparent FED screen.

List of Publications

1. **Zurita Zulkifli**, Subramanian Munisamy, Mohd Zamri Mohd Yusop, Golap Kalita, and Masaki Tanemura, "Fabrication of Nanostructured ZnO Films for Transparent Field Emission Displays", *Jpn J Appl Phys*, **52**, 11NJ07 (2013) (IF: 1.057)
2. **Z. Zulkifli**, M. Subramanian, T. Tsuchiya, M. S. Rosmi, Pradip Ghosh, G. Kalita and M. Tanemura, "Highly transparent and conducting C:ZnO thin film for field emission display", *RSC Adv.*, **4**, 64763-64770 (2014) (IF: 3.708)
3. **Zurita Zulkifli**, Golap Kalita and Masaki Tanemura, "Fabrication of transparent and flexible carbon-doped ZnO field emission display on plastic substrate", *Phys. Status Solidi RRL*, doi: 10.1002/pssr.201409557 (2015) (IF: 2.388)
4. **Zurita Zulkifli**, Subramanian Munisamy, Mohd Zamri Mohd Yusop, and Masaki Tanemura, "Effect of surface morphology on the field emission property of ZnO films", *Phys. Status Solidi C*, **11**, 1349–1352 (2014) – Conference Proceeding.

List of Conferences

1. Effect of Hydrogen Annealing on ZnO thin films.

   Zurita Zulkifli, M. Subramanian, Subash Sharma, Golap Kalita and M. Tanemura

   International Conference on Nanoscience and Nanotechnology 2013 (NANO-SciTech 2013)

2. Fabrication of Nanostructured ZnO Films for Transparent Field Emission Displays.

   Zurita Zulkifli, M. Subramanian, M. Zamri M. Yusop, Golap Kalita and M. Tanemura

   5th International Symposium on Advanced Plasma Science and its Application for Nitrides and Nanomaterials (ISPlasma 2013)

3. Effect of surface morphology on the field emission property for ZnO films.

   Zurita Zulkifli, M. Subramanian, M. Zamri M. Yusop and M. Tanemura

   The 16th International Conference on II-VI Compound and Related Materials (II-VI 2013)

4. Effect of Carbon Concentrations on Transparency and Conductivity of C:ZnO Thin Films.

   Zurita Zulkifli, Golap Kalita, M. Subramanian, and M. Tanemura

   12th International Conference on Atomically Controlled Surfaces, Interfaces and Nanostructures in conjunction with 21st International Colloquium on Scanning Probe Microscopy (ASCIN-12&ICSPM21) -2013

5. The emission performance of C:ZnO conical structure field emitters for transparent field emission display.

   Zurita Zulkifli, Subash Sharma, Takatoshi Sugiura, M. Zamri Yusop, Golap Kalita, M. Tanemura, *International Union of Materials Research Societies- The IUMRS International Conference in Asia 2014*